TRABAJO ESPECIAL DE GRADO

EXCAVACIÓN MECANIZADA EN ROCA: RESULTADOS OBTENIDOS TEÓRICA Y EXPERIMENTALMENTE A PARTIR DE ENSAYOS REALIZADOS CON UNA ILCM

TUTOR ACADEMICO: Profa. Aurora Pina

TUTOR ACADEMICO POLITECNICO DE TORINO: Profa. Marilena Cardu

Presentando ante la Ilustre
Universidad Central de Venezuela
Por el Br. Montes M.
Ramon A.
Para optar al titulo
de Ingeniero en Minas

Caracas, 2017

To my family and those who has put their faith on me

Acknowledgements

First, to god for giving me the health, intelligence, patience and wisdom necessary to overcome the task and challenges that arose during the making of this work.

To the Central University of Venezuela, Polytechnic of Turin and Environmental and Land Department for the opportunity of learning and growing either in classroom as personally.

To my tutors in Italy, Marilena Cardu, Giorgio Iabichino, Pierpaolo Oreste, for the opportunity of begin such interesting investigation as this one, for the time offered and specially for the knowledge shared during these months.

To my tutors in Venezuela, Aurora Piña and Miguel Castillejo for loving their jobs as professors and not only supporting me during my academical life but also to many others students.

Specially to Andrea Rispoli who contributed as no one on the good realization of this thesis, for not just taking part of his time for helping but for doing it exceptionally well. My eternal gratitude

To the researchers of the CNR, Igor, Simone e Giullia who always were there for giving a hand.

To Cristina Onate for her material collaboration during the execution of the study.

To Eliana Torres who more than provide me with a tool for writing this thesis has gave me a friendship.

Summary

Figure Index

Table Index

Introduction

Nowadays, using TBMs in hard rock has become the preferred choice for mechanized tunnel excavation. A good enough knowledge of geological conditions along the tunnel alignment is required as the tools used for excavation are not proper for large variation of material properties.

As quoted by (Maidl et al. 2008), in general, hard rock TBMs comprise four key sections, which make up the complete machine: boring section (cutterhead), the thrust and clamping section, the muck removal section, and the support section.

On the cutterhead are arranged the tools that interacts with the rock during excavation. These tools are fixed on a rotating bearing and roll in concentric circles on the face when the cutterhead turns. They are called cutter discs and its geometry depends basically on the rock characteristics and therefore, machine features as the thrust, torque and power. Also, space at the cutterhead and the maximum possible load on the disc cutter bearings are also crucial factors when choosing the appropriate tool size.

Based on the use or position at the cutterhead can be classified as follows: *single discs*, which is typically used in most applications, *double discs*, indicated for soft rocks and *twin discs* which are placed at the cutterhead periphery for doing the tunnel over breaking. It is important to choose the correct cutter for the machine and the geological conditions in order to get the best cost and risk balance.

Rock fragmentation requires a certain TBM performance. According to (Friant & Ozdemir, 1993) the cutting tools should be arranged and used in the manner which produces the possible largest size cutting. This is accomplished through the increasing load on the cutters. The purpose is to attain deeper penetrations into the rock front; so wider cutter disc spacing would be allowed.

According to (Innaurato, et al., 2006), the formation of size cutting or also called rock chip, initiates with a plastic deformation on the rock that produces the surface crushing which, at the same time, induces the formation of a cylindrical or spherical destruction nucleus. Then, the rock bounded by this nucleus starts to squash and spalls producing finally the crack propagation towards a free surface.

The chip formation takes place under a determined load, at a critical s/p ratio value where‘s’ is the spacing of the tools and ‘p’ the depth of the groove. Larger values of this ratio would not allow the chip formation because of the no crack intersection between grooves and shorter ones would represent an excessive crushing of the rock, in both cases increasing the values of specific energy.

(Gertsch, et al., 2007) establish that penetration is the essential rock cutting parameter. As penetration increases, damage to the rock increases, which manifests itself as increases energy consumptions, normal forces and rolling forces. Many researchers have constructed cutting and indentation predictive models that star with penetration.

For the case of cut spacing, the same authors postulate that an increase in the width of the chip must increases the normal force, because more rock is broken to the sides of the cutter. Both, too narrow and to wide spacing increases specific energy.

In general do exist two groups of model to predict the cutter disc performance, fully empirical and theoretical/empirical. The first one is based on data collected in the field and is merely a regression between machine parameters, rock properties and the penetration rate; an example could be the Norwegian Method (Bruland, 2014). The model also makes it possible to analyze the effect of variation on penetration rate, machine utilization and excavation costs.

On the other hand, the second group models are based on theoretical analysis of the rock fragmentation process with mechanical tools. For example the model proposed by (Rostami & Ozdemir, 1993) bases its prediction of normal forces on the pressure distribution under the cutter and area of cutter contact. The rolling forces are predicted by cutting coefficients and normal force. Instead, for (Roxborough & Phillips, 1975) normal force is a function of rock compressive strength and contact area of the cutter and the rolling forces are a function of these one.

The authors just quoted and some others: (Snowdon, et al ,1982), (Sanio, 1985) (Chang, et al., 2006), (Cho, et al., 2009),agree on the fact that the most reliable way to determinate the parameters related to the cutter discs performance is through a full scale linear cutting test which is carried out in a Linear Cutting Machine (LCM)..

Such machine was originally developed by the Colorado School of Mines (CSM). It has been used for designing TBM cutterheads for over 20 years. Consist on realizing with a cutter disc a set of grooves on the rock surface The main advantage is that parameters such as: cutter spacing, penetration depth, cutter thrust and cutting speed can be controlled. Tests done by (Chang, et al., 2006) were conducted in a LCM which has three moving parts used for controlling: cutter spacing conditions, cutting velocity and cutter thrust.

During the test, the linear cutting machine measures three forces: normal force, rolling force and side force. Determining these forces it is important for knowing TBM requirements. An estimated value of normal force allows calculating thrust requirements of the machine, so the cutter disc can penetrate effectively the rock. Also, rolling forces is used to calculate the torque, power and for estimating specific energy necessities.

Considering the facts above mentioned, can be affirmed that the linear cutting machine offers a good simulation of the actual conditions at excavation sites, and therefore can be considered as a reliable way for predicting cutter disc performance. However, the handling of such big samples, reaching dimensions of (1,1x0,8x0,6) m (Gertsch, et al., 2007) makes harder the execution of the test.

On the other hand, do exist methods based on laboratory tests reported in literature, for example those reported by (Innaurato, et al., 2006) (Nilsen & Ozdemir, 1993), which are practically simpler to carry out but do not allow suchlike parameter assessment offered by the LCM.

Taking this into account and the previous experiences at Istanbul Technical University; Environmental, Land and Infrastructures Deparment (DIATI) of the *Politecnico di* Torino in collaboration with the the Institute of Environmental Geology and Geoengineering of the National Research Council (CNR-IGAG), has developed a machine called the Intermediate Linear Cutter Machine (ILCM). In this study, the results obtained from a third round of tests, carried out on marble samples are presented. The variants are a new V-shaped cutter disc and the sample cementation as a way to confine it. These results are compared with a theoretical analysis done following the lines proposed by the Colorado School of Mines.

Chapter 1 Tunnel Boring Machine (TBM)

1.1. Generalities

TBM`s are used for full face excavation according to (Chapman, et al., 2010) "TBMs exist in many different diameters, ranging from microtunnel boring machines with diameters smaller than 1 m to machines for large tunnels, whose diameters are greater than 15 m… One of the general requirements for the use of a TBM is a consistent geology along the route of the tunnel as the different cutting tools are only suitable for a small variation in material characteristics. The combination of different cutting tools on the cutterhead can increase the application of machines to a greater range of ground conditions."

Although TBMs can have different mechanisms for moving through the ground, most have to start outside and hence need a reaction frame to start the drive, in figure 1.1 is shown an example of this kind of mechanism.

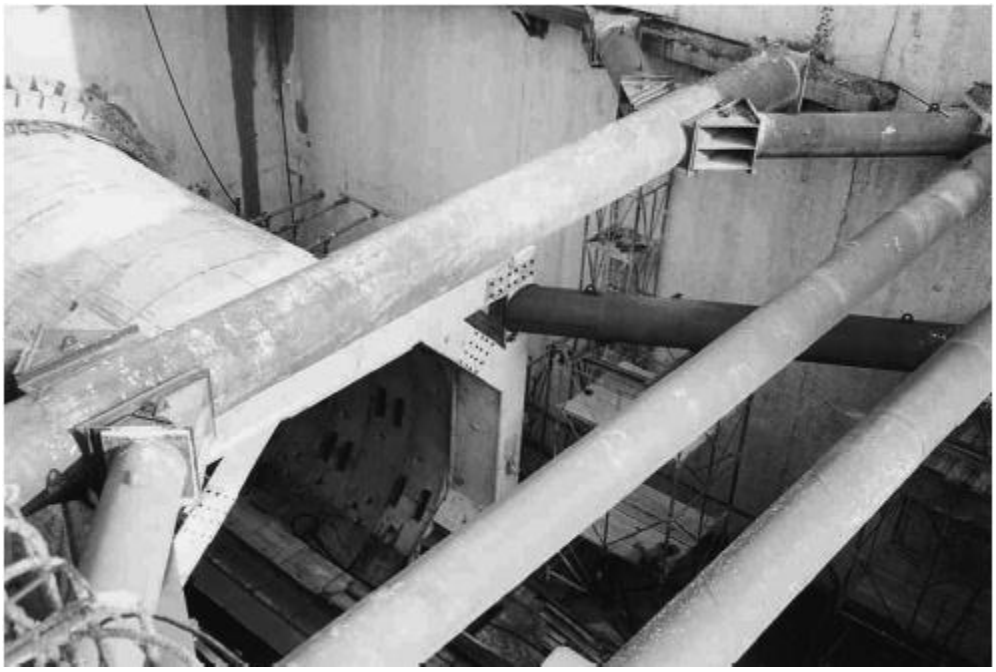

Figure 1-1-Example of reaction frame used to start off a TBM

(Chapman, et al., 2010) also states that "TBMs using segmental lining for the tunnel support need to have a tail seal at the rear end of the shield. As the tunnel segments are erected within the tunnel shield, there is a gap between the segments and the excavated ground. In order to achieve a rigid connection between the ground and the tunnel lining, thus preventing the ground from moving, the gap is injected with cement slurry. The challenge then is to keep the groundwater, soil and cement slurry out of the tunnel shield."

1.2. Tunnel Boring machine in rock

There are various mechanized full face tunneling techniques for hard rock and these depend on the quality of the ground. However, the final decision of which machine type to use always depends on controlling the stability of the ground during construction and the expected quantity of water ingress. It is these factors which dictate the final choice of TBM to be used in hard rock, either a Gripper TBM or a shielded TBM.

Hard rock TBMs comprise four key sections, which make up the complete machine (Maidl *et al.* 2008). These are the *boring section*, consisting of the cutterhead, the *thrust and clamping section*, which is responsible for advancing the machine, the *muck removal section*, which takes care of collecting and removing the excavated material, and the *support section*, where the tunnel support is erected.

1.2.1. Open tunnel boring machines

In stable rock conditions with low water ingress the gripper technique can be utilized (Chapman, et al., 2010). Figure 1-2 shows the principle of the gripper machine technique. The gripper machine locks itself against the ground laterally using 'gripper shoes' to establish the required face pressure. When the machine is locked, the tunnel is advanced by using hydraulic jacks which move the cutterhead forwards by approximately 0.7 to 1.2 m. Thereafter the cutterhead stops. In order for the tail of the machine to move forwards, auxillary supports are erected behind the cutterhead and at the rear of the machine and the gripper shoes are released. Now the hydraulic jacks that advanced the cutterhead can be retracted while the tail of the shield is pulled forwards. A new working cycle can begin when the gripper shoes of the machine are once more engaged.

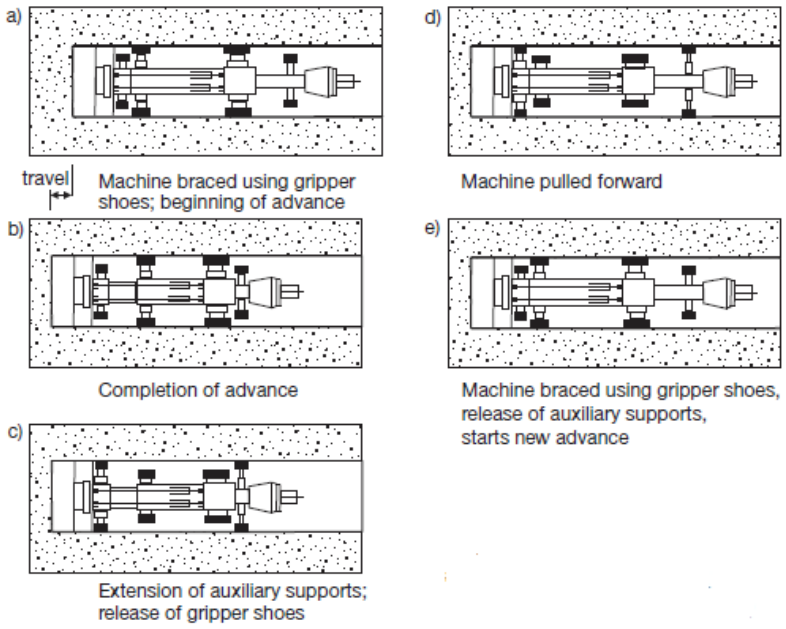

Figure 1-2- Principle of the gripper TBM technique (courtesy of Aker Wirth)

Unlike shielded TBMs, where tunnel support, e.g. segmental lining, is fixed and does not change during tunnel construction, the tunnel support system, when using a Gripper TBM, can vary depending on the ground quality. The appropriate rock support devices can be installed immediately behind the cutterhead. These devices can include anchors, steel arches and sprayed concrete and even segmental linings, as used in conventional tunneling methods. The gripper shoes can be moved hydraulically and can be adapted to the shape of the excavated rock surface. The allowable maximum gripper force is determined by the compressive strength of the rock and is in the range of two to three times the forward thrust

force of the machine (Maidl et al.2008). In figure 1-3 is showed a gripper TBM, also called Open TBM.

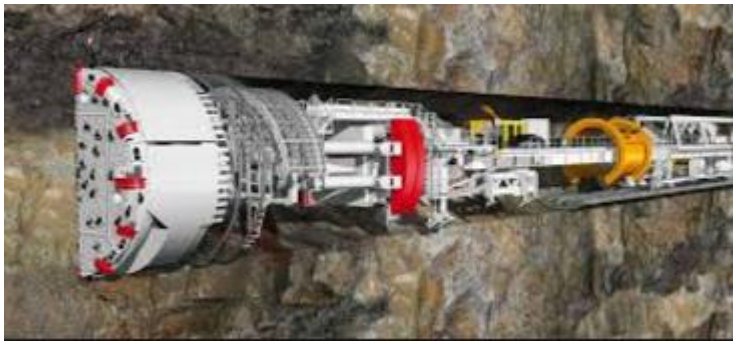

Figure 1-3- Gripper TBM scheme (courtesy of Herrenknetch)

1.2.2. Shielded tunnel boring machine

These kinds of TBMs have an extended shield over the front section of the machine. The shield has the function of supporting the ground and protecting the personnel, thus allowing safe erection of the tunnel lining. There are two basic types of shield TBMs for hard rock available; the single-shield and double-shield.

The single-shield TBM in hard rock, which is showed in figure 1.4, is mainly used in unstable conditions where there is a risk of ground collapse. With these machines, the pushing forces are maintained axially against the installed lining segments. One of the advantages of a single-shield machine is that it can be converted to a closed mode if high groundwater ingress is likely to be encountered.

On the other hand the double-shield machine (or telescopic shield) as it combines the principles of open machines and shielded machines, can be applied to a variety of geological conditions.

The double-shield machine consists of a front shield with cutterhead, as well as a gripper section with gripper shoes, a tail shield and auxiliary thrust jacks. Both parts of the machine are connected by a section called the telescopic shield. The operating principle is based on the gripper shoes pressing against the tunnel wall while excavation and segment installation are performed at the same time; the segment installation takes place at the rear of the whole machine. (Chapman, et al., 2010)

Figure 1-4- Single shield TBM (courtesy of BORETECH Industries)

Figure 1-5- Double shield TBM (courtesy of Robbins)

1.3. TBM performance in hard rock

There are three basics factors which affect the performance of hard rock TBMs: the characteristics of the rock, geometry of the cutter and the design features and capabilities of the TBM (Friant & Ozdemir, 1993). The significant elements of each are listed in the table 1-1.

Table 1-1- TBMs basic performance factors

Rock characteristics	-Unconfined compressive strength -Rock toughness -Fractures and joints
Geometry of the cutter	-Diameter -Blade width

TBM features	-Thrust per cutter available or structurally possible. -Spacing between cutters -Power (torque and rpm) available

A reliable estimation of excavation rates is needed for time planning, cost control and choice of excavation method in order to make tunnel boring economic in comparison with the classical drill and blasting method.

Performance prediction of TBM drives requires the estimation of both *penetration rate* (PR) and *advance rate* (AR). Penetration rate is defined as the distance excavated divided by the operating time during a continuous excavation phase, while advance rate is the actual distance mined and supported divided by the total time and it includes downtimes for TBM maintenance, machine breakdown, and tunnel failure (Alber, 1996).

Simple performance correlations have been developed from data on conventional rock strength testing at the laboratory scale. These equations relate the penetration rate with intact rock parameters like the uniaxial compressive strength, the rock tensile strength or the rock fracture toughness, showing good predictive ability in the case of homogenous low fractured rocks, as the case of the predictive model proposed by the Colorado School of Mines.

In jointed rocks the presence of discontinuities reduces the rock mass strength increasing the rate of penetration for a given TBM thrust (Wanner & Aeberli, 1979). Predictive equations should be based on rock mass properties rather than intact rock strength, for example, relating TBM performance with rock mass strength derived by standard geo-mechanical classifications.

Barton made the most progress in this direction. He proposed an expanded version of his well-known Q-system in which additional rock– machine–rock mass interaction parameters were introduced in order to take into account both the rock conditions and the reaction of TBM to the conditions. Q_{TBM} allows one to estimate TBM penetration and advance rate in a wide range of rock conditions even if, as pointed out by the same author, improvements and corrections are possible by testing new case records.

According to (Friant & Ozdemir, 1993), the fundamental principle governing rock fragmentation efficiency of a hard rock TBM is that system performance improves with the increasing size of cuttings produced. This means that the cutting tools should be arranged and used in the manner which produces the largest size cuttings. In a hard rock TBM this is accomplished by increasing individual cutters loads to attain deeper penetrations into the rock. Deeper penetration, in turn, allows wider cutter spacing, this relation will be explained in detail on chapter 2.

1.4. TBM choosing criteria

Choosing a machine for underground excavation requires accurate studies of some factors:

A. Geological study

Table 1-2- Geological consideration for choosing a TBM

Factor	Influence on the tunnel excavation
Structural features (layer orientation, fails)	Geological fails, where it could be found fragmented rock makes more convenient the use of shielded TBMs.
Stratigraphy features (variations along the alignment)	For heterogeneous lithology, a versatile TBM able to excavate in different abrasiveness, hardness conditions.
Mineralogical composition of rock mass	Cutting discs wear

B. Geotechnical and geo-mechanical studies: establishing the parameters listed on tables 1-3 and 1-4 is also crucial data needed for a proper machine choice.

Table 1-3- In situ tests for choosing a TBM

Test	Parameter	Importance for choosing
Geological and structural analysis	Geo-structural arrangement	First approximation choice of TBM type
Coring surveys	Stratigraphy details	
Drilling surveys	Compactness and fracturing degree	
Geo-electrical surveys	General statigraphy and presence of underground water	
Gravimetry	Voids and uncompressed zones	Tendency of using backfilling
Rock Quality Designation (RQD)	Quality Index	Setting of reinforcement machines in case of Open TBM
Discontinuities features (JRC,JCS, orientation)	Shear resistance of discontinuities	
Piezometry measures	Neutral pressure and underground water static levels	Possible drainage interventions during excavation
Lugeon	Secondary permeability	

Table 1-4- Laboratory test for choosing a TBM

Test	Parameter	Importance for choosing
Uniaxial compression	UCS and elastic parameters (E_t, E_s, υ_t, υ_s)	Estimation of machine parameters like: • Thrust • Torque • Power Cutting tools typology and arrangement on the cutter
Indirect traction (Brasilian test)	Traction resistance (T_o)	
Point load test	Point load resistance (Is_{50})	
Schimidt hammer	Hardness and estimation	

	of UCS	head
Punch test	Punching resistance	
Petrography analysis	Mineralogical composition, texture and internal structure	Type and wear of cutting tools
CERCHAR	Abrasiveness Index (CAI)	Cutting tools comsuption
Sievers'	Drilling index (S_j)	Excavation performance
DROP test	Fragmentation (S_x)	
Knoop	Micro hardness (HK)	

Considering the parameters charted above is extremely important so, during the advancement of a tunnel, changing ground conditions have to be expected and contingency plans must be in place. Traversing fault zones is manageable with TBMs, although with a potentially much reduced advancing speed. Very strong and frequently changing rock conditions can limit the use of a TBM, which is why a homogeneous and consistent ground is preferred. As a result, the investment required in the site investigation is larger than that required for blasting methods, for example, as the knowledge of the ground should be as comprehensive as possible (no gaps in data) because any modification of the machine during tunnel construction is limited.

Wearing caused by abrasive minerals is an essential aspect to take into account, since one of the most important cost considerations for TBMs is the cost of the cutting tools. Not only does the cost of the cutting tools themselves have to be included in the calculation, but also the downtime of the machine during the replacement of deteriorated cutters and the achievable tunnelling speed as this is related to the cutting rate of the bits. The final decision of which machine type to use always depends on controlling the stability of the ground during construction and the expected quantity of water ingress

Chapter 2 Discs as cutting tools

2.1. Generalities

The cutterhead is commonly arranged with cutters which crush or break the rock. The disc cutters are fixed on a rotating bearing and roll in concentric circles on the face when the cutter head turns. Depending on the type of cutter design, there are disc, toothed or button disc cutters and the rock is loaded either continuously or as a point load when the cutter head is pressed against the face as showed in figure 2-1.

There are others TBM cutter as: drag bits, toothed cutters and studded cutters. A drag bit simply gouges out a groove in the rock and is most suitable for soft rocks. The toothed cutter and the studded, suitable for harder rocks, cause failure by creating high stresses at the tip of the teeth or studs of the cutter and breaking out chips of rock between them.

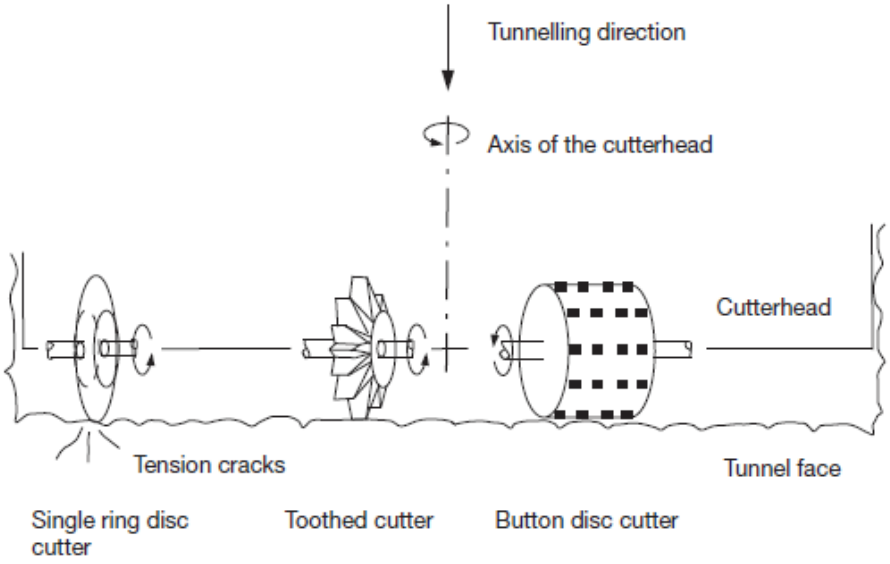

Figure 2-1- Different types of rotating excavation tools for hard rock (disc cutters, toothed cutters and button disc cutters) (Chapman, et al., 2010)

Through a combination of tensile and compressive forces, a local overstressing of the rock develops which results in its failure.

The deterioration of the cutters is mainly dependent on the hardness, fragmentation, abrasivity and ductility of the ground, in some cases the disc wearing could be as critical as it is showed in figure 2-2 The cutters should therefore not only be hard-wearing, but also easily replaceable. It is advantageous to be able to change the cutters from inside the machine in the protected area of the cutter head and not from outside.

The cutters furthest away from the centre of the cutter head are most prone to wear as they cover the longest distance at the face. The requirement for high abrasion resistance is also necessary for the cutter bit fixings and bearings, which also have to be designed for the high forces acting on them. In order to minimize deterioration large diameter roller cutters are used. However, cutters with a diameter of more than 17 inches (432 mm) are on the limit of

what can be manually handled, and with larger diameters it also becomes increasingly difficult to produce a robust construction of the bearings.

Figure 2-2- Worn disc cutter

It is possible with full face machines to drive through rocks with a uniaxial ground strength of 300 MPa or even higher. This is roughly equal to the maximum *in situ* uniaxial tensile strength for ground. This means that in theory there are technically no limits to the use of full face machines. The choice of tunneling using a full face machine is therefore mainly dependent on the costs.

2.2. Cutter disc design and components

The nature of the ground conditions determines the choice and positioning of the excavation tools for the cutterhead. Only if the tools are perfectly matched to the geology, the TBM can achieve high tunnelling performances. However, the respective ground conditions challenge the reliability of the tools in different places. In soft soils, precautions must be taken to stop the disc cutters from getting clogged. During excavation in hard rock, such as granite, the disc cutters must pass the absolute hardness test.

The correct steel mixture and an exact work process are of crucial importance in the materials composition and production of the disc cutters. The high-alloy tool steel of the cutting ring must not only be very hard to resist wear, the material toughness is also an important factor for its lifetime. Excessively brittle steel would lead to early material spalling at the cutting ring during rock bursts, which happen occasionally. According to the manganese composition quantity and the heat treatment process applied to the steel, cutter can be classified in: Standard, Heavy Duty and Extra Heavy Duty, showing the last one a larger ring life but also hard to afford costs.

In addition to the geology, limited space at the cutterhead and the maximum possible load on the disc cutter bearings are also crucial factors when choosing the appropriate tool size. The table 2-1 shows the maximum thrust force values for most used diameter rings types

Table 2-1- Maximun thrust force values.

Diameter (inches)	Thrust force (kN)	Thrust force (ton)
15,5	180	18

17	220	22
19	300	30

The tool is mounted on support rollers fixed to the cutter head by means of appropriate saddles. Inside the supports, there are bearings (figure 2.3), typically cylindrical or, alternatively, conical in shape. Seals retainers avoid dust to enter inside the bearings, which affects the rotational motion around the disc shaft, the disc cutter principal parts are showed in figure 2-4.

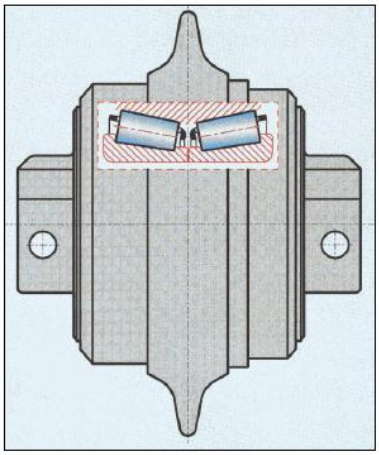

Figure 2-3- Cylindrical bearings of cutter discs (Peila D.,2013)

Figure 2-4- Principal components of cutter discs

Based on the use or the position occupied in the cutter head, cutter discs can be divided basically in three types:

Single disc

Double disc

Twin disc

The single disc is typically used in most applications; the double disc is indicated for soft rocks. In the case of twin discs which are placed on cutterhead periphery, do not rotate perfectly about the axis of the machine: instead these ones have the task of the tunnel over breaking (typically from 3 cm to 5 cm thick) with respect to the cutter head section. On large diameter TBMs are used cutter of 19 and 20 inch (483 mm and 508 mm). While it is

impossible to employ cutters so large on a small micro TBM. In figure 2.5 are showed the commercial diameters for these types of discs, according to the Herrenknecth Company.

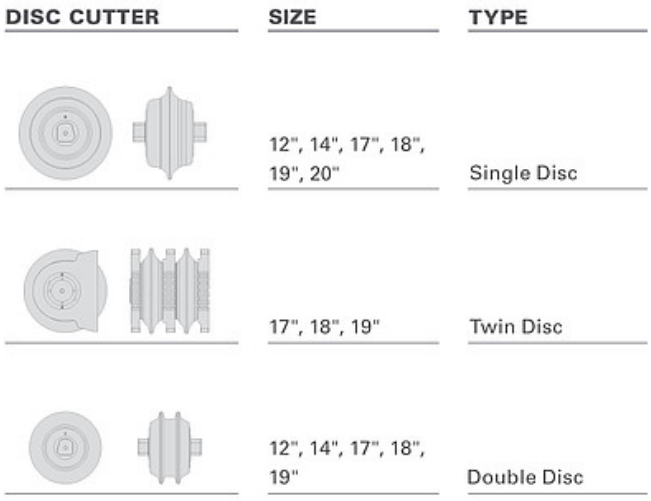

Figure 2-5- The Herrenknecht cutter disc portfolio

The disc cutter rings required to bore extremely hard rock are the most expensive of cutter rings; however, they provide little advantage in weaker rock formations where far less expensive rings will do the job as well. It is important to choose the correct cutter for the machine and the geological conditions in order to get the best balance of cost and risk.

(Roby, et al., 2008) establish that increasing the cutter ring tip width would reduce the contact stress, but also resulted in reduced penetration into the rock for a given cutter load, moving the problem from the cutter ring to the bearing. The lubricants recommended today are quite expensive, but their return on investment is substantial

To increase the wear volume one can increase the cutter ring tip width, the cutter ring diameter or both. Obviously, increases in cutter ring tip width have an adverse effect on cutter ring penetration into the rock. To achieve the same penetration, a cutter ring with an increased tip width would require an increase in thrust, which would have an adverse affect on the cutter bearing, as told before. However, an increase in diameter would have only a negligible effect on cutter load to achieve the same penetration. Essentially, one can increase the "tip length" to provide more wear volume in the ring. The risk of a longer cutter ring tip is the potential for fracturing of the long tip.

2.3. The mechanism of chip formation

Fragmentation or permanent deformation of the rock material using a tool can be achieved in different ways. According to (Innaurato, et al., 2006), chip formation under a tool includes phases such as:

- Rock deformation,
- surface crushing,
- formation of a destruction nucleus,
- squashing and spalling of the rock bounded by the destruction nucleus, and
- free crack propagation towards a free surface.

The nucleus (which may be cylindrical or spherical) acts as a fluid that is subjected to a hydrostatic pressure. If a free surface is sufficiently close to the tool, the formation of chips takes place under a determined load, at a critical value (s/p), where 's' is the spacing of the tools and 'p' the depth of the groove (interactive tools). For s=p ratios larger than the critical value, grooves are too far for interaction to occur, and ineffective chipping takes place independently from any further increase in groove spacing. In figure 2-6 is showed the formation of nucleus and the fractures intersection forming chips.

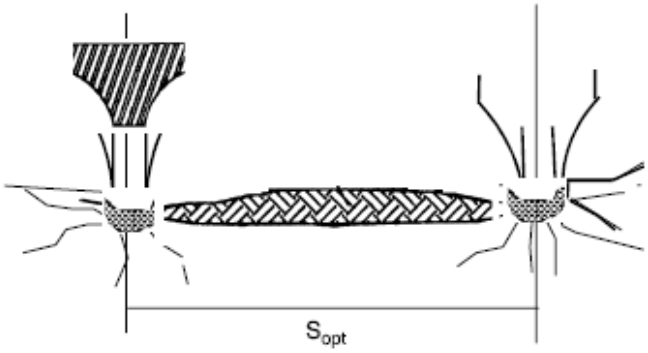

Figure 2-6- Rock destruction mechanism (Innaurato, et al., 2006)

When interaction between grooves is effective, two phases can be distinguished:

1. formation of a groove due to the disc and;
2. propagation of the fractures from a groove to the neighboring grooves.

Both these processes are dynamic rather than static, but most of the authors, for sake of simplicity, generally deal with the static aspect of the phenomena. The fracture propagation is however made easier by some inter-granular defects, the presence of schistosity, inter-strata planes and fissures.

The actual start of one or other failure mechanism depends on the scale of the phenomena involved. The action of a disc towards an already excavated groove is more effective than towards an adjacent disk.

2.3.1. Rock indentation

The indentation phenomenon is produced by the load transmitted from the disc in normal direction to the rock surface in contact with the tool. At this phase it is possible to distinguish three different zones (Figure 2-7) around the force application point of disc:

- Crushed zone
- Plastic zone
- Elastic zone

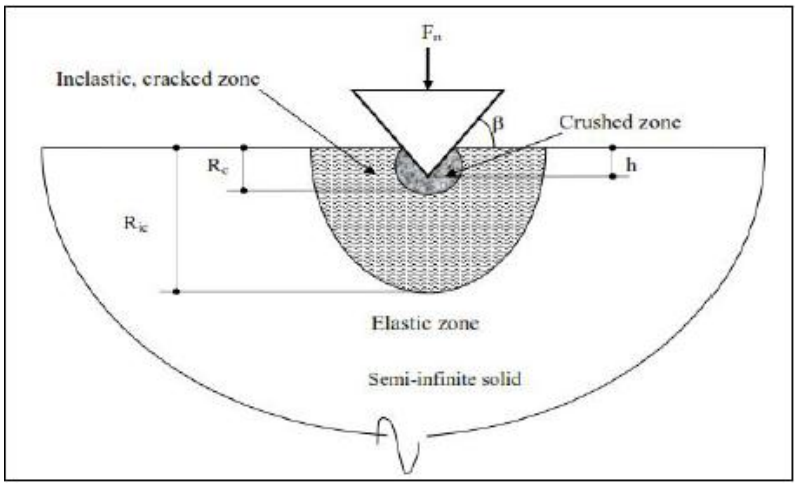

Figure 2-7- Fragmentation mechanism of rock submitted to indentation (Abd Al-jail, 2006)

In figure 2-8 it is assumed the mechanism of rock fragmentation under the disc cutter proposed by Rostami and Ozdemir in 1993.

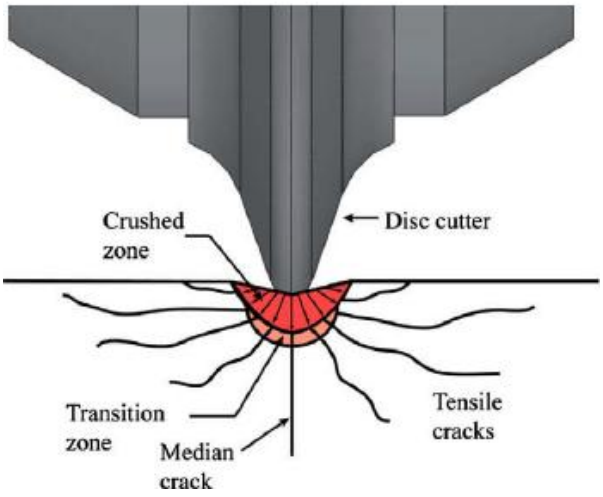

Figure 2-8- Mechanism of rock fragmentation by TBM disc cutters (Cho, et al., 2009)

The crushed zone (spherical or truncated ellipsoid shaped) is located immediately below the tool and is formed by pulverized and granular rock. Initially the load applied zone produces particles of variable size, thanks to the intersection of micro- and macro-fracture expanding from the point of contact between rock and disc.

The plastic mid-range zone is located between the bulb and the intact rock. Here the fractures generated in the crushed zones expand as far as the elastic zone begins Because of plastic condition, presents a stiffness lower than that of the intact rock.

2.3.2. Propagation of fractures

During the second phase, it is initiated the fracture formation between two adjacent grooves. At this stage occurs the chips detach and the reason is the surpassing of bulb pressure over the rock tensile strength that allows the fractures formation, which penetrates radially in the plastic behavior zone.

The chips detachment also depends on the fractures extension from the groove created by the tool to the point where fractures generated by an adjacent disc are able to reach, generating an intersection and therefore a chip. The efficiency of this process depends primarily on the rock characteristics, but also on spacing and penetration of the grooves produced by the cutters. Rock with a poor tensile strength and/or with numerous discontinuities represents the cases where the fractures propagation is the most effective.

2.4. Performance prediction of cutter discs

According to (Gertsch, et al., 2007) exist many performance prediction methodologies focus on predicting the cutting forces. If forces can be predicted for a given set of cutting parameters (spacing, penetration, disc diameter, disc tip width, and rock type), then predicting the rate of advance and cutting energy needed is relatively straightforward. Commonly, after postulating a failure mechanism and cutting geometry, the investigator develops a model that predicts cutting forces which arise from that mechanism. Cutting forces might be caused by the pressure needed under the cutter to cause tensile failure, the forces needed to penetrate the rock sufficiently to create a chip in shear, or the resistance of the rock to penetration defined by the rock compressive strength and the rock cutter contact

Penetration is the essential rock cutting parameter; if there is no penetration, there is no failure. As penetration increases, damage to the rock increases, which manifests itself as increased energy consumption, normal force, and rolling force. Increased damage also implies that deeper penetrations form more and/or larger cuttings. Because of the central role of penetration, many investigators constructed cutting and indentation predictive models that start with penetration. These models considered the normal force to be a function of penetration: the deeper the penetration, the higher the force. One reason why normal force penetration models are popular is that they are simpler to construct than rolling force models. Many of these models consider rolling force to be a function of normal force, which is not unreasonable.

The role of cut spacing in the performance model was either included with some difficulty, or essentially left out. However, these investigators recognized that spacing has an important role to play, because changes in spacing modify the forces acting on a cutter. Several investigators included a theoretical consideration of spacing, (Gertsch, et al., 2007) they postulated that an increase in the width of the chip (i.e., the spacing between the current cut and the last cut) must increase the normal force, because more rock is broken to the side of the cutter. Spacing affects the cut-to-cut interaction; both too narrow and too-wide spacings increase specific energy (SE), as shows figure 2-9.

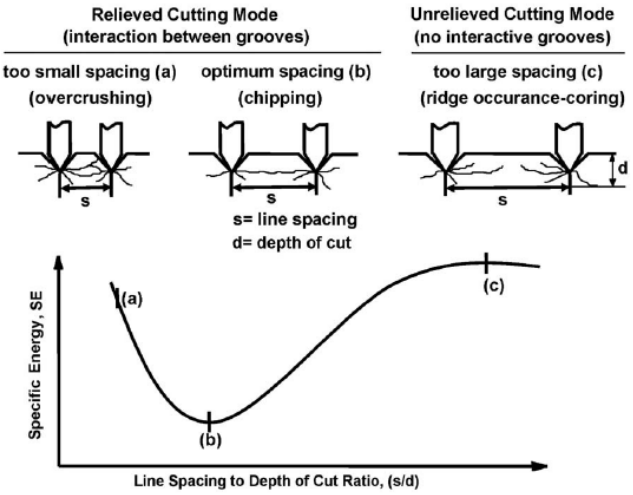

Figure 2-9- Effect of line spacing and depth of cut on specific energy and cutting efficiency. (Copur, 2010)

In Ozdemir's model wide spacings allow larger chips to form, but their formation can only be initiated by deeper penetration. The table 2-2 shows different prediction model for the performance of disc cutters. Therefore, spacing must be viewed in the context of penetration.

In addition to spacing issues, the models experience difficulty modeling and predicting the rolling force. They usually predict that rolling force increases with normal force. An increase in either spacing or penetration would thus increase the normal force and the rolling force would follow. The response of rolling force itself to spacing or penetration has been difficult to address. Further, the normal force-indentation models are quasi-static, but rolling force can only be dynamic.

Table 2-2- Performance prediction models for disc cutting tools

Model	**Normal force predictive basis**	**Spacing and rolling force**
Rostani and Ozdemir Pressure model	Pressure distribution under the cutter and area of cutter contact	-Spacing not modeled directly - Rolling forces predicted by cutting coefficient and normal force
Sanio Tensile failure-cutting pressure model	Normal force must create a pressure bulb sufficient to induce a crack to form a chip	-Spacing a function of the length of a chipping crack -Rolling force a function of normal force, when the resultant force causes zero torque on the cutter
Ozdemir and Miller Shear failure model	Normal force creates a chip in shear	-Spacing controls chip width and shear force -Rolling force related to normal force

Roxborough and Philips Compressive strength failure model	Normal force is a function of rock compressive strength and the contact area of the cutter	-Spacing not considered -Rolling force a function of normal force, such that the resultant force causes zero torque on the cutter -Indentation model only

2.5. Performance models for cutter discs

In general, the models can be divided into two main groups, fully empirical, and theoretical/empirical. The first group is based primarily on data collected in the field and is merely a regression between machine parameters, rock properties, and the penetration rate. A good example of this is the Norwegian (NTH) hard rock diagnostic system and predictor. The other group goes into more detail of the rock cutting process by estimating cutting forces acting on individual cutters to achieve a certain penetration. These models are based on theoretical analysis of the rock fragmentation process with mechanical tools. They are supported by data generated from various types of laboratory tests such as linear cutting test, punch penetration test etc. This group includes the CSM predictor model and some of the models developed by the manufacturers for estimating TBM penetration rate. (Rostami & Ozdemir, 1993).

2.5.1. Fully empirical models

This type of forecasting models was born for correlating laboratory index with the machine parameters, in terms of advancement rate and penetration. Provide empirical equations developed on a theoretical basis of balanced forces or energy conservation. In such models, geometric and stress distributions are simplified, in order to determine corrective coefficients to be apply on parameters determination without the use of databases.

The non-universality of application and the lack of completeness represent the limits. The objective of such methods is to predict the digging performance, correlating between them one or few rock properties with one or few machine parameters, thus not having a complete picture of the contour conditions that influence the penetration of the tools and the advancement of the machine. Then are showed some models proposed by different authors along the years.

2.5.1.1. Graham (1976)

Introduced a model in which the penetration per cutter head revolution is computed as a function of the normal forces per cutter, and the UCS of the rock. This model was applied in this study for the TBM performance in various lithological and structural conditions at different operational thrust per cutter.

$$P = \frac{3940.F_L}{\sigma_{cf}}$$

Where:

F_L= average cutter force (kN)

σ_{cf}= UCS of rock (kN/m^2)

P= penetration per revolution (mm/rev)

2.5.1.2. Farmer and Glossop (1980)

The model allows to derive the disc penetration considering the normal forces on it and the traction strenght of the rock. The method is developed from eight different TBM data, so this is its main limitation. Beside the fact that considers the rock as homogeneous and free of discontinuities and also overlooks the tool geometric characteristics.

$$P = \frac{624.F_L}{\sigma_{tf}}$$

Where:

F_L= average cutter force (kN)

σ_{tf}= traction strength of rock (kN/m^2)

P= penetration per revolution (mm/rev)

Nelson et al (1983)

It is based on the data of four sedimentary rock-excavated tunnels, the formulation is:

$$PR = 10{,}45 - 1{,}19.H_A$$

Where:

PR=penetration rate

HA= hardness estimated by Tarkoy & Hendron (1975)

The authors establish that penetration rate depends always on the cutter head thrust and the rock type. It is also proposed a correlation between the rock hardness and the normal penetration expressed in terms of developed thrust:

$$FPI = 5{,}95 + 0{,}18.H_T$$

$$H_T = H_R.\sqrt{H_A}$$

Where:

FPI= field penetration index (average thrust on cutter and penetration by round ratio) (kN/mm) (lbs/in)

HT= total hardness

HR= Schimdt hammer hardness

2.5.1.3. Bamford (1984)

Penetration rate is derived through a multi linear model according to the Schmidt hammer rock response, total thrust force, NCB index cone indenter and the friction angle:

$$P = 0{,}535.S - 8{,}49 - 0{,}00344.T - 0{,}000823.N + 0{,}00137.\phi$$

Where:

P= penetration rate (m/h);

S=Schimdt hammer rock response;

T= thrust total force (t)

N`= NCB index (N/mm)

ϕ= friction angle

Although a good correlation is obtained, the limits are multiple. First of all, it is based on the data obtained during one single tunnel excavation where it is not considered the dimensions of excavation. Furthermore, just are considered the intact rock properties and few machine parameters.

2.5.1.4. Hughes (1986)

Model inspired on the Graham model. The parameters considered are: average normal force per disc, uniaxial compressive strength of rock and rotation speed of the cutter head. There are also included the number of counterparts tools and the radius of the disc. This formulation is derived from analysis of data of full section machines operating in coal mines. It is possible to determine

$$PR = \frac{6.P^{1.2}.N.h}{\sigma_c^{1.2}.r^{0.6}}$$

$$PW = 28{,}45.D + 9{,}07.D^2$$

Where:

PR= penetration rate (m/h)

P= peripheral cutter force (kN)

N= cutter head rotational speed (rev/s)

h= counterparts cutters

σ_c= uniaxial compressive strength (kN/m^2)

r=cutter radius (m)

PW= power (kW)

D= TBM diameter (m)

2.5.1.5. Barton (2010)

In the Barton predictive formulation of TBM performance an appropriate rock mass quality index (Q_{TBM}) is introduced, in which the state of stress on the tunnel head is taken into account:

$$Q_{TBM} = \frac{RQD_0}{J_n}.\frac{J_r}{J_a}.\frac{J_w}{SRF}.\frac{SIGMA}{(F^{10}/20^9)}.\frac{20}{CLI}.\frac{q}{20}\frac{\sigma_1}{5}$$

Where:

Jn, Jr, Ja, Jw are the Q index parameters assessed for the most favourable TBM advance direction;

SRF is the rating for faulting, for strength/stress ratios and for squezzing or swelling behavior

RQD_0 is measured in the TBM advance direction;

SIGMA is an index related to the rock mass strength that depends on the uniaxial compressive strength in MPa and is expressed by the following equation:

$$SIGMA = 5.\gamma.\sqrt[3]{Q_c}$$

Where:

$$Q_c = Q.\frac{\sigma_c}{100}$$

γ is the rock density (t/m3);

F is the thrust applied on the disc (t)

CLI is the cutters life index according to the test carried out by the Technical University of Trondheim

q is the quartz contents (percentage)

σt (assumed equal to 2.po) takes into account the stress state acting on the tunnel head and is normalized to a depth of 100 m.

The instantaneous speed of the TBM is therefore given by the following equation:

$$\upsilon_{TBM} = 5.(Q_{TBM})^{-0,2}$$

2.5.2. NTH model or Norwegian method

According to (Bruland, 2014) the current model is based on data from 230km of tunnels, partly in very demanding rock conditions. The engineering geology of the tunnels has been carefully mapped and production and cost data have been analysed.

The step by step model estimates:

- Net penetration rate(m/h)
- Cutter life (h/cutter, sm^3/cutter)
- Machine utilization (%)
- Weekly advance rate (m/week)
- Excavation costs (NOK/m)

The prediction model also makes it possible to analyse the effect of variation in one or more factors on penetration rate, machine utilization and excavation costs

The input parameters of this method are listed on table 2-3. they can be considered as rock parameters and machines parameters.

Table 2-3- NTH method input parameters

Rock mass parameters	Machine parameters
Degree of fracturing by fracture class and the angle between the tunnel axis and the planes of weakness	Average cutter thrust
Drillability by the Drilling Rate Index DRI	Average cutter spacing

Abrasiveness by the Cutter Life Index CLI and the quartz content	Cutter spacing
Porosity is also included for some rocks	Cutterhead RPM
-	Installed cutter head power

The rock mass fracturing is by far the most important of the above mentioned rock mass parameters. The estimated penetration rate (m/h) is increased by a factor of five from homogeneous to well fractured rock mass. For homogeneous rock mass, estimated penetration rate will increase by a factor of two from extremely low to extremely high DRI values.

Since the net penetration rate is an important factor for the weekly advance rate, the cutter life and the excavation costs, it is obvious that great efforts should be made to establish a best possible model of the rock mass fracturing for a tunnel project.

On the other hand, the average cutter thrust (kN/cutter) is the most important machine parameter. Hence, the development has concentrated on larger cutter to be able to sustain the required thrust. In hard and homogeneous rock masses, a High Power TBM (483 mm cutters) will typically have a penetration rate (m/h) that is 40-50% higher than that of a standard TBM (432 mm cutters).

2.5.2.1. Net penetration

The basic philosophy of the prediction model is to combine the decisive rock mass parameters into one rock mass boreability parameter, the equivalent fracturing factor (k_{ekv}), and the relevant machine parameters into one machine or cutterhead parameter, the equivalent thrust (M_{ekv})

The equivalent fracturing factor is found by combining:

1. *Rock mass type of systematic fracturing*, estimated with the table showed on figure 2-10.

Fracture Class (Sp=Joints/St=Fissures)	Distance between Planes of Weakness [mm]
0	-
0-I	1600
I-	800
I	400
II	200
III	100
IV	50

Figure 2-10- Fracture classes for systematic fractured rock mass (Bruland, 2014)

2. Rock mass degree of systematic fracturing

3. Angle between planes of weakness and the tunnel axis

$$\alpha = \arcsin(sin\alpha_f . \sin(\alpha_t - \alpha_s))$$

Where:

α_f= dip angle of weakness planes

α_s= strike angle of weakness planes

α_t= tunnel of axis direction

Rock strength (drillability) expressed by DRI

These four factors mentioned above are required for using the abacus of figure 2-11.

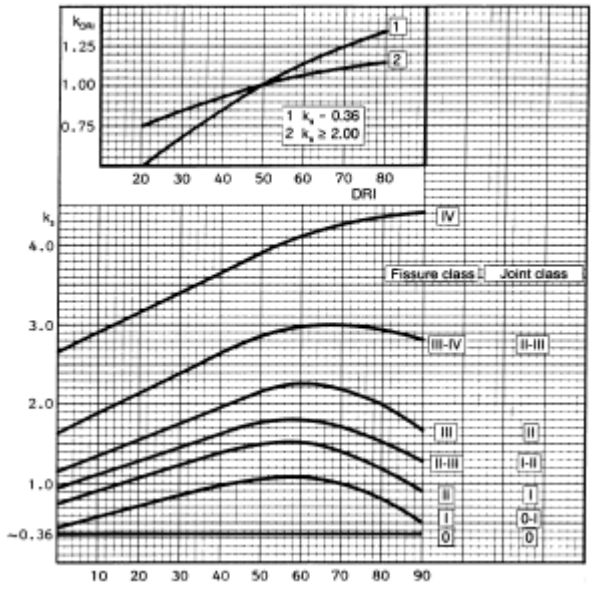

Figure 2-11- Fracturing factor (Bruland, 2014)

The basic penetration is expressed in mm per revolution of the cutterhead. Hence, the decisive machine characteristics are independent of the TBM diameter. The equivalent thrust is expressed as:

$$M_{ekv} = M_B . k_d . k_a$$

Where

M_B= gross average thrust per cutter (not the available thrust capacity of the machine, but the actual thrust (to be) used.

k_d= correction factor for cutter diameter; an indirect expression of the contact area under the cutter.

k_a= correction factor for average cutter spacing

Average cutter spacing is found by dividing the cutterhead radius by the total number of cutters on the cutterhead. The correction factors mentioned above are estimated through the abacus showed on figure 2-12 and figure 2-13 respectively.

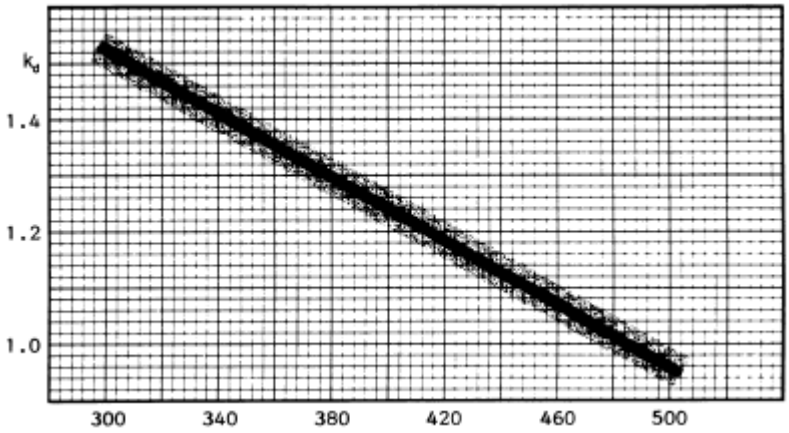

Figure 2-12- Correction factor for cutter diameter (Bruland, 2014)

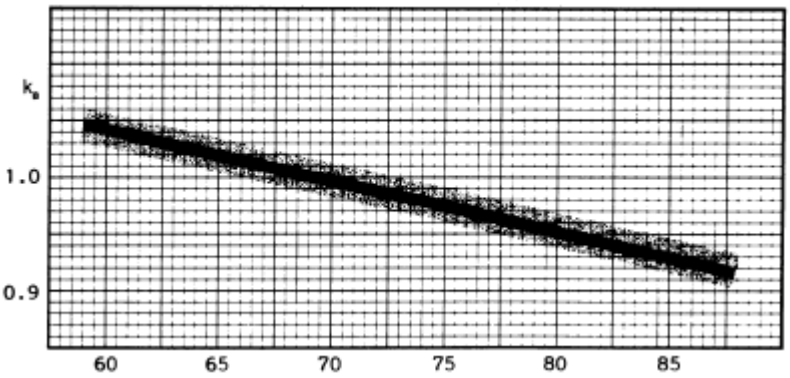

Figure 2-13- Correction factor for average cutter spacing (Bruland, 2014)

The estimated basic penetration rate should be checked with regard to the torque capacity of the cutterhead drive system. The basic penetration obtained in (mm/rev) obtained with the abacus of figure 2-14 can be expressed in (m/h) using the expression:

$$I = i_o . RPM . \frac{60}{1000}$$

Where:

i_o= basic penetration rate

RPM= cutterhead revolutions per minute

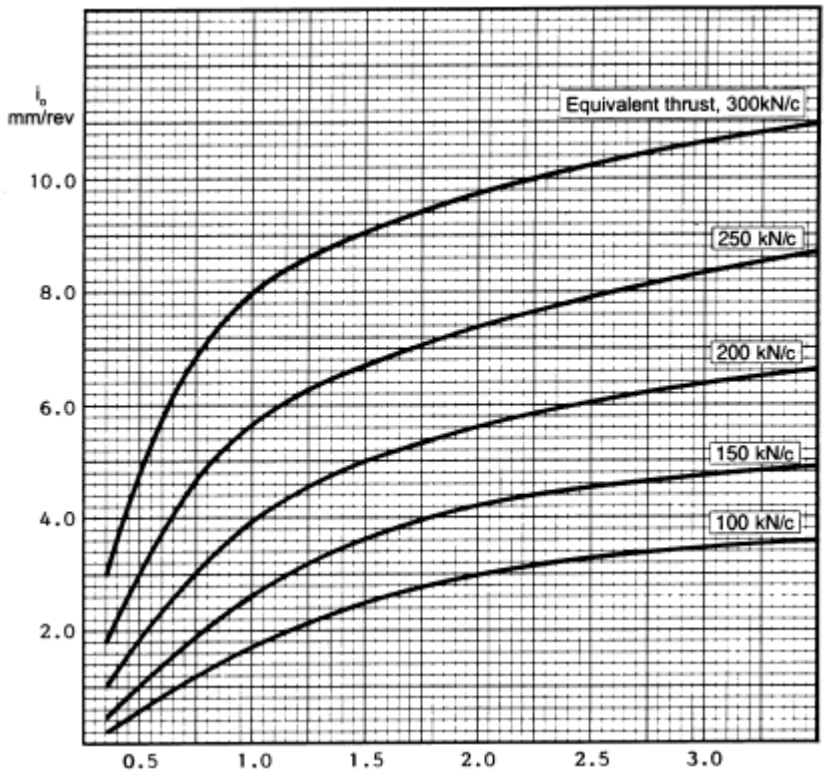

Figure 2-14- Basic penetration rate (Bruland, 2014)

2.5.2.2. Advance rate

(Bruland, 2014) states that "the gross advance rate is given as bored meters per week as an average for a longer period, and depends on net penetration rate, machine utilization and the number of working hours during one week. The machine utilization in net boring time in per cent of total tunneling time". The total tunneling time includes:

- Boring, T_b
- Regripping, T_t
- Cutter charge and inspection, T_c
- Maintenance and services of the TBM, T_{tbm}
- Maintanance and service of the back-up equipment, T_{bak}
- Miscellaneous activities T_a

$$u = \frac{100.T_b}{T_b + T_t + T_c + T_{tbm} + T_{bak} + T_a}$$

$$T_b = \frac{1000}{I}$$

$$T_t = \frac{1000.t_{bak}}{60.I_s}$$

Where:

l_s= stroke length, typically 1.5-2 m

t_{tak}= time per regrip, tipically 4-5 minutes

$$T_c = \frac{1000.t_c}{60.H_h.I}$$

Where:

t_c= time per changed cutter, typically 45-60 minutes

H_h= average cutter ring life

In the figure 2-15 is showed the abacus for the estimation of time consumption for TBM maintenance and services, back up and miscellaneous. For the total tunneling time, extra time must be added for:

- assembly and disassembly of TBM and back-up
- excavation of tip stations, niches, branching, etc
- rock support in zones of poor quality
- time for unexpected rock mass conditions
- complementary rock support and lining
- major tbm breakdowns (e.g. main bearing failure)
- dismantling of tracks, ventilation, cables, etc
- invert clean-up

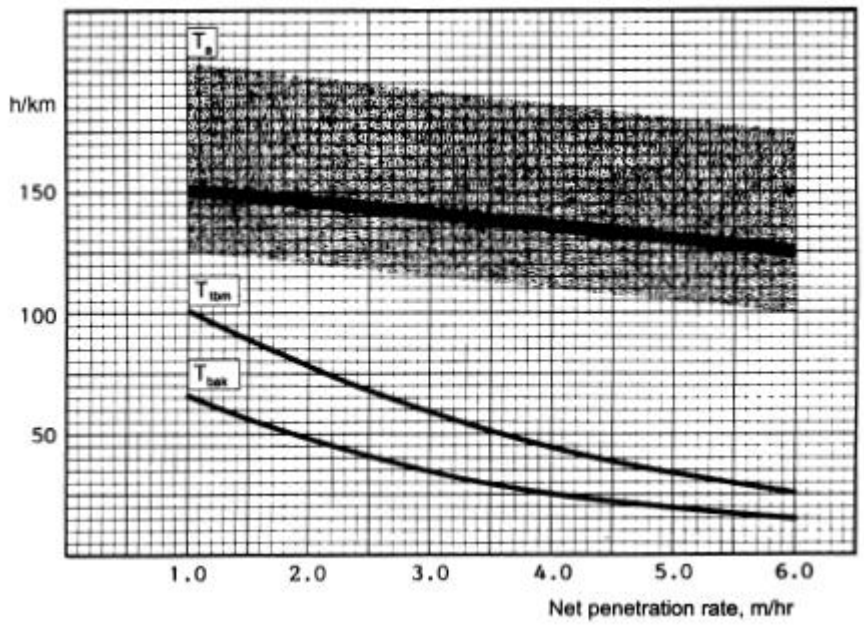

Figure 2-15- Time consumption for TBM, back-up and miscellaneous (Bruland, 2014)

2.5.2.3. Cutter consumption

According to (Bruland, 2014) cutter ring life is mainly dependent on the properties indicated on table 2-4

Table 2-4- Cutter life parameters

Rock Mass Properties	Machine Parameters
Cutter Life Index, CLI Rock content of abrassive minerals,represented by the quartz content	• Cutter diameter • Cutter type and quality • Cutterhead size and shape • Cutterhead rpm • Numbers of cutters

The average life of cutter rings is given by:

$$H_h = \frac{H_0 . k_D . k_q . k_{RPM} . k_N}{N_{tbm}} \left(\frac{h}{cutter}\right)$$

Where:

H_0= basic cutter ring life

k_D= correction factor for TBM diameter

k_q= correction factor for rock quartz content

k_{RPM}= correction factor for cutterhead rpm

k_N= correction factor for number of cutters

N_{tbm}= number of cutters on the cutterhead

$$k_{RPM} = \frac{{}^{50}/_{d_{tbm}}}{RPM}$$

$$k_N = \frac{N_{tbm}}{N_0}$$

Where:

d_{tbm}= TBM diameter

N_0= normal number of cutters on the TBM

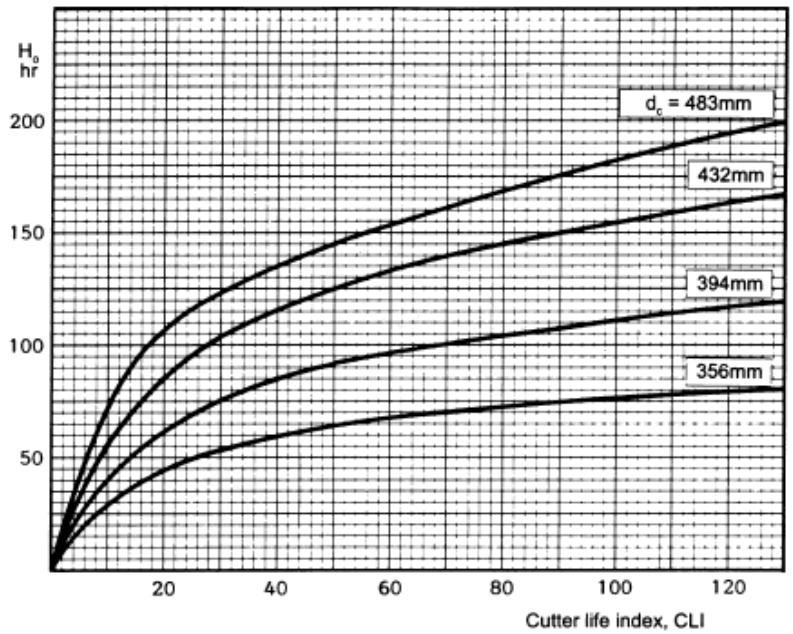

Figure 2-16- Basic ring life (Bruland, 2014)

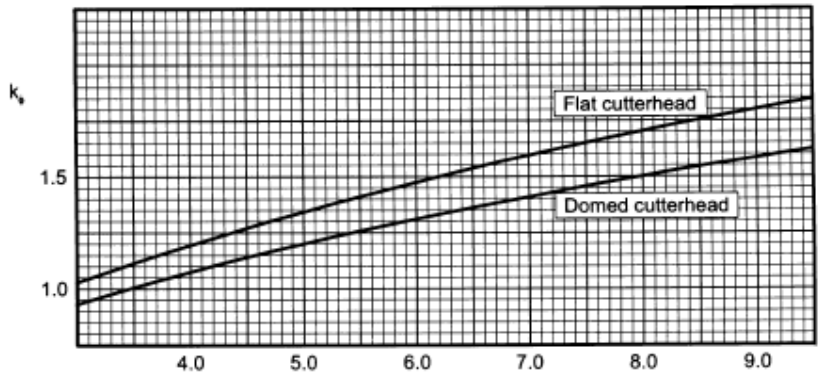

Figure 2-17- Correction factor for TBM diameter and cutterhead shape (Bruland, 2014)

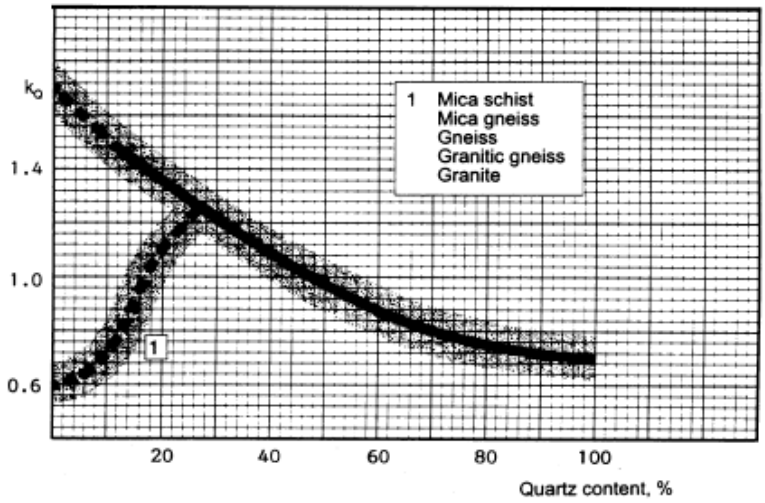

Figure 2-18- Correction factor for quartz content (Bruland, 2014)

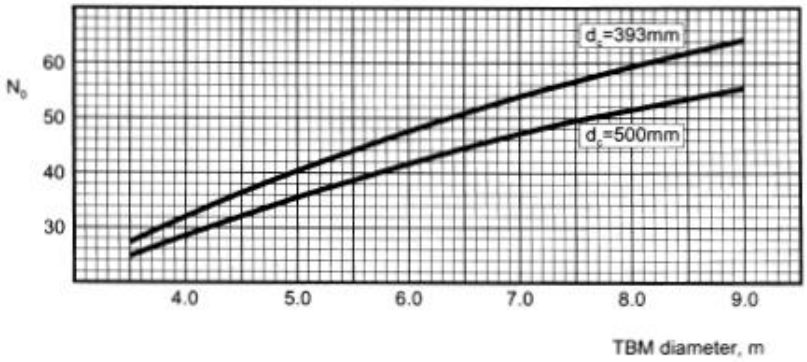

Figure 2-19- Normal number of cutters on a TBM

2.5.3. Theoretical empirical models

2.5.3.1. (Roxborough & Phillips, 1975)

Establish that an elementary analysis of the mechanics of disc operation can be provided by invoking several assumptions and approximations, none of which depart too far from reality, but the introduction of which considerably enhances mathematical simplicity.

Consider, as shown in figure 2-12, a disc of edge angle ϕ and diameter 'D', penetrating a rock surface to a depth 'p' under the action of a force F_T. As penetration increases, so does the chord length of contact 'l' such that

$$l = 2\sqrt{Dp - p^2}$$

It is assumed that the resistance to penetration is essentially compressive and that the force F_T is equivalent to a compressive stress acting over the projected area of disc contact 'A'. A precise determination of the area involves a complex expression, which to a first approximation can be simplified with negligible loss of accuracy to:

$$A = 2.p.l.tan\frac{\phi}{2}$$

The thrust force to affect a penetration 'p' may therefore, be written:

$$F_T = 4.\sigma.tan\frac{\Phi}{2}.\sqrt{D.p^3 - p^4},$$

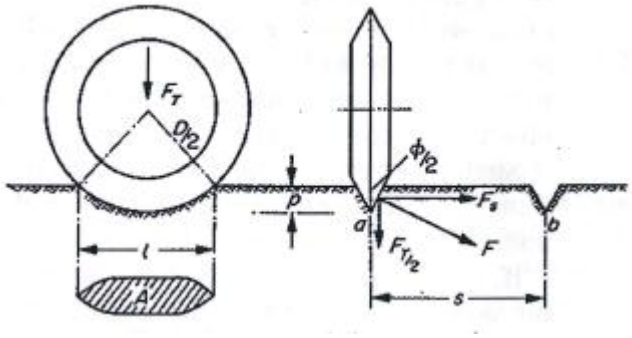

Figure 2-20- Geometry of disc penetration. (Roxborough & Phillips, 1975)

σ represents the compressive strength of the rock. Further analysis depends on the assumption that the value of F_T remains constant when the disc is made to roll.

Figure 2-13 represents a disc under the action of the two principal forces F_T and F_R. If the disc is free rolling and neglecting friction, then the line of action of the resultant R must pass through the centre of rotation to satisfy the zero net torque condition.

If now, R is assumed to act at the centre of the arc of contact 'acb' then for zero torque

$$F_R.\overline{of} = F_T.\overline{oe}$$

so that

$$\frac{F_T}{F_R} = \cot\psi$$

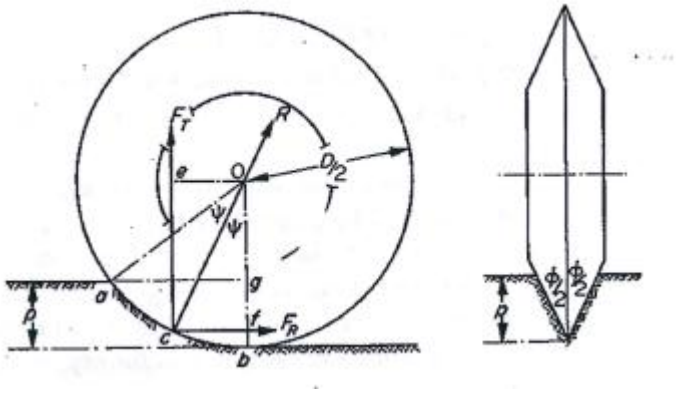

Figure 2-21- Orthogonal forces acting on a disc. (Roxborough & Phillips, 1975)

Finally, the expression that determinate theoretical value of rolling force F_R is:

$$F_R = 4.\sigma.p^3.\tan\frac{\Phi}{2}$$

2.5.3.2. (Rostami & Ozdemir, 1993)

The authors affirms that "…to estimate the forces acting on disc cutter, one should integrate force elements caused by pressure acting on disc cutter in 3D. Since a uniform crushed zone pressure around the cutter tip is assumed to exist, side forces can be neglected, as pressures on both sides of cutter tend to cancel out"

Along the cut, force elements can be integrated to obtain normal and rolling forces. For this purpose, a pressure distribution along the periphery of the disc cutter (within rock-cutter interacting area) as shown in Fig. is assumed to exist. This region of interaction can be specified by angle ϕ that is determined from cutter diameter and penetration as follows.

$$\phi = \cos^{-1}\left(\frac{R-p}{p}\right)$$

Where:

R= cutter radius or D/2

p =penetration

Magnitude of pressure P, at any point is function of the angle θ and the base pressure P'. This function can be written as:

$$P = P'\left(1-\frac{\theta}{\phi}\right)^{\psi}$$

P' =base pressure

θ = angle from the normal to face, ranging from 0 to ϕ

"This function can generate different pressure distributions as power ψ changes. For a linear distribution starting from zero in front of the cutter and maxing to P' under the cutter in a linear fashion with θ, ψ=1 is used (Figure 2-22.). A value of ψ=0 will generate a uniform constant pressure distribution along the cutter penetration edge. In general, increasing ψ will shift the pressure towards the normal line (vertical cutter axis) while decreasing it will shift the pressure forward (Figure 2-23). A negative value for ψ relates to higher pressures in front of the cutter. This shift in pressure in turn reflects the shift in position and angle of the resultant force F_t. In others words, decreased ψ will increased ratio of the rolling to normal forces, which is referred to as the Cutting Coefficient CC or Drag Factor. Normal and rolling forces F_n and F_r, are components of the resultant forces projected on the X and Y axes. The angle of resultant force with normal to the cutting face (or Y axis), β can be determined by estimating cutting coefficient as follows:

$$\beta = \tan^{-1}\left(\frac{F_r}{F_n}\right) = \tan^{-1}(CC)$$

Values of F_n and F_r for the linear distribution, ψ=1, can be estimated as:

$$dF = TPRd\theta = TRP'\left(1-\frac{\theta}{\phi}\right)d\theta$$

$$F_n = F_y = \int_0^{\Phi} dF_y = \int_0^{\Phi} dF.\cos\theta = \frac{TRP'}{\Phi}.(1-\cos\Phi)$$

$$F_r = F_x = \int_0^{\Phi} dF_x = \int_0^{\Phi} dF\sin\theta\,. = \frac{TRP'}{\Phi}.(1-\sin\Phi)$$

Where T= Cutter tip width

Hence the cutting coefficient for the linear distribution can be estimated by:

$$CC = \frac{\Phi - \sin\Phi}{\Phi - \cos\Phi}$$

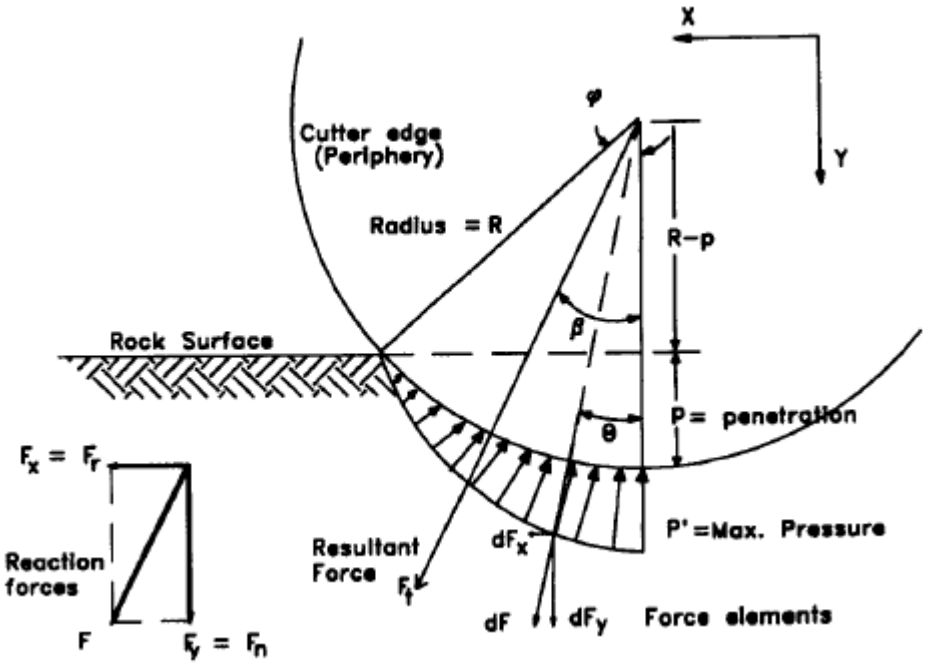

Figure 2-22- Linear pressure distribution along the disc periphery (Rostami & Ozdemir, 1993)

In order to determine cutting forces and CC in a general case with the power function, a new coordinate system is used to simplify calculations as in (Figure 2-23). Using a new positioning angle α, the pressure function changes to:

$$P = P'\left(\frac{\propto}{\Phi}\right)^{\psi}$$

$$dF = TPRd\alpha = TRP'^{\left(\frac{\alpha}{\Phi}\right)^{\psi}} d\alpha = \frac{TRP'}{\Phi} t^{\psi} dt$$

Where: t=a slack variable replacing $\frac{\propto}{\Phi}$

$$F_{y'} = \int_0^{\Phi} dF_{y'} = \int_0^{\Phi} dF.\sin\propto$$

$$F_{x'} = \int_0^{\Phi} dF_{x'} = \int_0^{\Phi} dF.\cos \propto$$

The angle of resultant force is:

$$\gamma = \tan^{-1}\left(\frac{F_{y'}}{F_{x'}}\right)$$

This angle can be related to β in normal coordinates and CC as:

$$CC = \tan\beta = \tan(\Phi - \gamma)$$

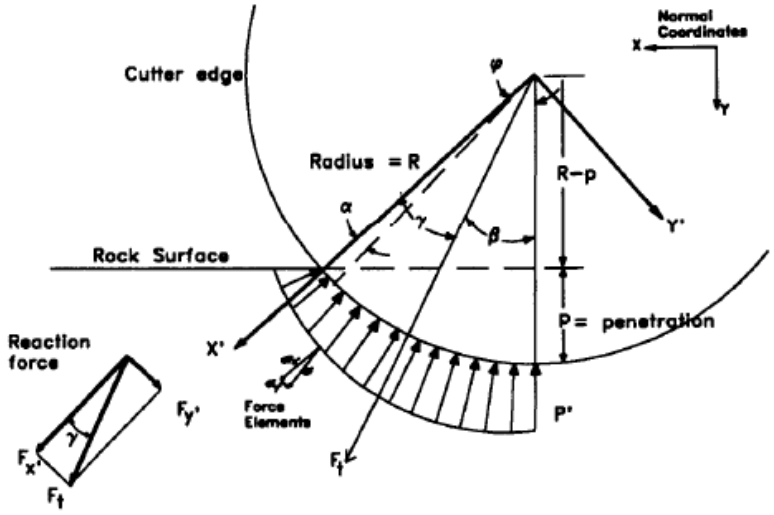

Figure 2-23- General shape of pressure distribution with power function (Rostami & Ozdemir, 1993)

According to the study a linear pressure distribution had been used in most modeling efforts before the time when this research was done but, the data available in that time shows tahta a uniform distribution is closer to reality. In general value of ψ depends of the shape of cutter tip. For V-shaped disc cutters, this value increased around. For CCS and blunt (or worn) cutters, ψ is closer to zero and decreases with increasing tip width. A nominal value of ψ=0 can be used for most cases in which CCS cutters with a tip width of about 12,5 mm (0,5 in) is used. Using this nominal value, the following is obtained:

$$\beta = \frac{\Phi}{2}$$

$$CC = \tan\left(\frac{\Phi}{2}\right)$$

The cutting forces F_n and F_r, are determined by using the total force F_t and CC or β:

$$F_t = \frac{P'RT\Phi}{\psi + 1}$$

$$F_n = F_t.\cos\beta$$

$$F_r = F_t.\sin\beta$$

2.5.4. Cutting force method, CSM model

According to (Rostami, et al., 1996) the basic philosophy behind this method " is to start from the individual cutter forces and determine the overall thrust, torque and power requirement of the entire cutterhead. The estimated values are then compared to the machine installed or available thrust and power, the maximum achievable penetration is obtained. The estimate of the cutting forces may be provided by the actual full size cutting test, which is the most reliable and accurate method, or estimated based on the available formulas…"

Also, the formulas developed for estimation of forces are merely based on the full size cutting tests of different cutters in various rock types. The models use some rock property values such as compressive and tensile strength and combined with cutting geometry and cutter information, they give an estimate of cutting forces, namely normal and rolling forces. Examples of such formulas can be found in (Roxborough & Phillips, 1975). The later one which was developed at the Colorado School of Mines, has been used in various project with a high degree of success. The original formula to estimate the total force (combination of rolling and normal) was as follows:

$$F_t = \frac{P^0 . \phi . R . T}{1 + \psi}$$

Where:

F_t= total of resultance force

R = cutter radius

T = tip width or thickness

ψ = constant for the pressure distribution function (typically 0.2 to-0.2 decreasing with the increased cutter tip width)

ϕ = angle of contact between the rock and cutter disc

$$\phi = \cos^{-1}\left(\frac{R - p}{R}\right)$$

p = penetration per revolution

P^0 = pressure of the crushed zone, estimated from the rock strength and cutting geometry as $P^0 = f(\sigma_c, \sigma_t, S, T, R, p)$

σ_c = uniaxial compressive strength of rock

σ_t =tensile strength of rock

S = spacing between the cuts

The original formula for the pressure of the crushed zone was obtained from the regression analysis of the data available at the time and several formulas were offered in the references. Naturally, these formulas were limited in their application by the range of data that was in the data base. The limits were at the time both in the rock strength properties and cutter size and geometry. Recently, these equations were up dated with cutter sizes from 125-480 mm (5-19 in.) and rock strengths form 30-250 MPa (5-40 ksi) and the range of several other parameters were extended. A new equation for the pressure of the crushed zone was derived by regression analysis of the new database. This equation, being the result of

regression analysis, is not dimensionally correct if a linear or polynomial combination of variables is used. Yet, if a logarithmic regression is used the right combination of parameters may be derived. The results of the later analysis is very close to the right dimension, which is the force over the area (same as pressure or stress). In order to correct the dimensions for the above formula, the pressure formula can be expressed as:

$$P^o = C.\sqrt[3]{\frac{S}{\phi\sqrt{R.T}}\sigma_c^2.\sigma_t}$$

In this formula C is a coefficient (about 2,12) and similar to ϕ (angle), it is dimensionless. The dimension of the overall formula is the same as pressure. In either case, to estimate the normal and rolling forces, the following formulas can be used.

$$F_n = F_t.\cos\frac{\phi}{2} \text{ and } F_r = F_t.\sin\frac{\phi}{2}$$

This is based on the assumption of a uniform pressure distribution (β= ϕ/2 angle of the resultant force from the normal) in the contact area, which has been proved to be true. The following steps to complete the performance prediction with this method are as follows:

1. Calculate the total thrust requirements as: $Th^* = \sum_1^N F_n \approx N.F_n$
2. Calculate torque as: $Tq^* = \sum_1^N F_{ri}.R_i \approx 0{,}3.D.N.F_r$
3. Calculate rotational speed as: $RPM = \frac{V}{\pi.D}$
4. Calculate power requirement of the head $HP^* = \frac{Tq^*.RPM}{5250}$
5. Calculate installed thrust and power by using an efficiency factor η (i.e. $Th=Th^*/\eta$

Where:

D= TBM diameter

N= total number of cutters

V= linear velocity limit of the cutters (i.e. 150 m/min=500 ft/min for 17" cutters)

With all the parameters fixed in a certain rock type using a specific machine, penetration is the only variable that can be increased till one of the limits is reached. In other words, the penetration rate of the machine is the maximum penetration per revolution that can be achieved within the available machine parameters.

2.5.5. Comparison between CSM model an NTH model

(Rostami, et al., 1996) affirms that the rock properties used in the CSM model are very basic common tests provided by most geotechnical reports, including compressive and tensile strength. On the other hand, inputs to the NTH model consists of the indices related to the same rock strength parameters but tested and measured in term of a special indices.

Also, for cutter life estimates, CSM model utilizes the Cerchar Abrasivity Index (CAI) whereas NTH model uses specialized abrasiveness value (AV). The authors establish the interrelation between these factors.

The CSM model can generate a thrust-torque-penetration relationship for a certain machine, from which the penetration rate be estimated. The NTH model, similarly, can estimate the penetration rate for a given level of machine thrust. As shows figure 2-22, both models use standard utilization factors to estimate the advance rate.

The two prediction models have been compared several times with the results being very close to each other. Specifically, in intact rock where boreability is not affected by joints and discontinuities the results are almost one to one.

	CSM Model		NTH Model	
	Parameter	Units*	Parameter	Units**
Input	Cutter Radius	(in)	Fracturing	Classes (0-IV)
	Tip Width	(in)	Brittleness	S_{20} Index
	Spacing	(in)	Drillability	Sievers' J Index
	Penetration	(in)	Abrasiveness	AV index
	Rock UCS	(psi)	Porosity	%
	Tensile strength	(psi)	Cutter Dia.	(mm)
	Existing TBM Diameter	(ft)	Cutter Load	(kN)
	RPM	rev/min	Spacing	(mm)
	Num. of cutters	#		
	Thrust	(lbs)	Machine's	
	Torque	(ft-lbs)	Diameter	(m)
	Power	(hp)		
Output	Cutting Forces	(lbs)	Num. of cutters	#
	Normal-Thrust	(lbs)	RPM	rev/min
	Rolling / Torque	(lbs/ ft-lbs)	Thrust	(Ton)
	Power	(hp)	Power	(kW)
	Basic Penetration	(in/rev)	Basic Penetration	(mm/rev)
	Rate of Penet.	(ft/hr)	Rate of Penet.	(m/hr)
			Torque	(kN-m)
	Head Balance	force/moments		
	Machine spec.'s	(th, tq, hp, etc.)	Utilization	%
	Perform. Curve	Graph (rop-vs-th tq-vs-th)	Advance Rate	(m/day)
			Cutter Life	(hr/cutter)
	Utilization	%		
	Advance rate	(ft/day)		
	Cutter Life	(hr/cutter)		

* Proper conversion in formulas and constant required for Metric system.

** Special tests and indices at NTH

Figure 2-24 Table of input and outputs of the two models (Rostami, et al., 1996)

Chapter 3 Linear cutting machine

The LCM, which was originally developed by the CSM, has been actively used to design the TBM cutterheads for over 20 years in four countries such as the United States, the United Kingdom, Japan and Turkey. The biggest advantage of the LCM is that the design parameters such as cutter spacing, cutter penetration, cutter thrust and cutting speed can be controlled. Moreover, it was reported that the size effect could be eliminated in the linear cutting test (Nilsen & Ozdemir, 1993)

LCM is composed by several parts as it is observed in (Figure 3-1), research tests by (Chang, et al., 2006) were developed with a LCM which have three moving parts, including:

1. Part controlling cutter spacing conditions;
2. Cutting velocity controlled part and;
3. Servo controlled hydraulic actuator simulating cutter thrust.

Three-directional component of loads acting on a cutter can be measured simultaneously by a three-directional load cell directly attached to the cutter housing part.

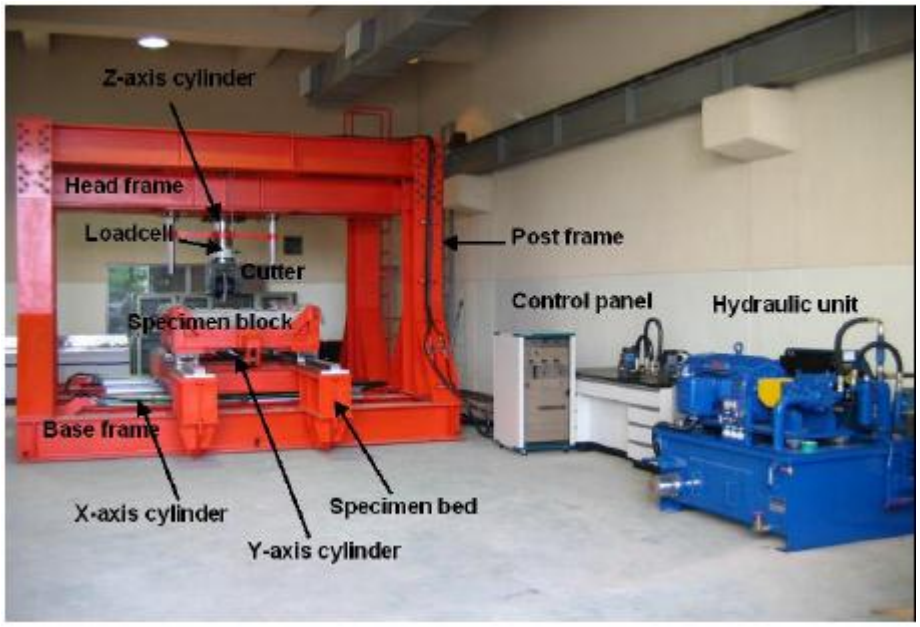

Figure 3-1- Overview of the Linear Cutting Machine (Chang, et al., 2006)

The cutting forces are measured in three directions (normal, rolling, and side; Figure 3-2) while the cutter was forced through the surface of the rock sample at a preset penetration depth for each individual cutter spacing. The linear cutting machine possesses sufficient stiffness to isolate the response of the cutter to the rock from the response of the cutting machine itself. (Gertsch, et al., 2007).

From the measured cutting forces, several parameters are calculated which are commonly used in performance prediction and analysis. These are going to be discussed in the next sections.

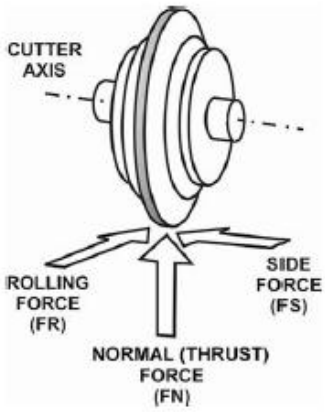

Figure 3-2 Three components of forces acting on a disc cutter. (Balci, 2008)

3.1. Full scale linear cutting test

Full-scale testing minimizes the uncertainties of scaling and any unusual rock cutting behavior not reflected in its physical properties. The rig can accommodate block rock samples up to 1.0 x0.7 x 0.7 m size. A high quality aircraft aluminum block equipped with strain gauges is used as a dynamometer to record thrust forces up to 500 kN. A data acquisition system is used to record the cutter forces in three perpendicular directions. The data acquisition card includes eight independent channels and monitors the excitation voltage ranging from 0 to 10 V. The hydraulic cylinders can move the sample box in which the rock sample is cast in concrete to eliminate pre-failure of the specimen. The cutter is fixed with a tool holder directly to the dynamometer. The depth of cut is adjusted with hydraulic cylinders. However, the depth of cut is kept constant using a mechanical device to fix the adjusted depth of cut, which is measured with a depth gauge, at each cut. (Balci, 2008). In figure Figure 3-3 is showed another schematic view of the full scale rock cutting rig.

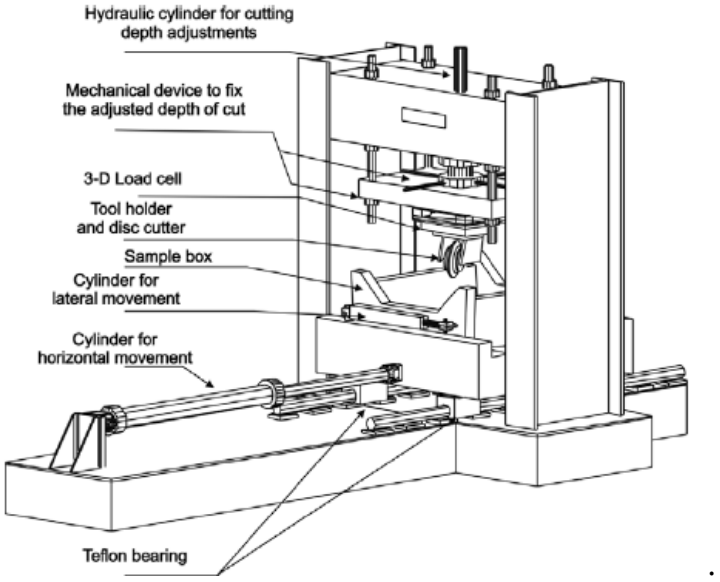

Figure 3-3- Full scale rock cutting rig. (Balci, 2008)

The normal force (the average force required to be applied to the perpendicular direction of rolling, to maintain the disc at the prescribed level of penetration) recorded by the LCM is used to calculate thrust requirement of the machine. This is important to ensure that the machine is able to provide the necessary thrust, so the cutters can effectively penetrate the rock.

The rolling force (the average force required to be applied in the direction of cutting to cause the disc to roll at the prescribed level of penetration) recorded during LCM testing is used to calculate the torque and power requirements for excavating the rock. The rolling force is directly related to the torque requirement of an excavator, and is also used to calculate the specific energy requirement. The side force may be used along with normal and rolling force to balance the cutterhead design.

According to (Balci & Bilgin, 2007) the independent linear cutting test variables consist of three major variables:

- rock type;
- depth of cut; and
- cutter spacing.

The dependent variables are:

- mean and maximum cutter forces (rolling and normal forces);
- yield; and
- specific energy values.

The constant variables through the testing program are:

- cutting sequence;
- attack angle;
- cutting speed;
- skew angle;
- tilt angle;
- cutter type; and
- data sampling rate.

During the execution of this test, two cutting types can be performed, (Balci & Bilgin, 2007) explains that in the case of unrelieved cutting there is no interaction between cutting grooves (Figure 3-4). On the other hand, for relieved cutting there should be interaction between grooves (Figure 3-5).

The initial linear cutting tests are carried out in unrelieved cutting mode to find out the variation of specific energy with the depth of cut. This helps to find out the optimum depth of cut value (d_{opt}) at which the relieved cutting tests are usually performed for determination of optimum specific energy and cut spacing at which the machine excavates the rock with the most energy-efficient manner

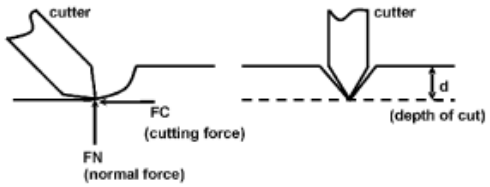

Figure 3-4- Unrelieved cutting mode (no interactive grooves). (Balci & Bilgin, 2007)

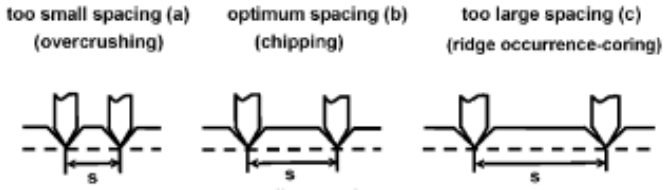

Figure 3-5- Relieved cutting mode at different cut spacing. (Balci & Bilgin, 2007)

The individual cutters on a TBM always operate on a rock surface damaged from the previous pass of the cutters. A pass is defined as a group of cuts at the preset spacing and penetration across the width of the sample. This situation is simulated in the laboratory by cutting several passes with a disc cutter before data recording, which is called ‘‘surface conditioning”. After conditioning, one or two passes (layers) of unrelieved cuts, which means no interaction between the cutting grooves, are performed by cutting over the every other cut lines. After unrelieved cuts completed, at least two passes of conditioning cuts are performed and then relieved cuts, there is interaction between cutting grooves, are performed by cutting over the each cut lines. A schematic drawing explaining the nomenclature is presented in Figure 3-6.

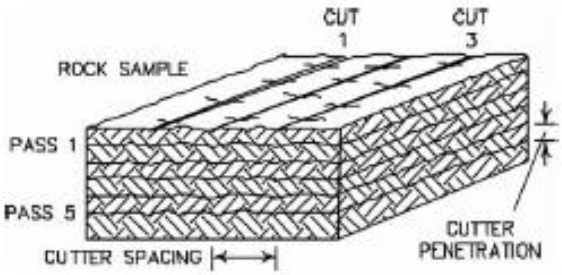

Figure 3-6- Schematic of a LCM sample and nomenclature (Balci, 2008).

From the measure of cutting forces, some parameters can be calculated and therefore used for the final scope, performance and prediction analysis.

3.1.1. Specific energy

It is defined as the amount of energy required to excavate a unit volume of rock. Using the specific energy (kWh/m^3), achievable production rates are calculated for a machine with a known horsepower available on the cutterhead. (Balci, 2008)

Early studies carried out by (Balci & Bilgin, 2007) establish that the specific energy is calculated as follows:

$$SE = \frac{F_R}{Q}$$

Where:

$SE =$ specific energy (MJ/m^3)

$F_r =$ rolling force (kN)

$Q =$ yield per unit length of cut (m^3/km)

(Chang, et al., 2006) estipulate an analogous equation of specific energy based on the cutting volume, as follows.

$$SE = \frac{F_r . D}{V}$$

Where:

D =cutting distance

P =penetration depth

S =cutter spacing

3.1.2. Net cutting rate

Also called instantaneous cutting rate (ICR), predicts the rock volume excavated in an interval of time. For estimating this parameter is possible to use the specific energy method. This method uses machine installed power, total system efficiency and the specific energy required for cutting a particular rock type with a certain type of tool (Rostami, et al., 1994)

$$ICR = k . \frac{P}{SE_{opt}}$$

Where:

ICR =net cutting rate (m^3/h)

P =power consumed in optimum conditions (kW)

k =energy transfer ratio from cutterhead to tunnel face, usually taken as 0,85-0,90 for TBM.

SE_{opt} =optimun specific energy (kWh/m$^{3)}$

The predicted net cutting rate by using the expression mentioned above is valid for competent rock conditions and does not include the effect of rock mass properties (Bilgin, et al., 2005).

3.1.3. Cutting coefficient CC

It is the ratio of the rolling force to the normal force, expressed as a percent. This is considered an indicator of the amount of torque needed for a given amount of thrust; the higher the CC, the higher the torque needed by the tunnel boring machine. It also relates the rolling force to the normal force (Gertsch, et al., 2007)

The same authors affirm that if the relationship is consistent, knowing a rock's CC would allow performance models to readily predict rolling force after normal force is determined.

Since some investigators start by predicting normal force, a predictable CC would be a means to predict the rolling force.

3.2. ILCM at “Politecnico di Torino”

3.2.1. Generalities

Currently, the ILCM is used at few research centers such as: Colorado School of Mines (CSM), the Korea Institute of Construction Technology (KICT) and the Istanbul Technical University, in which was set up in 1996 with the collaboration of the CSM.

From 2010, also the Environmental Engineering Land and Infrastructure Department, (DIATI) of the Polytechnic of Turin in collaboration with the Institute of Environmental Geology and the National Researching Geoengineering Council (CNR-IGAG), it is provided with a Intermediate Linear Cutting Machine.

This ILCM allows to conduct the Linear Cutting Test by mounting different types of tool and also to insert them coupled. The variation on the position of the transversal beam in regard to the machine support plane can be set up to 1525, 1815 and 2110 mm. Therefore it is possible the installation of the whole range of disc cutter available on market, from mini-discs up to 19-inch ones. In Figure 3-7 and Figure 3-8 are represented schemes of the ILCM (Rispoli, 2013).

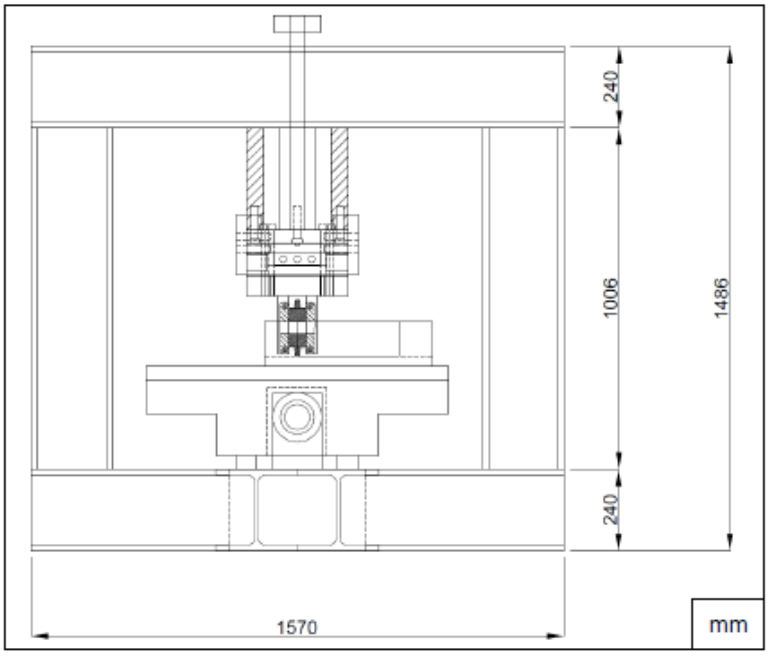

Figure 3-7- Frontal view (Rispoli, 2013)

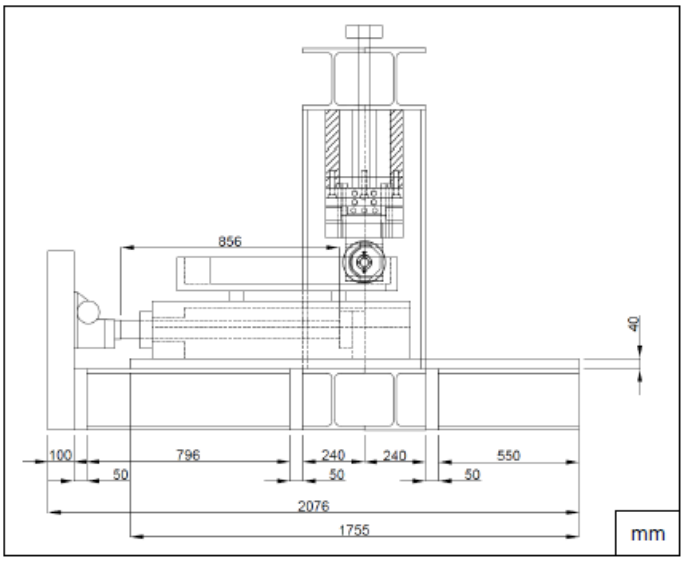

Figure 3-8- Transversal view (Rispoli, 2013)

3.2.2. Components

The principal ILCM components, as showed in Figure 3-9, are:

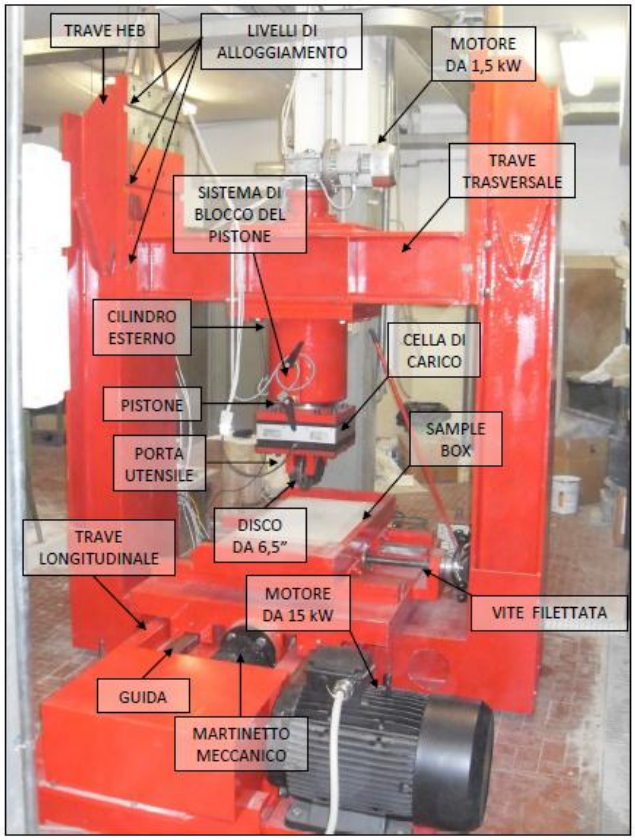

Figure 3-9- ILCM at "Politecnico di torino". (Rispoli, 2013)

- a solid steel frame portal of 2225 x 1810 mm format by a solid steel frame It is formed by two HEB beams coupled (240mm);

- a longitudinal beam on which two polizene self-lubricating guides are installed (Sintered polyethylene of high density at low pressure). The length is equal to 1755 mm;
- a transverse beam having a length of 1245 mm, which can be housed on one of the three fixed levels and on which is mounted the outer cylinder (Figure 3-10).

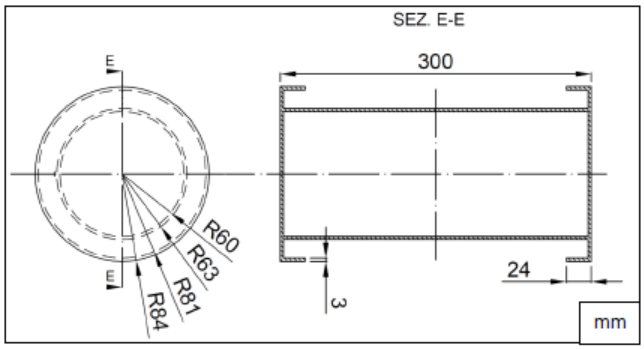

Figure 3-10-Outer cylinder section (Rispoli, 2013)

- a piston on which is installed the load cell and the tool holder. Inside of it there is a endless screw that adjusts the vertical translation with a stroke of 300 mm;
- a 960 x 495 mm stainless steel sample box where can be accommodated a rock sample with maximum dimensions of 890 x 470 mm. The sample can be move horizontally moved with a threaded screw;
- a direct start engine (1.5 kW) with reverse and peak absorption of about 4 A, which allows the vertical movement through the piston endless screw;
- a direct start three-phase asynchronous engine (15 kW) with reverse and a peak current of about 30 A, which allows the longitudinal movement through the two metal rails;
- one mechanic jack type SEP 200, a rotary screw TPN 65x12 mm, completely on B14 bronze outer spiral, with a nominal capacity of 200 kN and useful stroke of 800 mm. Reduction ratio of 1/24, able to move the sample-boxes at a speed of about 12.5 mm/s;
- a load triaxial cell (Figure 3-11) with capacity up to 20 t in the Z direction and 10 t in the X and Y.
- a 6.5 in steel disc tool, reinforced with Carbide Tungsten "Widia";
- a transducer of position made by DSPM Industrial, powered with 12 V. Range of 2 m and sensitivity of 0.48781 mV / mm. Used for the sample box horizontal displacement measurement;
- a position transducer made by Kubler, powered with 12 V. Range of 2 m and 0.1 mm sensitivity. Used for measurement of the piston vertical displacement.

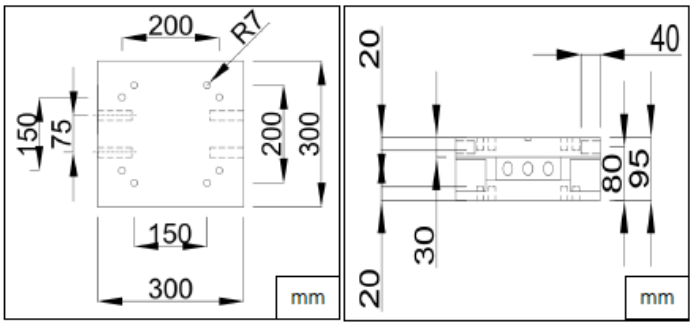

Figure 3-11- Plant and transversal view of Triaxial load cell (Rispoli, 2013)

The machine function principle contemplates three types of movement:

1. Sample box longitudinal movement along the guide rails started by the 15 kW engine through the mechanic jack.
2. Piston vertical movement activated by the 1,5 kW and transferred to the tool holder.
3. Manually activated transversal movement of sample box through the knob that adjusts the threaded screw.

The vertical and transversal movements allow to set up respectively, penetration depth and the desired cutting spacing. These parameters are fixed before starting the test. During the test there is only the longitudinal movement that allows the disk to reach the contact with the rock. The piston therefore, it has not only the function of providing the vertical motion, but also maintaining the desired penetration depth. The exchanged disc-rock forces are measured by the load triaxial cell between the piston base and the tool holder.

During the test, the piston is fixed through the clamping system, composed of a sled forced by two screws against the piston outer wall. This allows the efforts transfer required during the tool-rock contact. The tightening operation also ensure to read the correct force to which the load cell is subjected.

The engine motors supply is provided by an 400 V electric panel (Figure 3-12) which allows two motion modes: automatic and manual. Does also exist a mobile command for remote controlling of the engines.

Electrical panel also has the feature of viewing, the real time electrical absorption of engines, thanks to a double-setpoint controller ATR121. With this device it is possible, during the test, to highlight the based time trend of energy absorption during the rock cutting, and determine the existence of any additional correlations with other machine acquirable test parameters

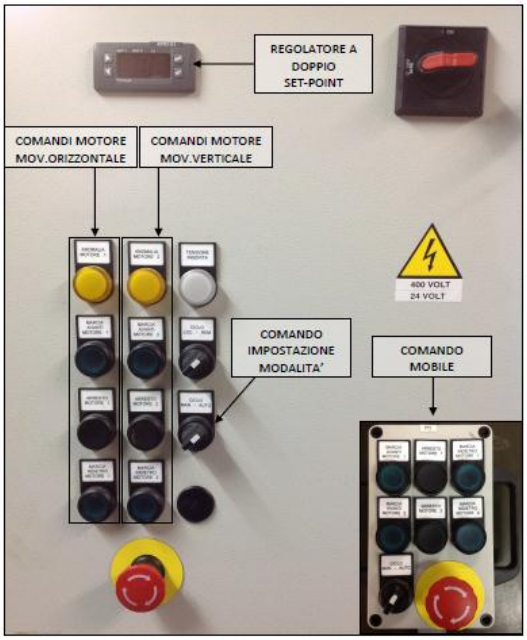

Figure 3-12- Electrical power panel (Rispoli, 2013)

3.2.3. Data Acquisition System

The data acquired with this ILCM is:

- Three channels for the triaxial load cell referred to: normal force, rolling force and side forces.
- One channel for the position transducer relative to the sample box horizontal motion (Figure 3-13)
- One channel for the position LVDT transducer relative to the piston vertical motion (Figure 3-13)

Figure 3-13-Transducers for horizontal and vertical motion. (Rispoli, 2013)

The measurement just named is transmitted by the transducers to an electronic measuring system (Spider8) developed by HBM .This one is provided with 8 channels and has the function of digitalize the data obtained during the test. Then, the data values are visualized on the computer with Catman software, also developed by the same test and measurement house. Later the employment of Microsoft Excel is essential for treatment data.

3.2.4. Calibration System

The output signal from the triaxial load cell is converted to return values acquired in kg_f. Initially the force values returned by the acquisition system were expressed in kg_f; then an appropriate conversion was implemented to obtain values expressed in kN, as the International System of units (Rispoli, 2013). The conversion expression are:

$$kg_{(x)} = \frac{(Volt.x - offset.x) * F.S._{(x)}}{V_{alim} * f.c\ (x) * f.a.} * 1000$$

$$kg_{(y)} = \frac{(Volt.y - offset.y) * F.S._{(y)}}{V_{alim} * f.c\ (y) * f.a.} * 1000$$

$$kg_{(z)} = \frac{(Volt.z - offset.z) * F.S._{(z)}}{V_{alim} * f.c\ (z) * f.a.} * 1000$$

Where:

kg= returned value in kg_f from 3 channels (x,y,z)

$Volt$ =volt value acquired

$offset$ =slipping in volt applied to the data acquired on calibration phase

$F.S.$= triaxial load cell full-scale in kg_f, (10.000 kg_f for X axis and 20.000kg_f for Y and Z axis)

V_{alim} = electrical tension which powers the cell (equal to 5 V)

$f.c$ = corrective factor for each X,Y,Z axis channel (equal to 1,846-1,827-1,517, respectively)

$f.a.$= amplification factor (equal to 64)

Then (Rispoli, 2013) affirms that the position transducer (wire potentiometer) calibration is obtained comparing the detected signal with the one obtained through a mechanical transducer. The conversion expressions verified are as follows:

$$mm_{(h)} = \frac{(Volt.h - offset.h)}{V_{alim} * f.c\ (v)} * 1000$$

$$mm_{(v)} = \frac{(Volt.v - offset.v)}{V_{alim} * f.c\ (v)} * 1000$$

Where:

mm= returned value in mm from transducers

$Volt$ =volt value acquired

$offset$ =slipping in volt applied to the data acquired on calibration phase

V_{alim} = electrical tension which powers the cell (equal to 12 V)

$f.c =$ corrective factor; 0,48681 mV/V for horizontal transducer and 1,014 mV/V for the vertical one.

3.2.5. Signals

(Rispoli, 2013) in order to determine the output data reliability during LCM tests has evaluated the signals obtained from each measurement channel. Is has been done a comparison between the detected signal without any processing and the filtered signal. The data was obtained with the machine stopped and with no contact with rock.

3.2.5.1. Side forces

The not filtered signal is in a range between +500 kg and -400 kg. After filtering the range get reduces around 5 times, the difference is clearly observed in Figure 3-14. The mean values are 24,4 kg_f and 25,6 kg_f, respectively. The author affirms that the values gap is due to the processing data mobile mean, which take into account the variation detected in a fixed set of values preceding the single data provided.

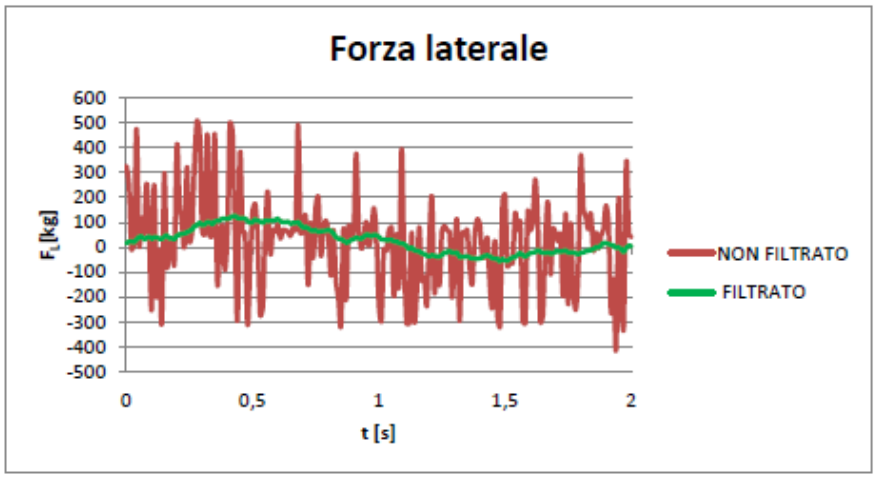

Figure 3-14- Side forces comparison signals. (Rispoli, 2013)

3.2.5.2. Rolling forces

In this case the not filtered signal interval range goes from +150 kg_f to -100 kg_f, while the filtered is between +50 kg_f and -10 kg_f (Figure 3-15). The mean value is 20 kg_f and the variability ±30 kg. Rispoli assure that this result is acceptable since the magnitude of rolling forces is greater than these statistical values, from 500 kg_f to 1200 kg_f. The mean filtered data was equal to 23,5 kg_f while the not filtered 26,3 kg_f.

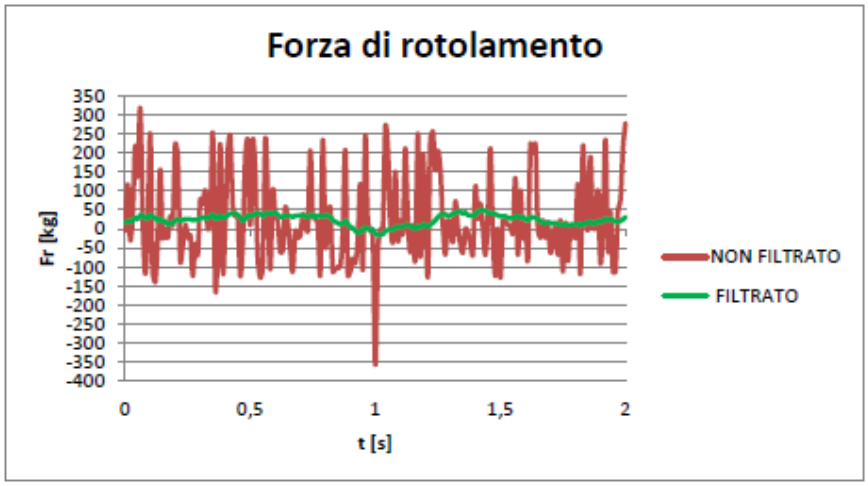

Figure 3-15- Rolling forces comparison signals (Rispoli, 2013)

3.2.5.3. Normal forces

Processing normal forces allows the noisiness reduction. Fluctuations of (+1000 kg_f to -700 kg_f) can be reduced until (+100 kg_f to -50 kg_f). Considering that the minimum values detected part from 6000 kg_f, the maximum noisiness of 2% is acceptable. The mean filtered normal force was equal to 49,5 kg_f while the not filtered 67,8 kg_f.

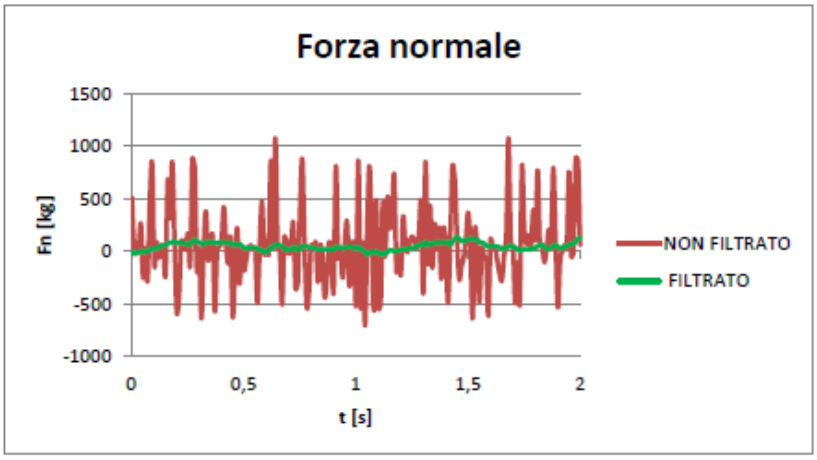

Figure 3-16- Normal forces comparisons signals. (Rispoli, 2013)

3.2.5.4. Horizontal displacement

Output data has a low variability due to the filtering. The graph on Figure 3-17 shows as the variability is minor to 0,01 mm. The horizontal displacement mean value of the signals filtered and not are equal to 47,12 mm.

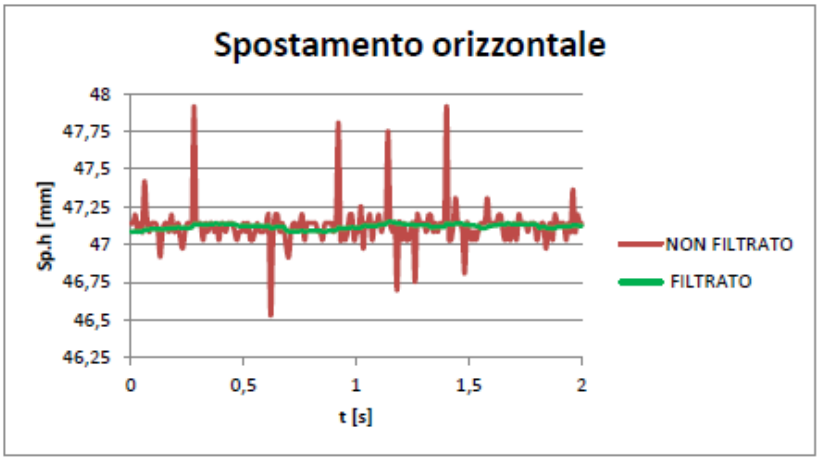

Figure 3-17- Horizontal displacement comparison signals. (Rispoli, 2013)

3.2.5.5. Vertical displacement

The filtering greatly reduces the noisiness obtained as shows Figure 3-18. Nevertheless, referring to the Figure 3-19, it is evident as the output filtered data varies around the 0,5 mm in the measured interval. Considering the values of depth penetration of 2 and 4 mm, the author considers the result as unacceptable. In the case of these value cannot be considered mean values but must be controlled regularly and precisely.

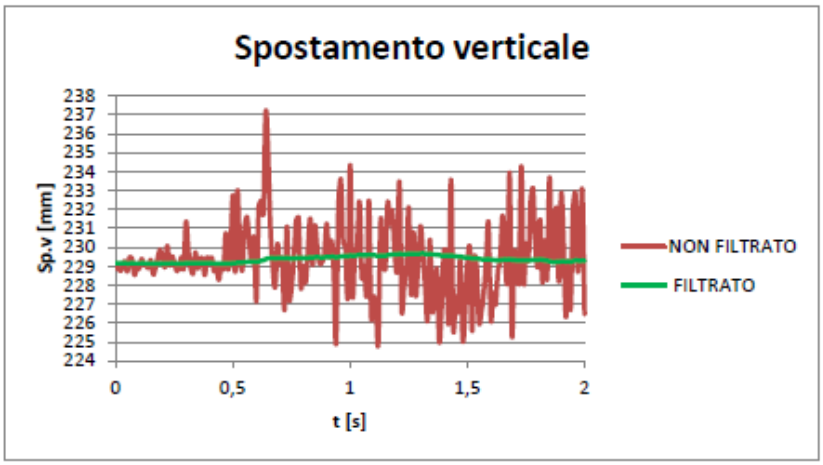

Figure 3-18- Vertical displacement comparison signals. (Rispoli, 2013)

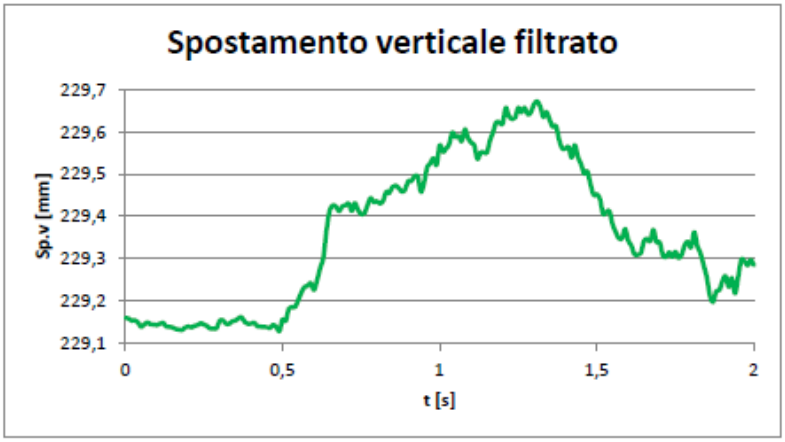

Figure 3-19- Vertical displacement filtered data. (Rispoli, 2013)

Chapter 4 Intermediate Linear Cutting Machine test background at "Politecnico di Torino"

Polytechnic of Turin's ILCM project was implemented at 2010, since then they have been developed some research tests, among them two master degree thesis. On this chapter will be summarize and describe the results obtained during these researches in order to set a reference which supports the results obtained from this study.

4.1. (Rispoli, 2013)

Tests were conducted on three different rock types. Rock samples have a prismatic geometry and dimensions of (50x30x20) cm. In Table 4-1 are listed physical and geo-mechanical properties of these lithotypes.

Table 4-1 Rock samples properties (Rispoli, 2013)

"**Vico" Diorite**				
Density (kg/m^3)	C_o (MPa)	$\sigma_{t,fle}$ (MPa)	E_t (MPa)	Knopp Hardness (MPa)
2620	124	21,3	63	4261
"Luserna" Stone				
Density (kg/m^3)	C_o (MPa)	$\sigma_{t,fle}$ (MPa)	E_t (MPa)	Knopp Hardness (MPa)
2790	120	19,8	35	1286
"**Prali" White Marble**				
Density (kg/m^3)	C_o (MPa)	$\sigma_{t,fle}$ (MPa)	E_t (MPa)	Knopp Hardness (MPa)
2814	215	21,1	45,7	4115

4.1.1. "Vico" Diorite

There were evaluated just the forces developed during the test, regarding sample non planarity effect. Sample presented a slight inclination on the sample box along the cutting direction. It was decided to set up the test differencing between the going cuts (positive slope) and the return ones (negative slope). Table 4-2 shows the results obtained.

Table 4-2 "Vico"Diorite results (Rispoli, 2013)

Cut N	**p (mm)**	**s (mm)**	**s/p**	**Peak F_n (kN)**	**Peak F_r (kN)**	**CC (%)**
1 (going)	1,5	-	-	104,97	4,85	4,6
2 (return)	1,5	-	-	98,87	7,67	7,8
3 (going)	1,5	15	10	94,49	4,05	4,3
4 (return)	1,5	15	10	87,00	4,73	5,4
5 (going)	1,5	20	13,3	98,95	4,60	4,6
6 (return)	1,5	20	13,3	89,86	5,90	6,6

There were taking into account just peak forces because of the non significant mean values. Figure 4-1and Figure 4-2 illustrate the graphs which confront them with the spacing cut.

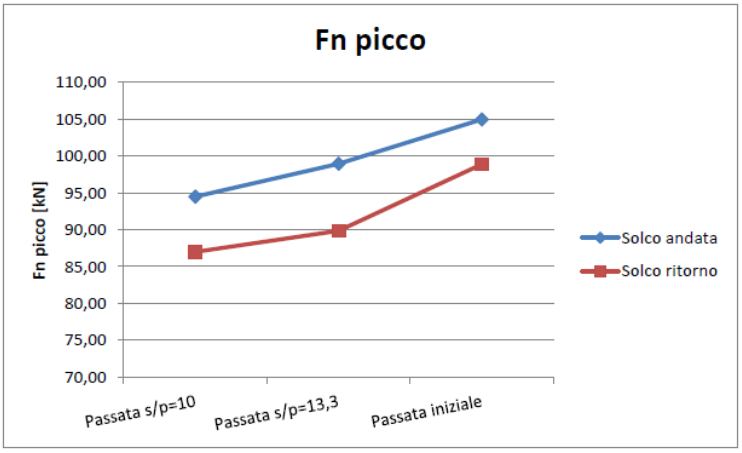

Figure 4-1Peak normal force behavior. (Rispoli, 2013)

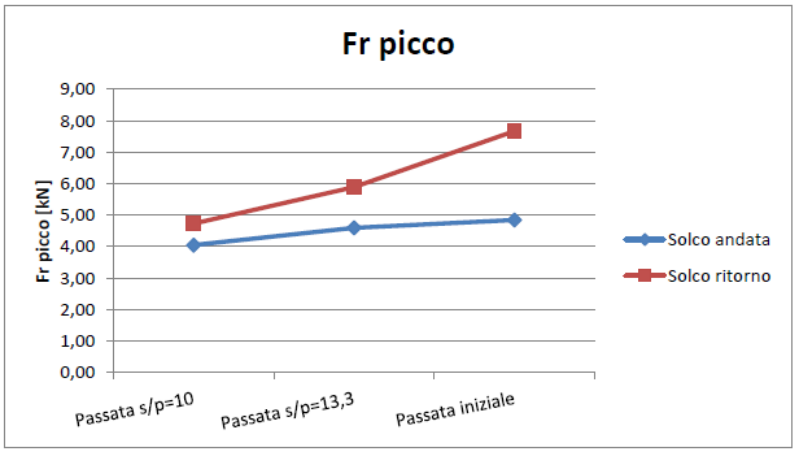

Figure 4-2 Peak rolling force behavior. (Rispoli, 2013)

These studies evidenced how the normal and rolling forces increased as spacing cut did, resulting maximum when the first cut was done. Regarding the going and return cuts, it is noted that for the going cut the normal force is greater than for the return cut. Contrary, the rolling forces resulted greatest when the return cuts were done. According to the results obtained, rock sample inclination affects the F_r/F_n ratio, also called cut coefficient Cc.

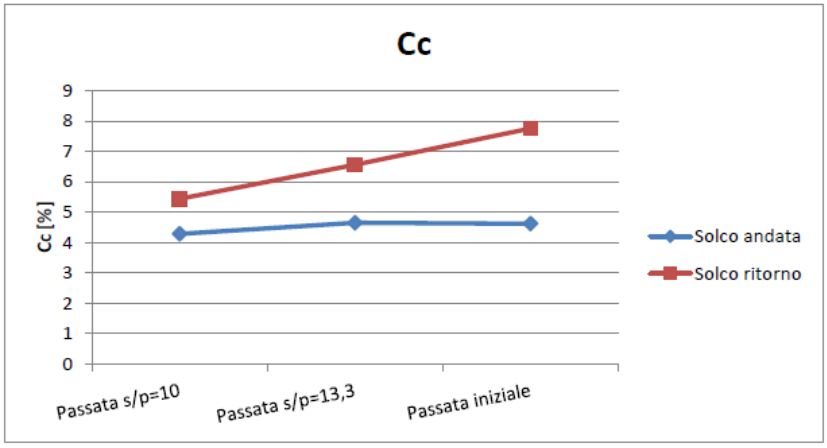

Figure 4-3 Coefficient cut behavior. (Rispoli, 2013)

Figure 4-3 explains the variation of this mentioned Cc. The coefficient remains constant as going cuts were excavated. In contrast the return cuts, due to the bigger differences between forces (by increasing of rolling forces), evidenced a greater variation

4.1.2. "Luserna" Stone

In this case was evaluated the specific energy SE. The confinement of the detritus was done with pieces of paperboard surrounding the disc tool. Despite of the primitive of the technique, it was possible to weight effectively the detritus produced with the disc tool.

The Table 4-3 shows the results obtained for each cut done on the "Luserna" Stone. Also, Figure 4-4 and Figure 4-5 show as the normal and rolling forces are bigger in function of s/p ratio increasing and, the graph of Figure 4-6 indicates that there is a contained variability of Cc values that goes around 8% and 10%.

Table 4-3 Measured forces on "Luserna" Stone. (Rispoli, 2013)

Cut N	p (mm)	s/p	Mean F_n (kN)	Peak F_n (kN)	Mean F_r (kN)	Cc (%)
6	3,9	7,6	74,32	149,89	7,05	9,5
12	3,95	8,0	76,72	118,09	7,17	9,3
7	4,2	9,3	93,02	152,90	7,62	8,2
9	3,8	10,8	102,93	162,74	10,06	9,8
13	4,07	11,1	114,32	139,05	10,10	8,8
10	4,2	12,2	123,19	162,69	11,80	9,6

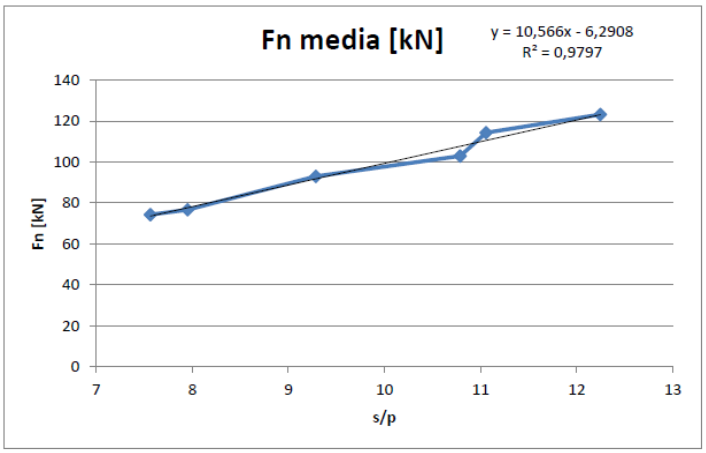

Figure 4-4 Mean normal forces behavior. (Rispoli, 2013)

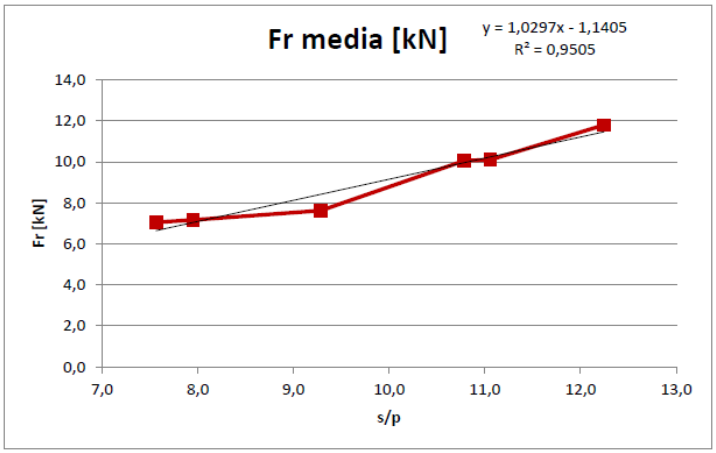

Figure 4-5 Mean rolling forces behavior.(Rispoli, 2013)

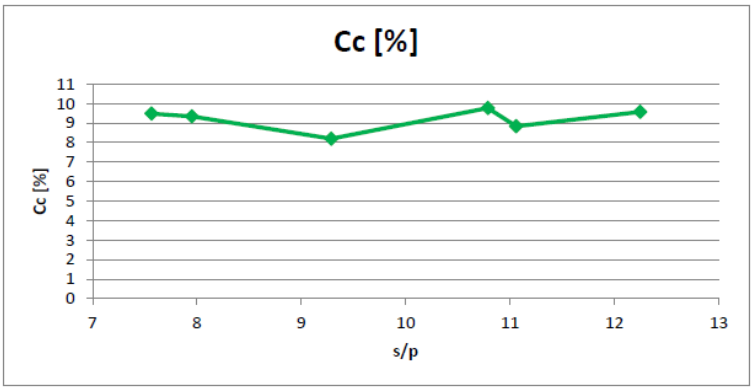

Figure 4-6 Cut coefficient behavior (Rispoli, 2013)

Regarding the specific energy SE the results obtained are contained in Table 4-4. These SE values were estimated through the expression:

$$SE = \frac{F_r * L_{solco}}{V}$$

Where:

SE = specific energy in MJ/m^3

F_r = rolling forces in kN

L_{solco} = cut length in mm

V = detritus volume excavated during the cutting test in mm

Table 4-4 Results of Specific Energy measured on "Luserna" stone. (Rispoli, 2013)

Cut N	s/p	Mean F_n (kN)	Cut lenght (mm)	Weight (kg)	V (kN)	SE (MJ/m^3)
6	7,6	7,05	240	0,04980	19	9,5
12	8,0	7,17	245	0,05753	22	9,3
7	9,3	7,62	235	0,06430	24,5	8,2
9	10,8	10,06	250	0,07808	29,8	9,8
13	11,1	10,10	235	0,07472	28,5	8,8
10	12,2	11,80	245	0,08205	31,3	9,6

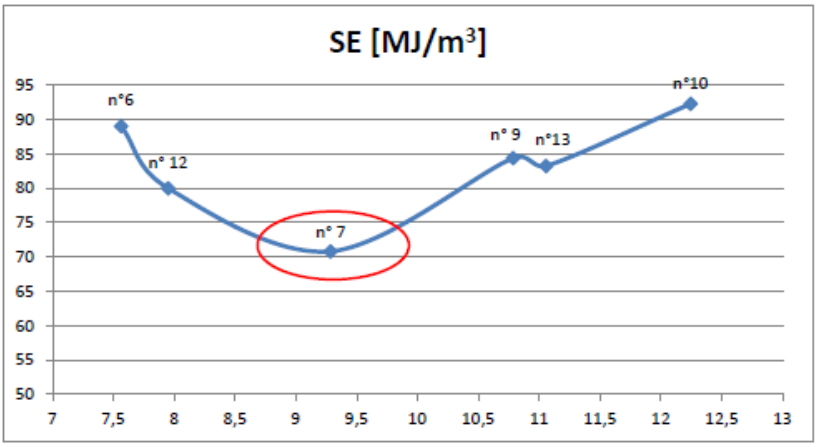

Figure 4-7 Specific energy values for "Luserna" stone. (Rispoli, 2013)

On the base of the results obtained as from these tests, the optimal s/p ratio for this lithotype varies from 8,5 to 10. As it can be seen in the graph in Figure 4-7 exists an anomaly on SE values. The specific energy of Cut n 13 was minor than needed for Cut n 9, presenting s/p values of 11,1 and 10,08 respectively. The reason of this anomaly was told to be the no increasing on detritus volume of Cut n13 respecting Cut n 9. The next contributing factors were the possible reason given for this issue to happen:

- Inferior cutting length
- Penetration depth gap
- Anisotropy influence during Cut n 13
- Detritus collection and removing errors

4.1.3. "Prali" White Marble

As it can be seen from the Table 4-5, the s/p ratio shows a larger variability regarding the values obtained with the "Luserna" stone. The behavior of the forces and curt coefficient are represented in the next figures.

Table 4-5 Measured forces on "Parni" White marble. (Rispoli, 2013)

Cut N	p (mm)	s/p	Mean F_n (kN)	Peak F_n (kN)	Mean F_r (kN)	Cc (%)
8	3	7,3	58,03	83,40	4,77	8,2
2	2,85	9,0	70,74	86,86	5,08	7,2
4	2,85	11,0	71,62	104,32	6,92	9,7
5	2,8	11,9	75,71	99,00	7,95	10,5
6	2,85	13,5	83,02	104,33	8,16	9,8
9	2,95	15,3	94,60	102,63	8,86	9,4
10	2,95	16,2	102,99	112,50	9,39	9,1
11	2,95	16,9	106,76	110,60	9,71	9,1
12	2,9	17,5	108,95	111,7	9,89	9,1

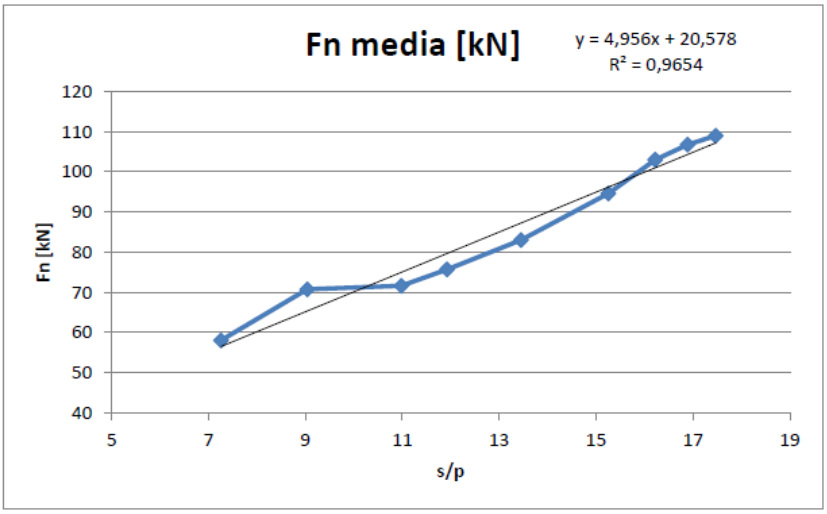

Figure 4-8 Mean normal forces behavior.(Rispoli, 2013)

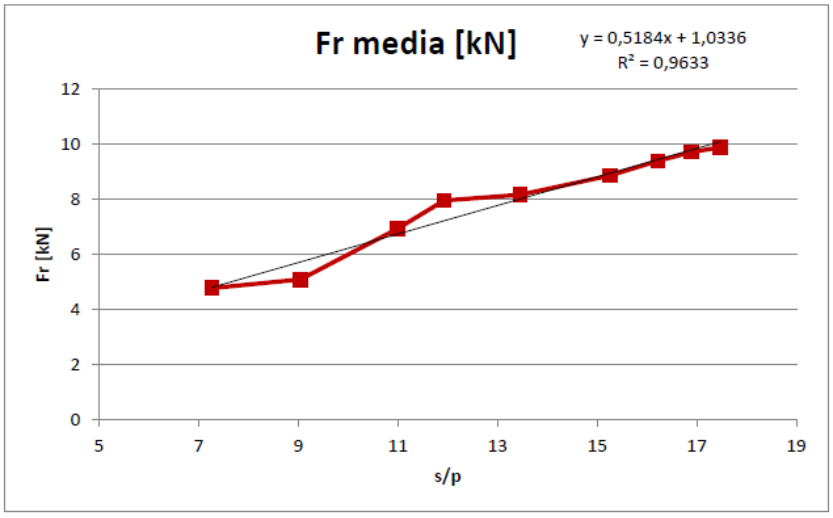

Figure 4-9 Mean rolling forces behavior.(Rispoli, 2013)

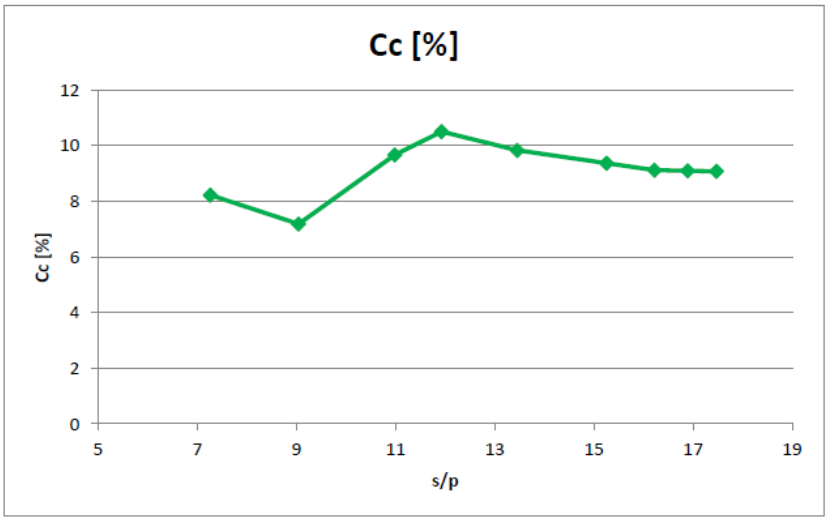

Figure 4-10 Cut coefficient behavior (Rispoli, 2013)

In this case the s/p optimal ratio was among 15 and 16. In Figure 4-11 is proved as s/p values above 16 represent the beginning of a too wide spacing cut and hence greater SE values.

Table 4-6 Results of Specific Energy measured on "Parni" white marble. (Rispoli, 2013)

Cut N	s/p	Mean F_n (kN)	Cut lenght (mm)	Weight (kg)	V (kN)	SE (MJ/m^3)
8	7,3	4,77	205	0,06205	22,2	43,97
2	9,0	5,08	210	0,07161	25,7	41,57
4	11,0	6,92	200	0,09616	34,5	40,16
5	11,9	7,95	210	0,11936	42,8	39,03

6	13,5	8,16	225	0,15482	55,5	33,08
9	15,3	8,86	210	0,20999	75,3	24,72
10	16,2	9,39	215	0,20918	75,0	26,93
11	16,9	9,71	220	0,19823	71,1	30,07
12	17,5	9,89	220	0,19365	69,4	31,35

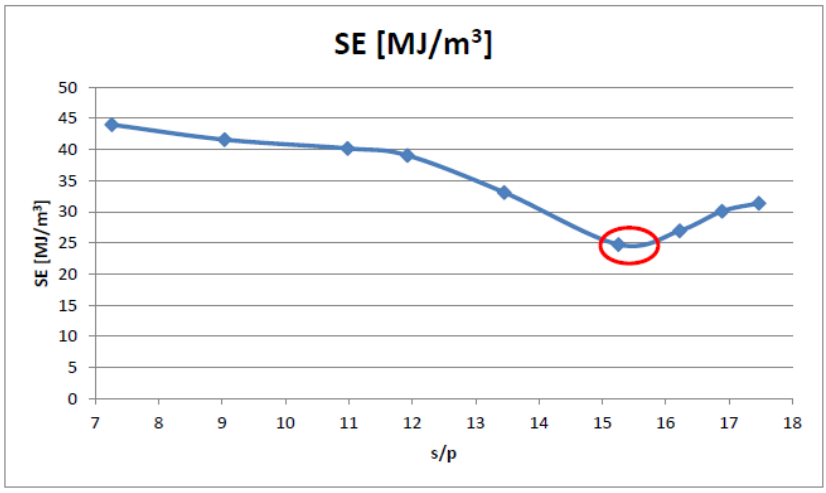

Figure 4-11 Specific energy values for "Parni" white marble. (Rispoli, 2013)

4.2. (Vagnon, 2013)

The study consisted on the use of analytical and numerical models in order to predict brekage penetration depths and normal and rolling forces acting on a linear cutting test and the correlation between models.

Analytical models were based on the Spherical Voids method proposed by (A. Lembo-Fazio, R. Ribacchi, 1986) used for estimating the tensile-strain state at the excavation front of a tunnel (Figure 4-12). The analysis was made for three different rock types, classified as optimal quality, medium quality and low quality rock. The parameters used for the analysis were:

- Peak friction angle θ_p
- Residual friction angle θ_r
- Peak cohesion c_p
- Residual cohesion c_r

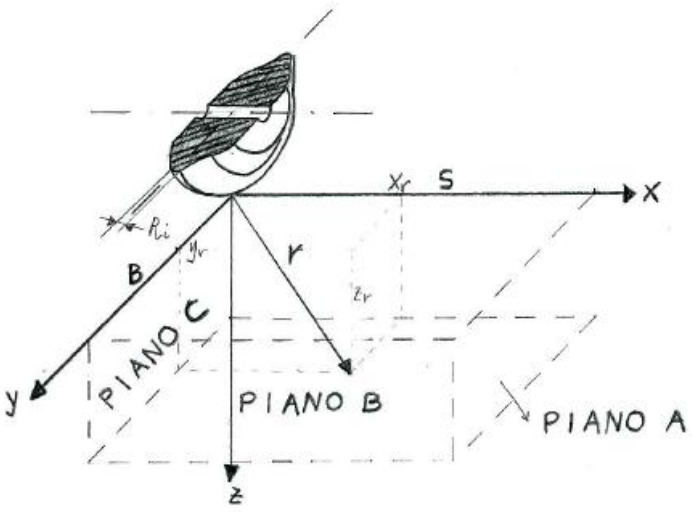

Figure 4-12 Model scheme. (Vagnon, 2013)

Taking the base of Hoek & Brown failure theory and the σ_{ci} values proposed by (Hoek et al., 1996) were estimated the parameters (Table 4-7) used for checking each rock type analytical models.

Table 4-7 Rock parameters used on the analytical model. (Vagnon, 2013)

	Optimal quality	Medium quality	Low quality
Parameters			
σ_{ci} (MPa)	150	80	20
m	25	15	8
θ_p and θ_r	44	37	32
c_p (MPa)	50	28	7
c_r (MPa)	50	28	7

The checking was done for three planes indicated with letter A (horizontal), B (vertical) e C (parallel to cut direction) Figure 4-12). On the three plane on study is possible to identify an alignment form which are calculated the model parameters. The model considers a spacing cut S of 80 mm, a chip length B of half S, internal radius equal to 6,5 mm and maximum force of 200 kN. The objetive's model was to estimate the penetration depth for chip formation.

4.2.1. Optimal quality rock analysis

From the cohesion and friction angle values were defined the critical pressure (62,41 MPa) and the plastic radius (32 mm). In the graph shows in Figure 4-13 is noted as, for the case of plane A, the main breakage mechanism is due to shearing forces. These increase as penetration depth increases. It is also evidenced as closer to the cut the forces are greater.

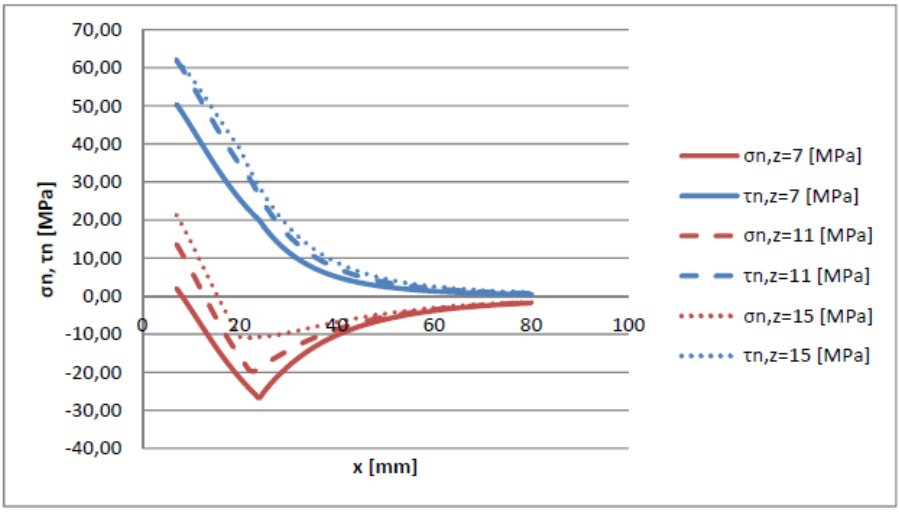

Figure 4-13 Shear and normal stresses variation for different z values in function of the spacing cut (x axis) and with aligment y=B/2. (Vagnon, 2013)

Penetration depth estimation (chip formation) was equal to 8 mm. and it was estimated through the variation of a security factor given by the expression,

$$F.S = \frac{\tau_{lim}}{\tau_n}$$

$$\tau_{lim} = \sigma_n . \tan \vartheta_r + c_r \quad for\ plastic\ condition$$

$$\tau_{lim} = \sigma_n . \tan \vartheta_p + c_p \quad for\ elastic\ condition$$

Where:

τ_{lim} = shear resistance determined by the Mohr-Coulomb criteria

τ_n = shear stress parallel to the cutting surface

the minimum FS value is reported in the Figure 4-14

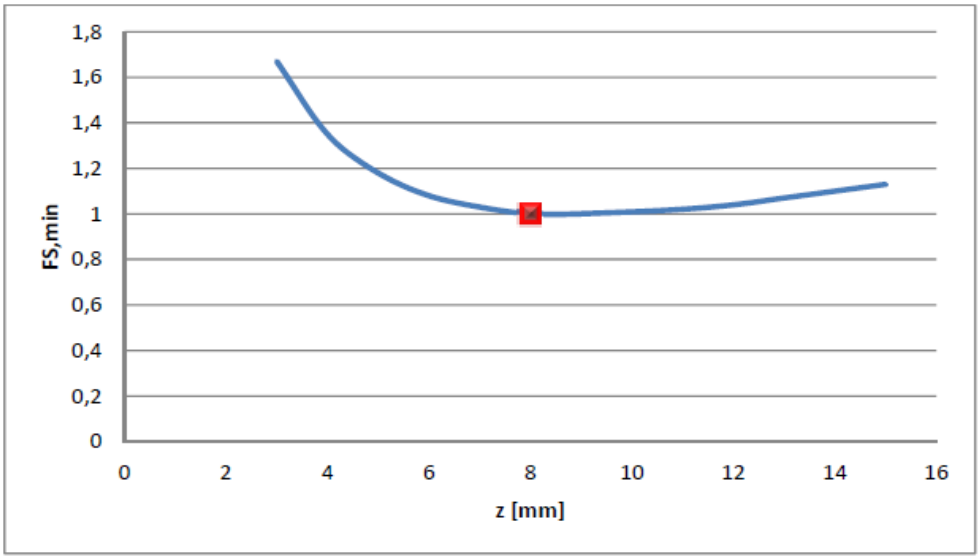

Figure 4-14 F.S. variation in function of depth penetration (z axis). (Vagnon, 2013)

For plane B, transversal to the disc direction and orthogonal to plane A, with a constant penetration depth of 4 mm the breakage mechanism is also a shear breakage mechanism but it decreases as the disc rolls (Figure 4-15).

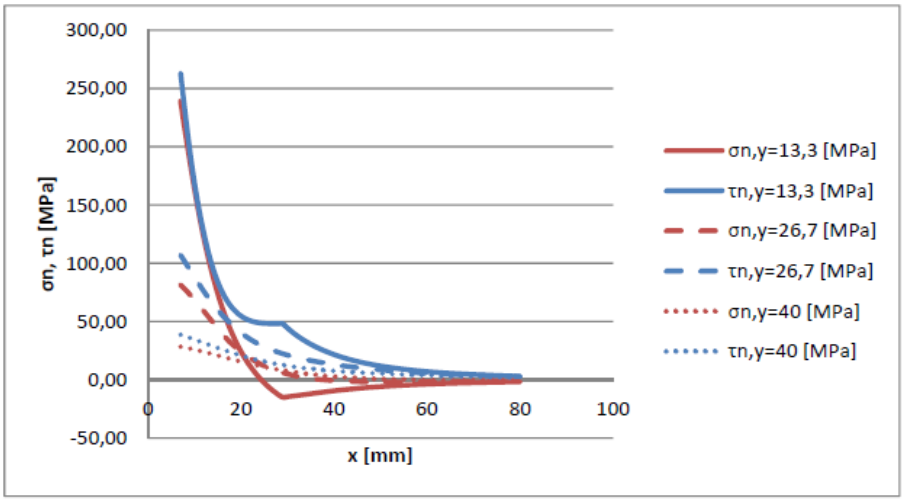

Figure 4-15 Shear and normal stresses variation for different z values in function of the spacing cut (x axis) and with alignment y=B/2. (Vagnon, 2013)

The graph in Figure 4-16 indicates that the breakage on plane B occurs in consequence of the chip formation on plane A. In other words the shear stress generated is not enough to generate a breakage.

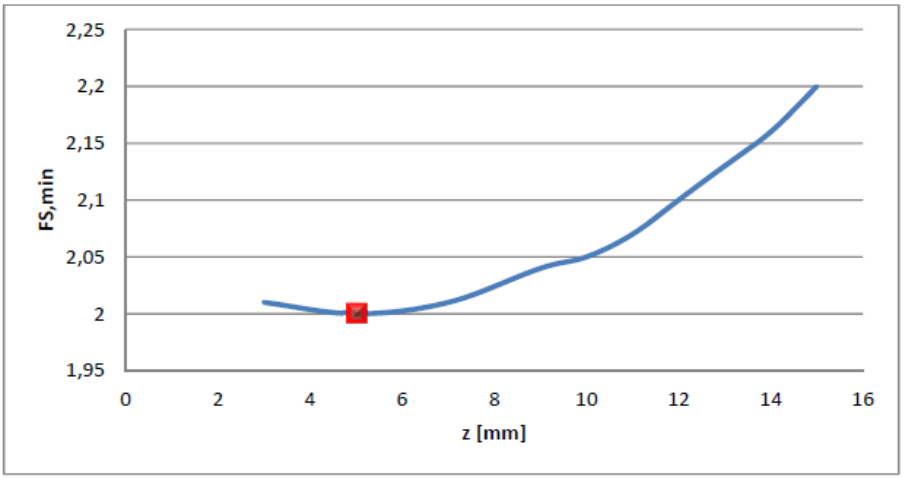

Figure 4-16 F.S. variation in function of depth penetration (z axis). (Vagnon, 2013)

In contrast in plane C existed a traction breakage mechanism when σ_θ becomes negative (Figure 4-17) or at distance of around half plastic radius (Figure 4-18). The compression breakage mechanism prevails until a distance equal to the plastic radius (Figure 4-19).

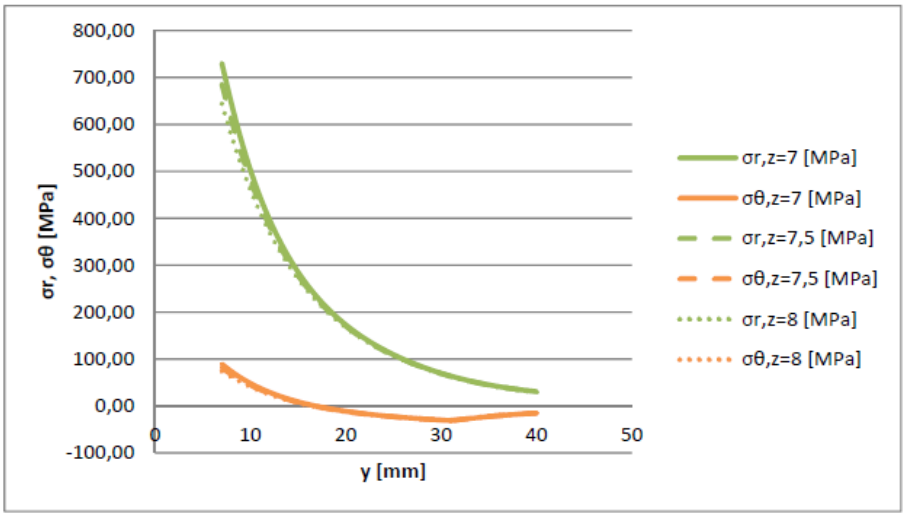

Figure 4-17 σ_r and σ_ϑ variation in function of position on disc trajectory (Vagnon, 2013)

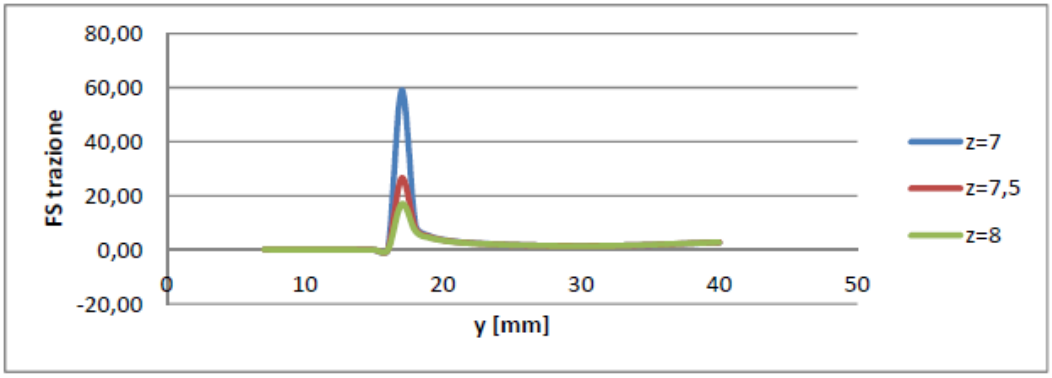

Figure 4-18 F.S. variation in function of position on disc trajectory (y axis). (Vagnon, 2013)

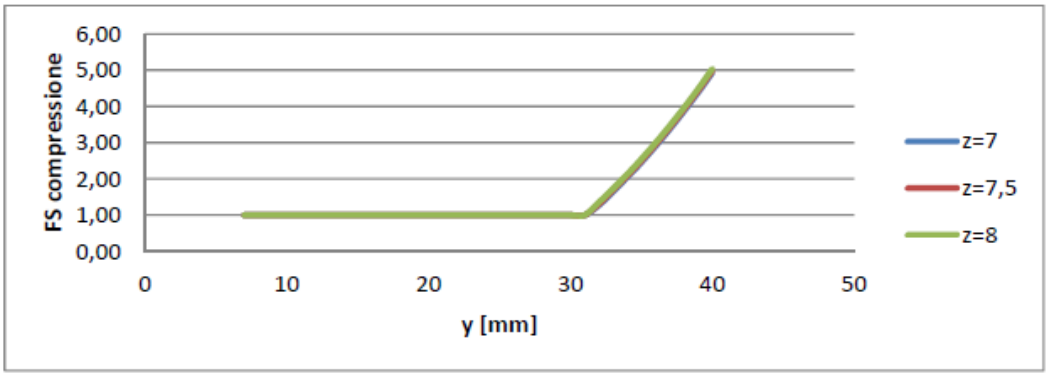

Figure 4-19 F.S. variation in function of position on disc trajectory (y axis). (Vagnon, 2013)

4.2.2. Medium quality rock analysis

In this case the critical pressure resulted equal to 37,30 MPa and the plastic radius 48,87 mm. In the same way than before the graph showed in Figure 4-13 that for the case of plane A, the main breakage mechanism is due to shearing forces. These increase as penetration depth increases. It is also evidenced as closer to the cut the forces are greater.

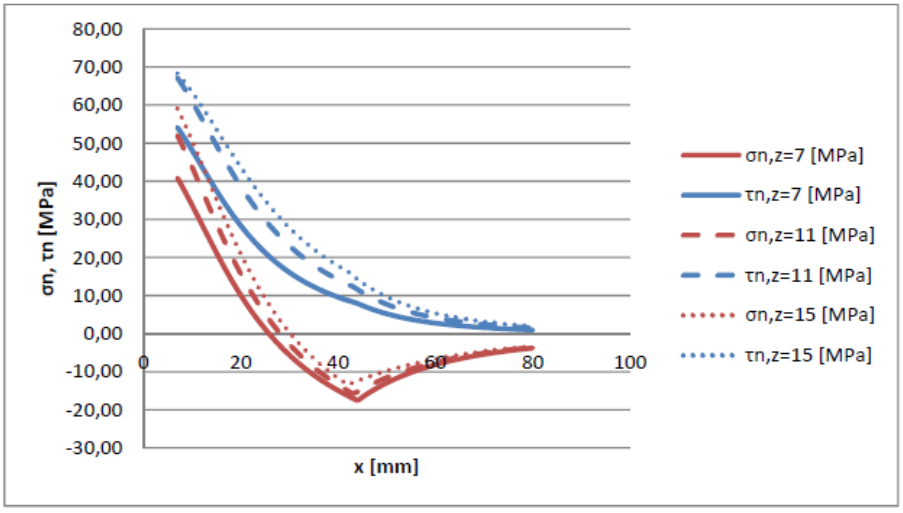

Figure 4-20 Shear and normal stresses variation for different z values in function of the spacing cut (x axis) and with aligment y=B/2. (Vagnon, 2013)

The optimal penetration depth in function of the minimum F.S was equal to 10 mm.

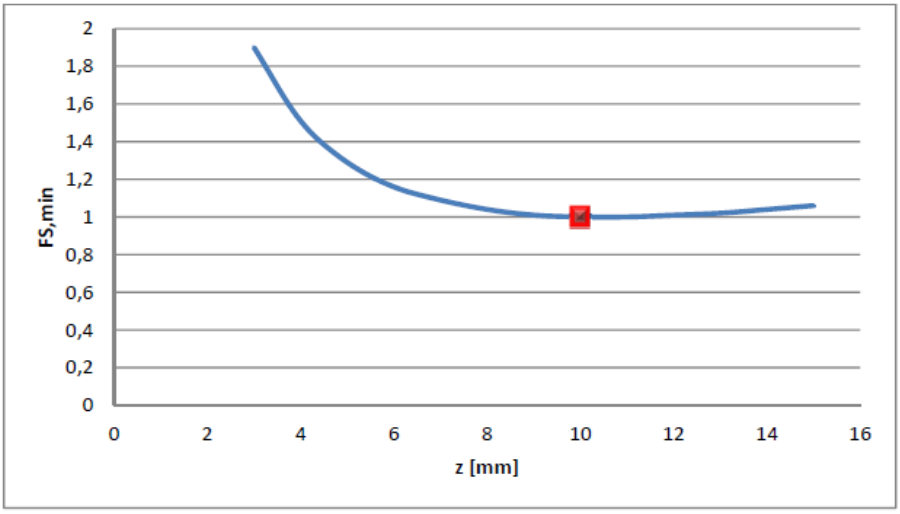

Figure 4-21 F.S. variation in function of depth penetration (z axis). (Vagnon, 2013)

On the vertical plane B, the stress behavior was substantially the same of the optimal quality case. Prevailed the shear stresses as shows Figure 4-22. For any value of depth penetration among 3 and 15 mm the shear breakage of rock occurs at y=40 mm.

For the plane C the same considerations made before, about traction breakage mechanism were valid (Figure 4-24). The compression failure extended until the elastic zone for surpassing the compression resistance (Figure 4-25). The theoretical chip dimension obtained were 80x44x10 mm, comparable with TBM excavated chips.

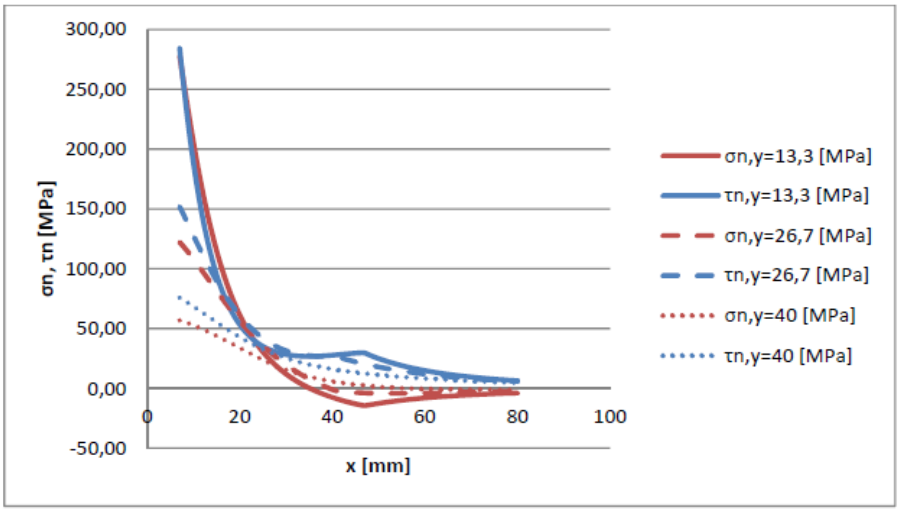

Figure 4-22 Shear and normal stresses variation for different z values in function of the spacing cut (x axis) and with aligment y=B/2. (Vagnon, 2013)

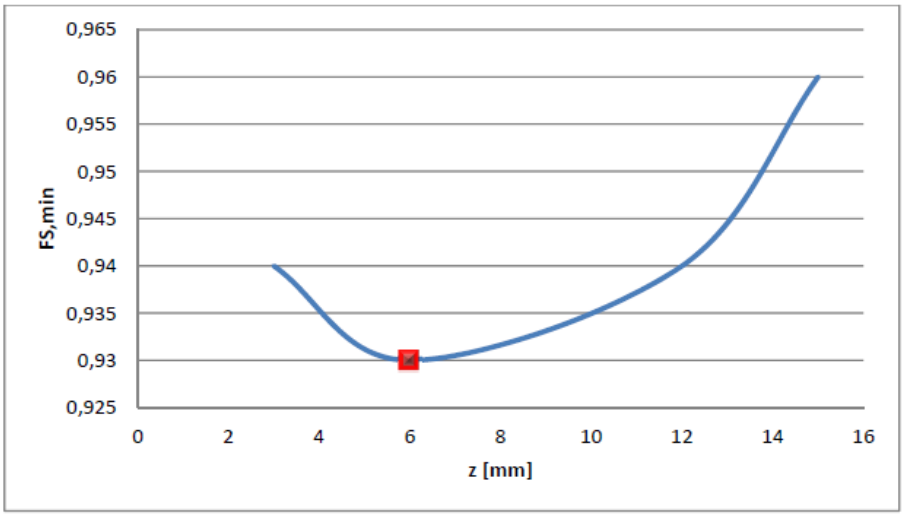

Figure 4-23 F.S. variation in function of depth penetration (z axis). (Vagnon, 2013)

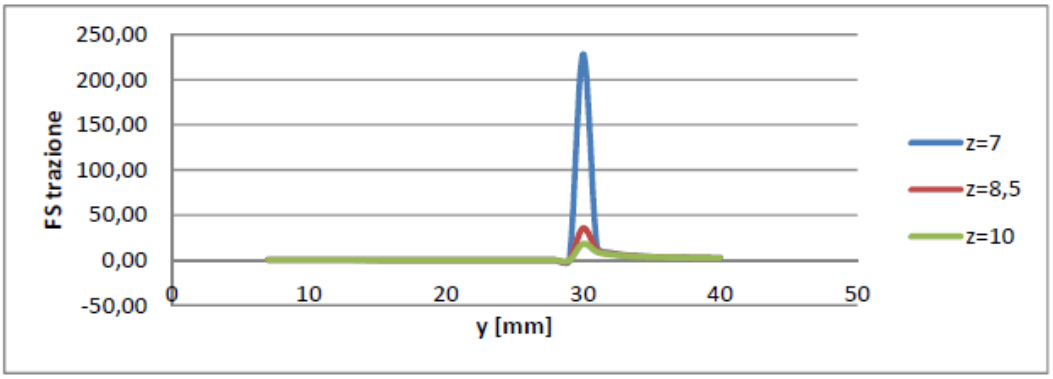

Figure 4-24 F.S. variation in function of position on disc trajectory (y axis). (Vagnon, 2013)

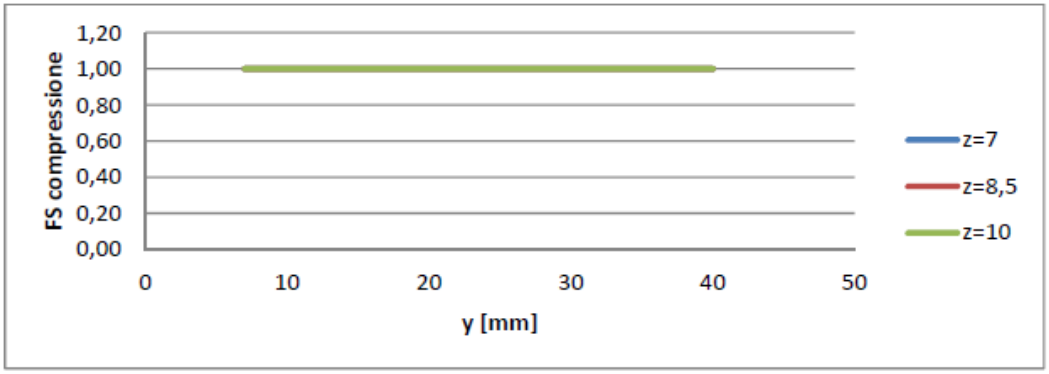

Figure 4-25 F.S. variation in function of position on disc trajectory (y axis). (Vagnon, 2013)

4.2.3. Low quality rock analysis

In this case the critical pressure resulted equal to 9,61 MPa and the plastic radius 143,71 mm. The poor geo-mechanical properties caused different results in comparison with the two others analysis. The prevalent stress on plane A is normal instead of shear stress, and both are of compression (Figure 4-26). The optimal penetration depth was 11 mm (Figure 4-27).

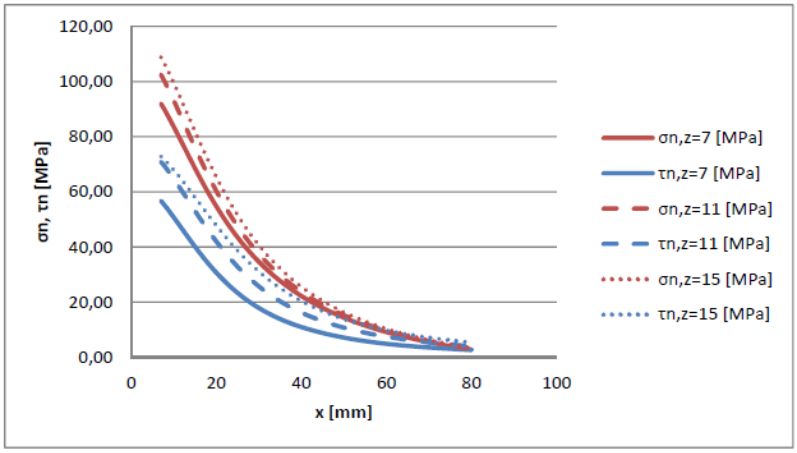

Figure 4-26 Shear and normal stresses variation for different z values in function of the spacing cut (x axis) and with aligment y=B/2. (Vagnon, 2013)

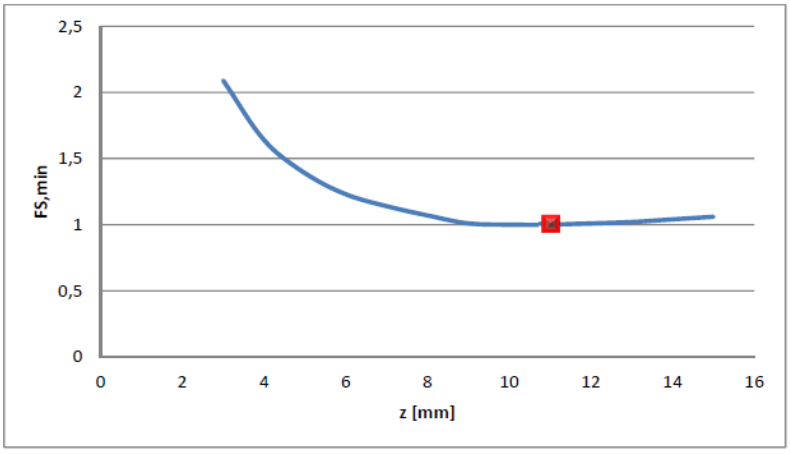

Figure 4-27 .F.S. variation in function of depth penetration (z axis). (Vagnon, 2013)

For plane B the situation was slightly different respecting the plane A. Near to the disc prevailed the normal stresses. Contrarily while "y" increased just shear stresses did (Figure 4-28). The author affirms that chip formation at the plane y=40 mm occurs surely because of the low F.S values obtained (Figure 4-28). However, due to the fact that for F.S=1 is obtained at y=146, the parameters obtained are not considered as reliable. On the plane C the failure is due to traction stresses (Figure 4-29).

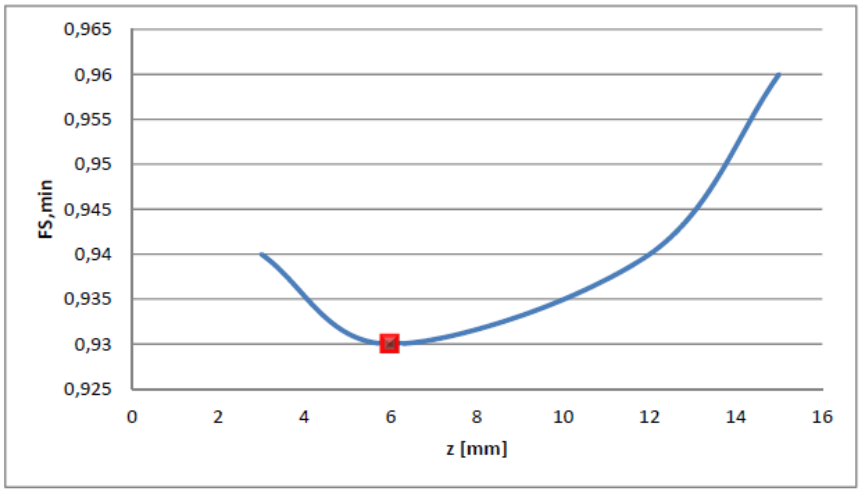

Figure 4-28 F.S. variation in function of depth penetration (z axis). (Vagnon, 2013)

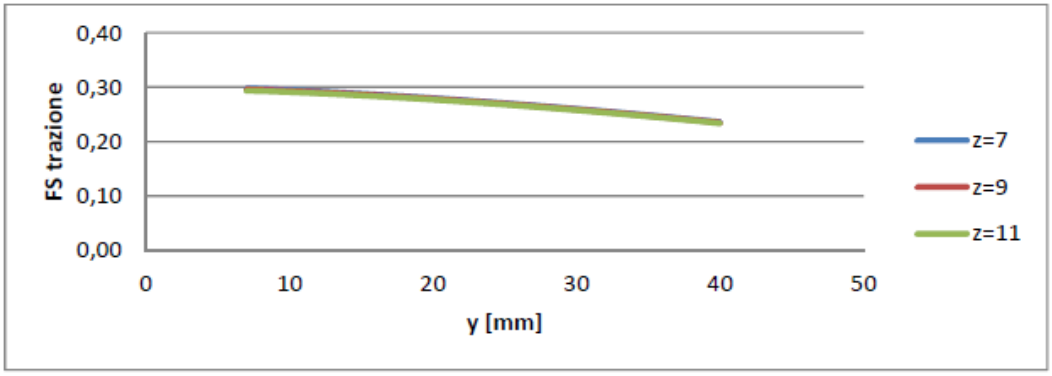

Figure 4-29 F.S. variation in function of position on disc trajectory (y axis). (Vagnon, 2013)

The chip dimensions estimated in this case were 80x148x11 mm. Is is obvious as the length is greater than one obtained with a TBM.

Chapter 5 Experimental and theoretical analysis

5.1. Generalities of experimental phase

Tests were performed with the ILCM of *Politecnico di Torino* on a single marble block (Figure 5-1), having dimensions of (50x40x25) cm and characteristics described on the next section. The cutter disc used was a V-shaped one (Figure 5-2) which dimensions are listed on (Table 5-1).Said cutter disc is tungsten carbide (widia) madden and this has been the first time on being used.

Figure 5-1 Cutter disc after excavating a groove on marble-cement block

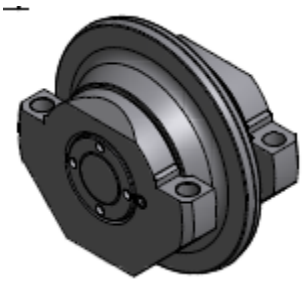

Figure 5-2 Cutter disc design. Courtesy of Palmieri S.P.A

Table 5-1 Cutter disc dimensions

Diameter (mm)	170
Tip width (mm)	0,2
Shaft width (mm)	102,5
Shaft lenght (mm)	152,5
Contact angle with surface ()	45

It is suggested by the cutter disc producer (Palmieri SPA) to not exceed, as mean value, the 5 ton of applied force during the test. These suggestions were kept during almost all of the tests in order to preserve the disc useful life for futures researches.

The ILCM' sample box has a rectangular area (Figure 5-3) with dimensions of (89,5x47) cm. The vertical barrier which partially closed this area has a height of 10 cm.

Figure 5-3 Sample box of ILCM

The rock sample is confined onto the sample box with a water-cement mix. The cement's commercial name is EMACO® S55, which can be applied easily and has the advantages of having a high compressive strength, high fluid consistency and it is free of bledding. For a mix volume of 0,1 m^3 are used five 25 kg. EMACO® S55 bags. The water/cement relation is kept as producer suggestion, being of 0,16. The preparation and cement characteristics are explained in detail on section 5.3. The entire marble-cement block must be also confined with iron fasteners like those on figure Figure 5-4.

The sample is cut by levels with the same cutting space of 40 mm but with different depth penetrations. In function of its purpose the levels can be classified in: trimming levels, conditioning levels and data levels. The trimming ones are done just for the first two cuts in order to guarantee a regularized surface. The conditioning levels have the function of preparing the rock surface for the data levels at which are excavated the grooves used for calculating the specific energy in function of s/p ratios (final goal of testing): these two should have the same penetration depth. At section 5.4 are explained in detail the steps to follow.

Figure 5-4 Iron fasteners pressing the block against the sample box

5.2. Rock characteristics

The marble rock sample was taken from the Carrara quarries at Alpuane Alps in Toscana - Italy (Figure 5-5). It is called "Veined Statuary White", according to (Blasi, 1998) this kind of Carrara's marble has so prominent vein patterns that i forms band a few centimeters thick. The colour may vary from grey to light yellow and sometimes a greenish colour. It is commercially knows as Calacata (Figure 5-6) and its production amounts to less than 5% of the total.

Figure 5-5 Geographical scheme of Alpuane Alps. (Criscuolo & Lisi, 2016)

Figure 5-6 Calacata or Veined Statuary White. (Blasi, 1998)

The mean mineralogical composition of Carrara's marble is listed on Table 5-2 and the geo-mechanics properties on

Table 5-3.

Table 5-2 Mean mineralogical composition

Calcium Carbonate $CaCO_3$	~98%
Dolomite $CaMg(CO_3)_2$	1,76%
Magnesium oxide MgO	1,32% mol
Silicon oxideSiO_2	0,71%
Estroncio Sr	114-160 ppm
Rest	1,37%

Table 5-3 Geo-mechanicals properties

Density	27,05 kN/m^3
Uniaxial compressive strength	131 MPa
Tangent elastic modulus	75000 MPa
Secant elastic modulus	83550 MPa
Poisson's Ratio	0,274

5.3. Test methodology

The linear cutting test carried out can be described as a succession of steps listed as follows:

5.3.1. Setting up phase

5.3.1.1. Doing the formwork

First of all, for obtaining more realistic forces values during the test, the marble rock was bounded with a cement-water mix. So, it was necessary to assemble a formwork Figure 5-7. It was formed by four wooden planks. One pair had dimensions of (47x25) cm, put on the shorter side of the sample box and the other one (88,7x25) cm for the longer one. The thickness for both of them was equal to 0,4 cm.

Figure 5-7 Assembled formwork mounted on the sample box before cement casting

5.3.1.2. Placing the block onto the sample box

An estimated weight of the block is 135 kg, because of that it was use a wheeled hoist (Figure 5-8) for handling and moving it. Two strings held up by the hoist were put under it. Then, with extremely care the block was placed over two wooden wedges which allow placing straight and symmetrically the sample on the box as shows Figure 5-9.Later, before starting the cement cast they were removed.

Figure 5-8 Marble block raised by a hoist

Figure 5-9 Marble block on the sample box

5.3.1.3. Mixing and casting the cement

As mentioned on section 5.1, it was mixed EMACO® S55 with water in a relation of 0,16. In other words for each 25 kg of cement there were added 4 liters of water to the cement mixer . After 4-5 minutes the mixing was stopped and then casted between the block and the formwork (Figure 5-10). The mix was hardening for 4 days until the start of the tests.

Figure 5-10 Cement mix casted inside the formwork

Figure 5-11 Sample ready to be tested

Table 5-4 shows some cement characteristics given by the producer

Table 5-4 EMACO® S55 characteristics. Provided bi BASF The Chemical Company

Product chemistry	Minerals filler and cement
Compressive strength TS EN 196 (1day) (7days) (28 days)	 >30 N/mm^2 >50 N/mm^2 >60 N/mm^2
Elasticity modulus TS EN 13412 (28 days)	> 20.000 N/mm^2
Application temperature	+5 C- +30 C
Water quantity	0,16 liters per kg
Mixed density	~2,20 kg/liters

5.3.2. Cutting phase

5.3.2.1. Putting the cutter disc above the sample

The transversal movement of sample box was activated manually through the knob that makes twist the threaded screw. At the beginning, when the sample box is at the end of its guide rails, the disc is placed just over the sample. Exactly, at 25 mm from its left edge as shows Figure 5-12.

Figure 5-12 Cutter disc over the sample

It was necessary to cut and break one of the angles of the block (Figure 5-12) for allowing the vertical piston to carry the tool down to the penetration depths.

It is important to clarify that it was chose as first cutting space 25 mm and not 40 mm (as the rest of the cuts) in order to take advantage of the block edges' weaknesses. In this way, in theory, there would be not a great breakage of rock-cement and therefore big block pieces will not break apart (Figure 5-13). However, this method did not work well for depth penetrations below 4 mm.

Figure 5-13 Partial breakage of cement block

5.3.2.2. Confining with iron fasteners

Because of rock-cement detachments, it was decided to subsequently confine it with iron fasteners, pressing against the sample box on both extremes (Figure 5-13). The method proved to be effective also avoiding the transversal movement of the block.

5.3.2.3. Fixing cutting spacing

The initial thought was to create ten grooves on the surface rock (

Figure 5-14) at each one of the 14 levels planned. However, taking into account the facts explained on sections 5.3.2.1 and 5.3.2.2, from level 3 onwards there were done just five of them (Figure 5-15). The lists the three types of levels done as the block is excavated with the disc.

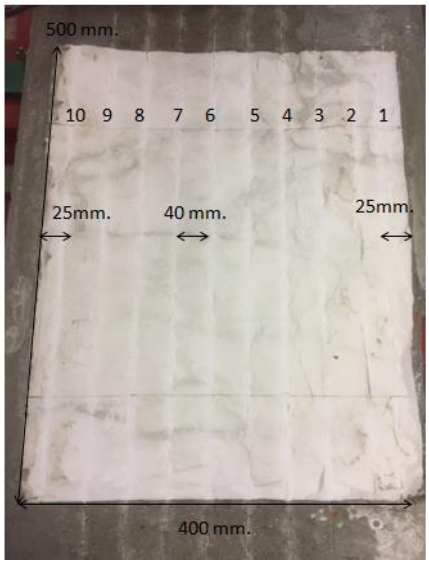

Table 5-5 Levels of cutting

Level	**Type**	**Level**	**Type**
1	Trimming	8	Data
2	Trimming	9	Conditioning
3	Conditioning	10	Data
4	Data	11	Conditioning
5	Conditioning	12	Data
6	Data	13	Data
7	Conditioning		

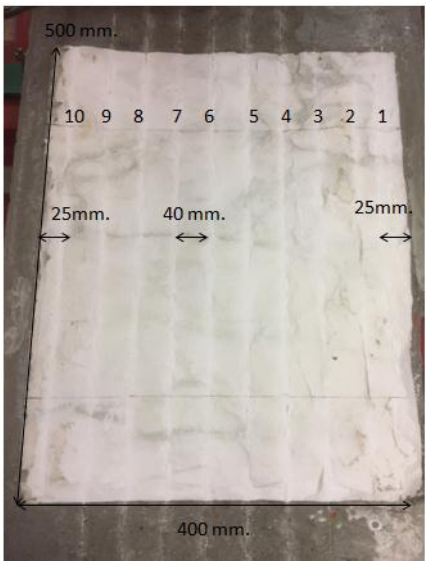

Figure 5-14 Initial grooves by level

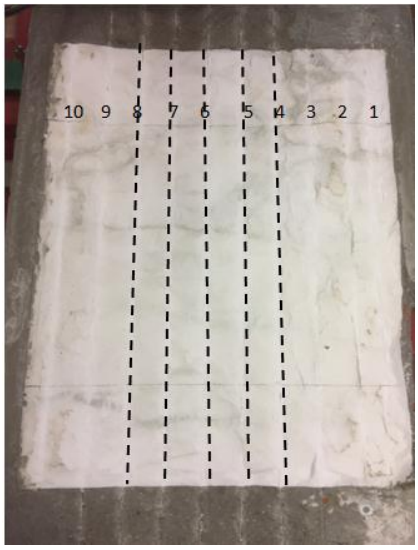

Figure 5-15 Final grooves by level

5.3.2.4. Creating the grooves

The depth penetration value is set using a LVDT transducer (Figure 5-16) which converts vertical movement of piston into an electrical signal. Said signal is acquired with the acquisition system Spider 8 that transfers it as a digital signal to the computer and finally with Catman software the "p" value is measured.

Figure 5-16 LVDT transducer

Once known the value, the piston's nuts (Figure 5-17) is tighted with a force of 15 kgf. in order to create a contrast that could react against the normal force induced on the piston by the block during the cutting . Then, the longitudinal movement of the sample box along the guide rails is started by the 15 kW electrical engine (Figure 5-18). The grooves are excavated as long as the engine is stopped. Later, the sample box is transversally moved with the threaded screw until put the disc above the next groove. The process is repeated as far as the level is finished.

Figure 5-17 Piston's nuts to be tighten

Figure 5-18 15 kW electrical

Table 5-6 Depth penetration by levels

Level	**Type**	**Depth penetration (mm)**
1	Trimming	4,2
2	Trimming	5
3	Conditioning	4,94
4	Data	4,94
5	Conditioning	5,45
6	Data	5,45
7	Conditioning	4,47
8	Data	4,47
9	Conditioning	3,96
10	Data	3,96
11	Conditioning	3,51
12	Data	3,51

13	Data	3,51

The decision of not excavating the closer grooves to the block edges (Figure 5-15), explained on section 5.3.2.3 in order to prevent the sample breakage did create a sort of valley on the rock surface (Figure 5-19). This fact forced to eventually pass the cutter disc near to the extreme grooves (Figure 5-20) with a penetration depth above the current level being excavated. The reason was the great forces measured on the cutter disc during the excavation of them, because of the sharp quotes differences that both damage the tool and modify the actual results.

Figure 5-19 Valley created at the centre of the sample

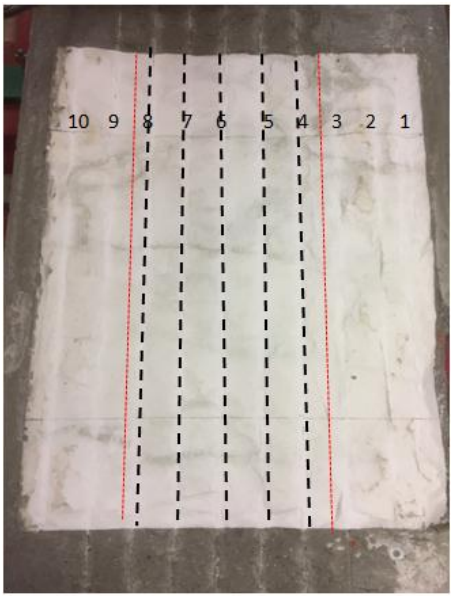

Figure 5-20 Auxiliar grooves

5.3.2.5. Collecting and weighing out detritus

After each groove is completely cut, the detritus must be removed for making easier the pass of the disc on the next one. The removal is done with a vacuum cleaner as showed in (Figure 5-21).

Figure 5-21 Detritus removal with vacuum

At each data level, the detritus formed from central cuts (Figure 5-22) besides being removed should be collected and weighted. For this purpose is used a plastic bag at the inside of the vacuum which is weighted before and after the collection plus the dust filter With this data it is possible to estimate, as explained on section 2.5, the specific energy of excavation. The results obtained are showed on the next section.

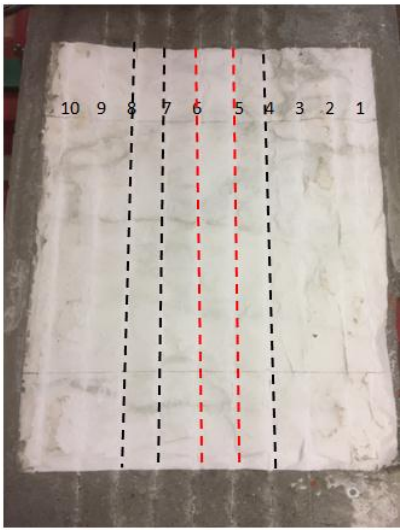

Figure 5-22 Grooves for estimating specific energy

5.4. Test results

On the next sections are showed the results obtained after the testing phase. The most of the data was collected from the cuts done on the data levels mentioned on Table 5-6. The parameters of study are the variation of penetration depth along the cuts excavated with the disc, the forces variation in function of the penetration depth an s/p ratio and finally the specific energy. Also are put on discussion some force variations as mineral presence occurred on the marble surface.

5.4.1. Depth penetrations

The data was taken from the grooves that were object for specific energy calculation i.e. grooves 6 and 5 (Figure 5-22). For the five penetration depths in study there was not a great variation along the block length, conversely the values did just oscillate more or less in a range of 0,15 mm. Another aspect to emphasize is that the block length on study does not include the first and last 100 mm of the marble block, as shows Figure 5-23 the yellow and green colored areas are excluded from data collection.

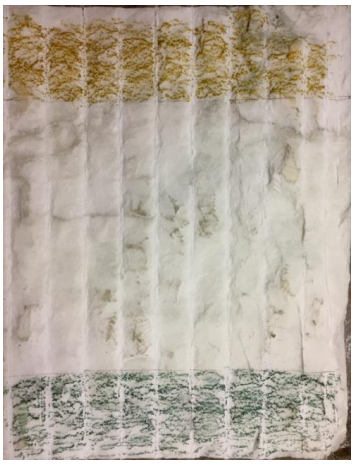

Figure 5-23 Block length on study

For the case of p=5,45 mm. on both grooves the "p" value does not evidence a variation greater than 0,15 mm. It is also observable as at the beginning of the block length under study the penetration is slightly shallower respect to the mean. On the opposite, at the end it is deeper.

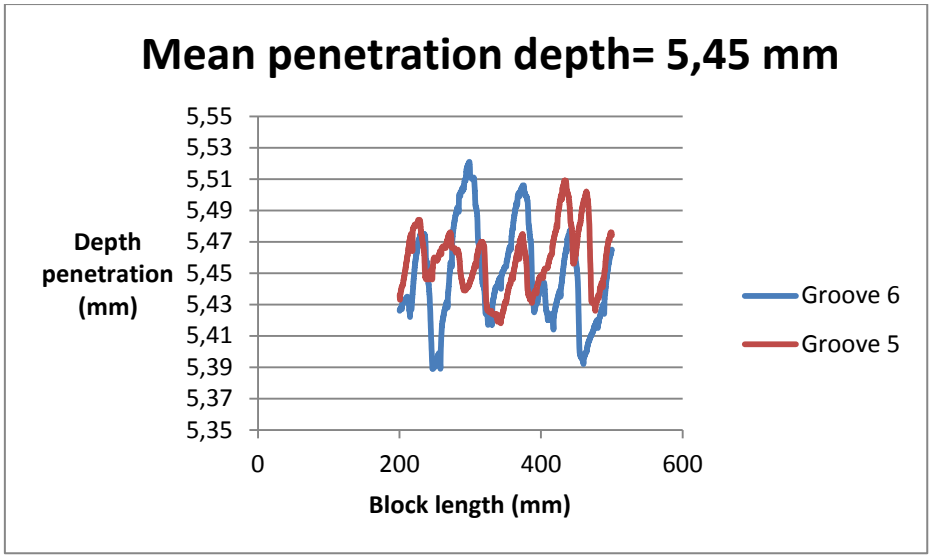

Figure 5-24 Variation of depth penetration along the cut for a prefixed "p" value of 5,45 mm.

In this case the variation range is even smaller than with the previous one, about 0,10 mm. It can be appreciated on Figure 5-25 as "p" sharply rises and decreases inside the interval length.

On the next prefixed penetration value of 4,47 mm the range is also of 0,10 mm. but the variation is less sharpen. Figure 5-26 shows that in this case the initial and final penetration depth are shallower than deeper than the mean for both grooves.

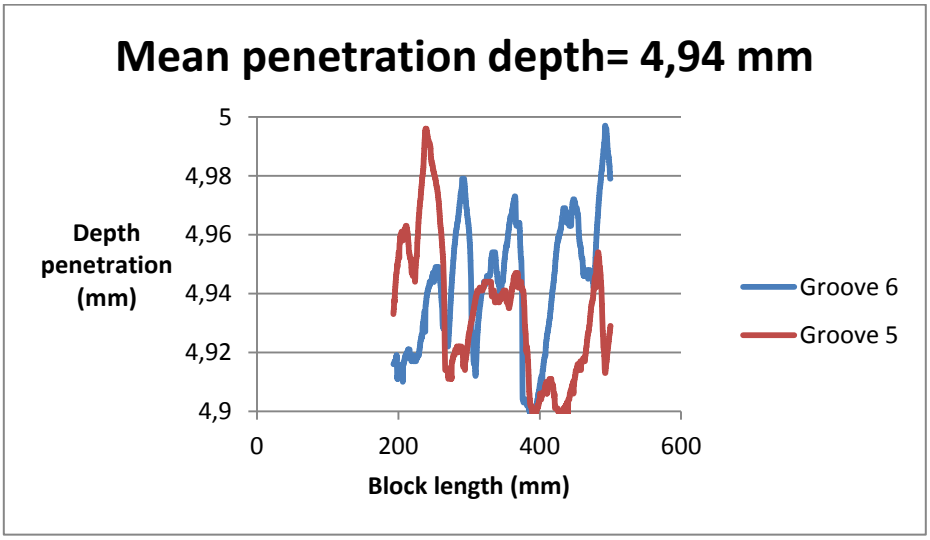

Figure 5-25 Variation of depth penetration along the cut for a prefixed "p" value of 4,94 mm.

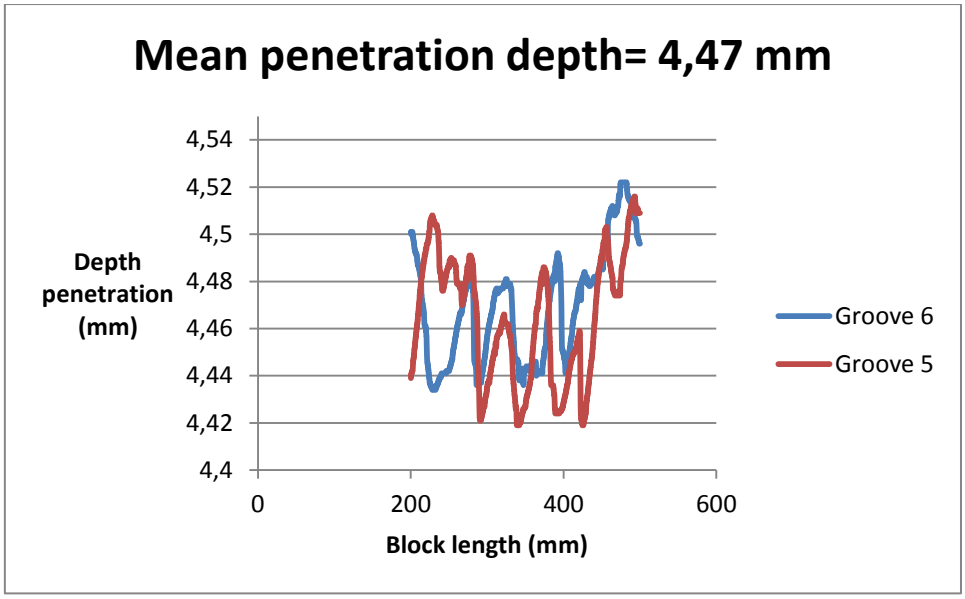

Figure 5-26 Variation of depth penetration along the cut for a prefixed "p" value of 4,47 mm.

Finally, also for this fifth p value the graphs showed on Figure 5-28 were created from data obtained of two grooves excavated on different data levels (12 and 13). Nevertheless, the penetration variation is not superior to 0,15 mm., thus is taken as good any of the two mean p values obtained.

Figure 5-27 Variation of depth penetration along the cut for a prefixed "p" value of 3,96 mm.

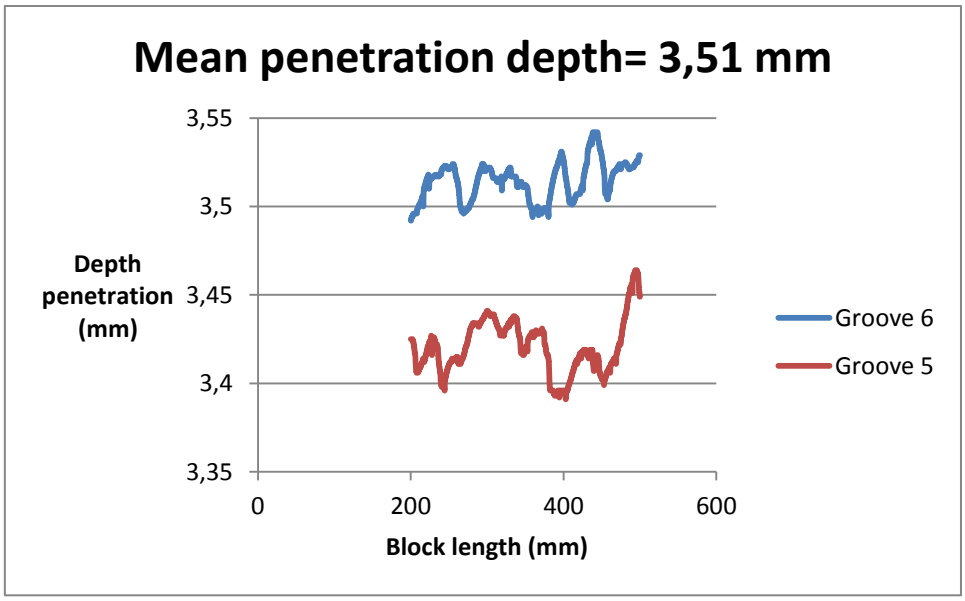

Figure 5-28 Variation of depth penetration along the cut for a prefixed "p" value of 3,51 mm.

5.4.2. Rock cutting behavior

5.4.2.1. P= 5,45 mm.

For each of the data levels elaborated has been taken one groove to show the force behavior on normal and rolling directions along the cut length. On Figure 5-29 is showed the maximum normal force, being of 69 kN and a mean of 34 kN. Instead, the rolling forces represented on Figure 5-30 have a maximum of 11,5 kN and a mean of 7 kN.

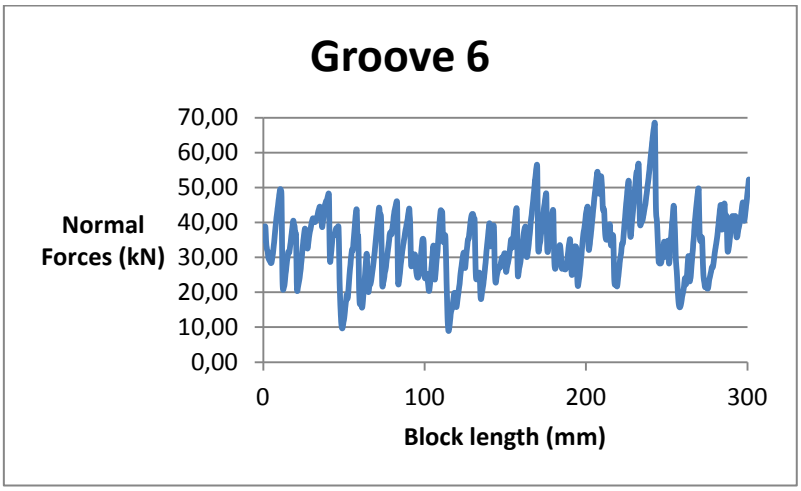

Figure 5-29 Normal force behavior for p=5,45 mm.

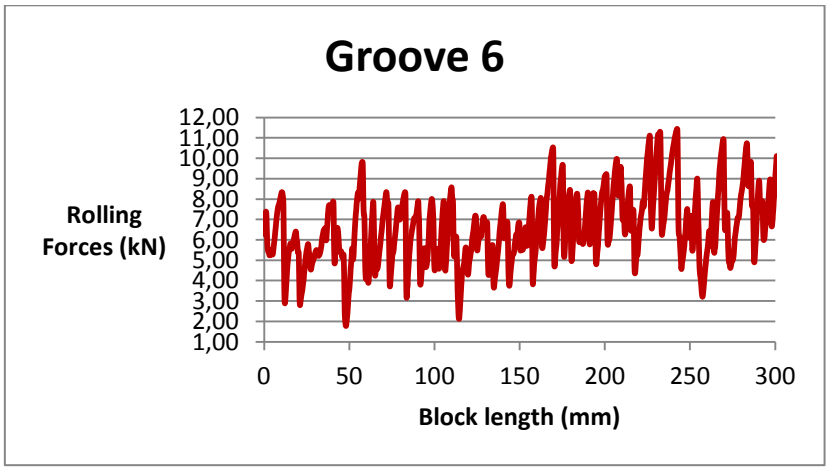

Figure 5-30 Rolling force behavior for p= 5,45 mm.

The forces also were measured on the rest of grooves; the variation is in the range of 10 kN for the groove 4 to the groove 7. The normal forces (Figure 5-31) developed on groove 8 is about 20 kN bigger than the mean of the other ones. In the case of rolling forces the difference is almost 3 kN. This considerable difference between these values is due to the block surface conditions where was located this groove, as explained on section 5.3.2.4.

Table 5-7 Force values for penetration depth of 5,45 mm.

	Fr mean (kN)	**Fn mean (kN)**
Groove 4	6,68	37,52
Groove 5	6,29	34,15
Groove 6	6,62	33,87
Groove 7	6,07	31,77
Mean 4-7	**6,42‡0,08**	**34,33‡5,67**
Groove 8	9,24	53,53

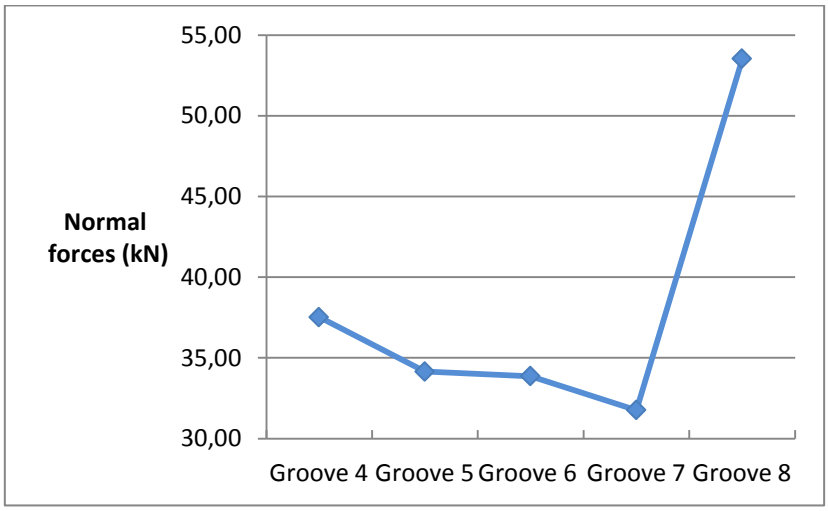

Figure 5-31 Variation of forces in normal direction on each groove

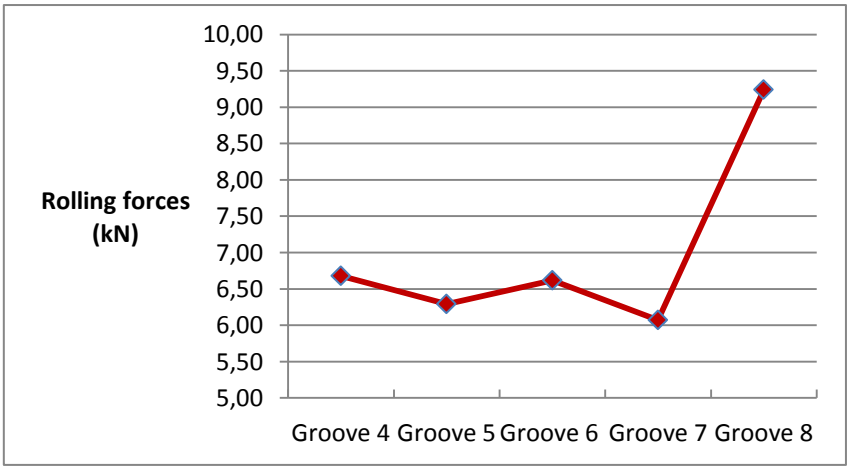

Figure 5-32 Variation of forces in rolling direction on each groove

5.4.2.2. P= 4,94 mm

For this groove at this penetration depth, the maximum normal force is about 55 kN and a mean of 33 kN. Instead for rolling forces the maximum is around 10 kN and the mean is 6 kN.

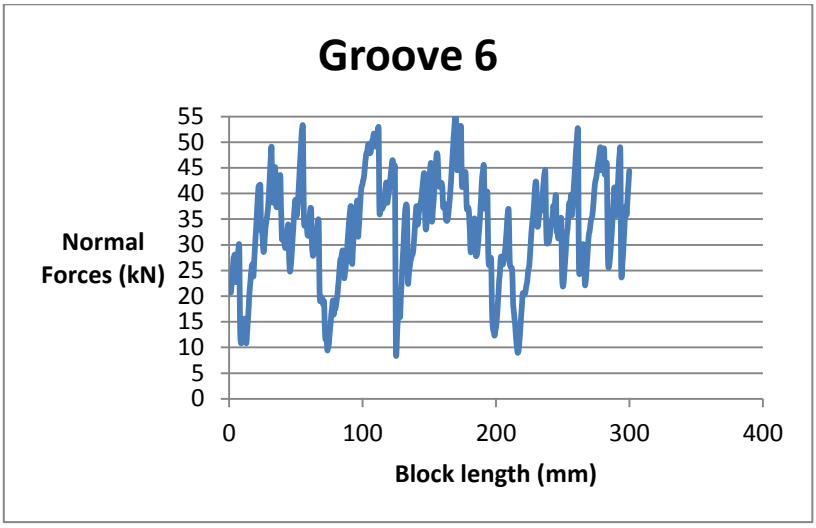

Figure 5-33 Normal force behavior for p=4,94 mm.

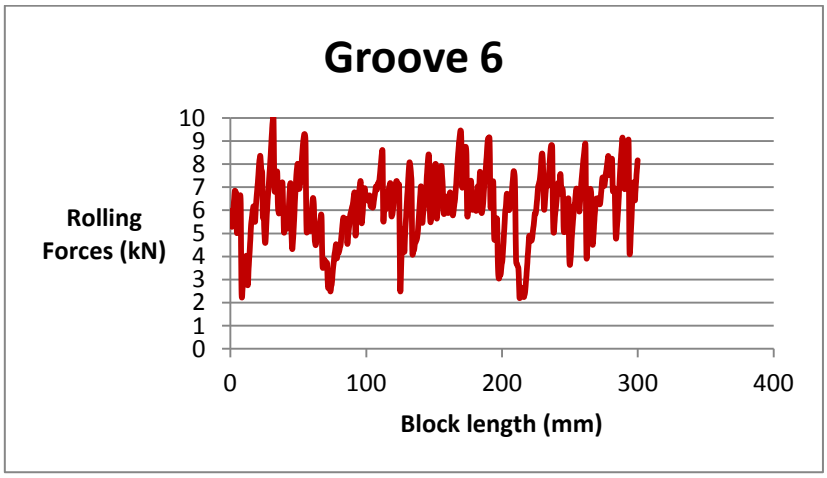

Figure 5-34 Rolling force behavior for p=4,94 mm.

The data showed on Table 5-8 evidences as the differences discussed above are slightly smaller. In the case of rolling forces, it is almost of 2 kN while for normal forces is a little more than 10 kN. The variance are 0,17 kN and 3,98 respectively, more or less the same as reported on Table 5-7.

Table 5-8 Force values for penetration depth of 4,94 mm.

	Fr mean (kN)	**Fm mean (kN)**
Groove 4	5,27	29,03
Groove 5	5,82	32,82

Groove 6	6,17	33,22
Groove 7	5,39	30,39
Mean 4-7	**5,66‡0,17**	**31,36‡3,98**
Groove 8	7,58	42,05

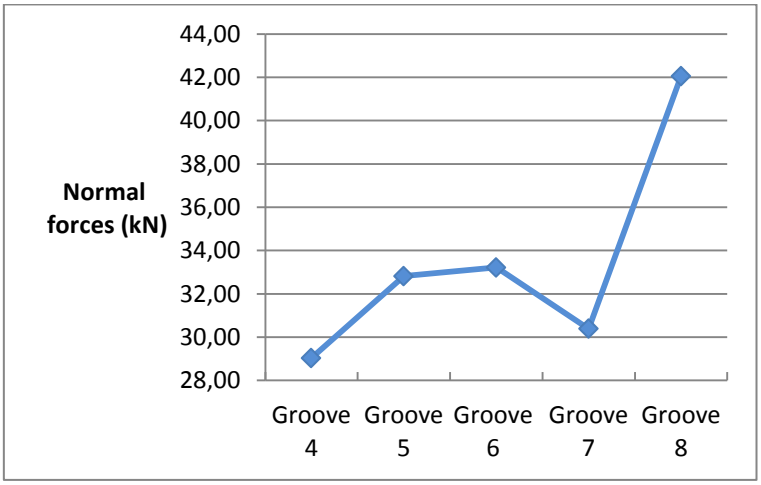

Figure 5-35 Variation of forces in normal direction on each groove

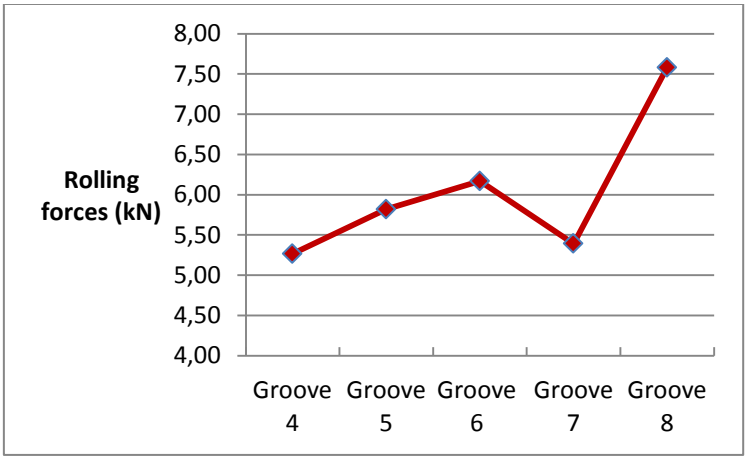

Figure 5-36 Variation of forces in rolling direction on each groove

5.4.2.3. P=4,47 mm

According to Figure 5-37 the maximum normal force is about 56 kN and the mean is 30 kN. While rolling forces the maximum is around 8 kN and the mean is 5 kN. It is noticed how the forces have decreased their values as the penetration depth is reduced.

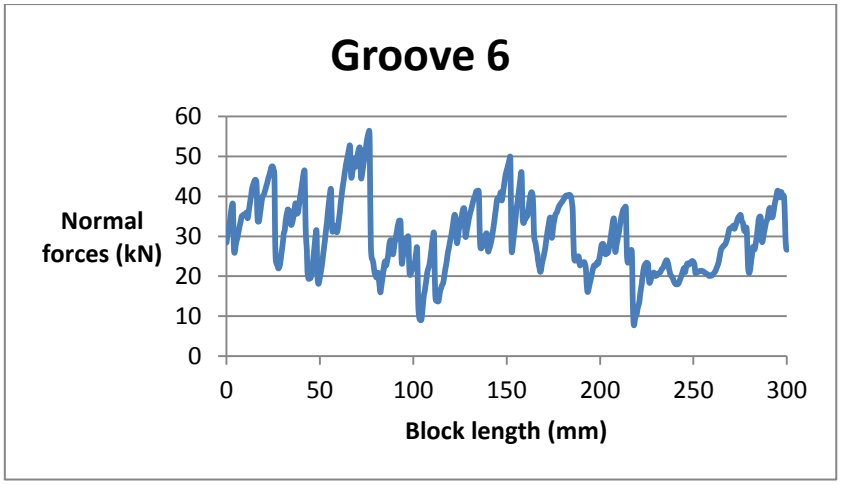

Figure 5-37 Normal force behavior for p=4,47 mm.

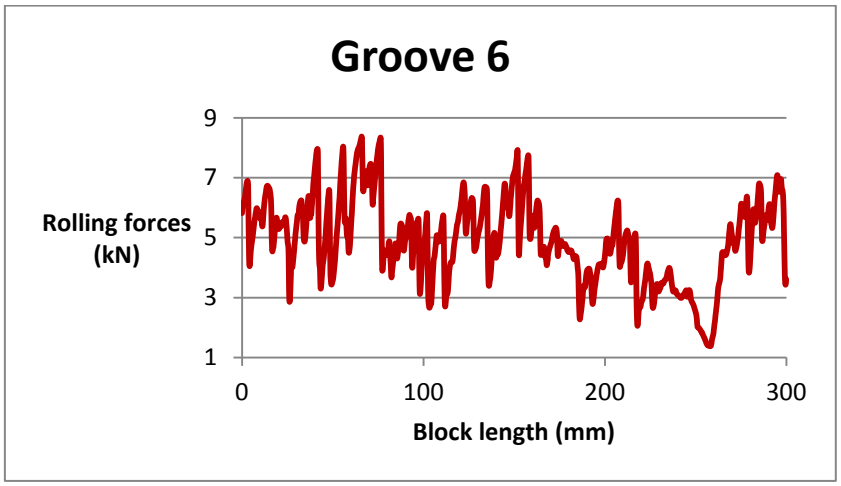

Figure 5-38 Rolling force behavior for p=4,47 mm.

The data showed on Table 5-9 shows as the mean value of rolling forces from groove 5 to groove 7 is 5,14 kN with a variance of 0,04 kN. The normal forces exhibit a mean of 30,38 kN and a variance of 0,97. In this case the analogous values for the groove 8 are not so far in magnitude, showing a smaller difference than the two penetrations describes above. This behavior is also well represented on Figure 5-39 and Figure 5-40 where it can be seen as the graph is more linear for both cases. The reduced difference mean and forces on groove 8 is due to the auxiliary grooves that were started to be excavated from this data level (see Figure 5-20)

Table 5-9 Force values for penetration depth of 4,47 mm.

	Fr mean (kN)	**Fm mean (kN)**
Groove 5	5,18	29,56
Groove 6	4,92	30,10
Groove 7	5,32	31,47

Mean 5-7	**5,14‡0,04**	**30,38‡0,97**
Groove 8	6,43	38,25

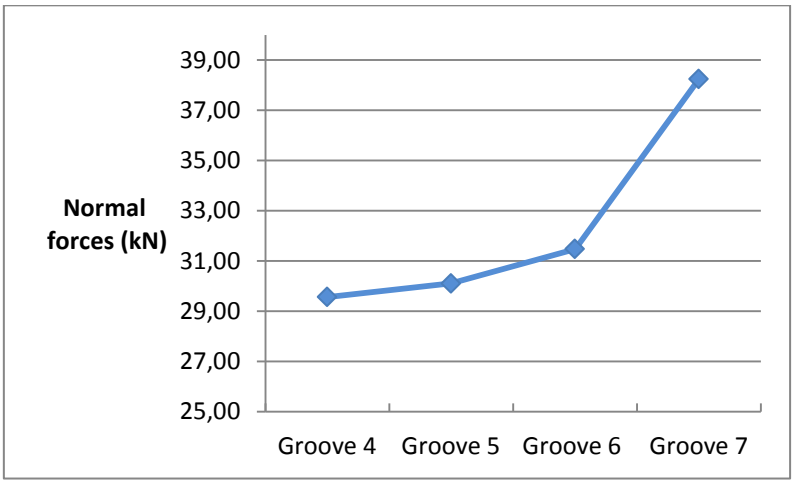

Figure 5-39 Variation of forces in normal direction on each groove

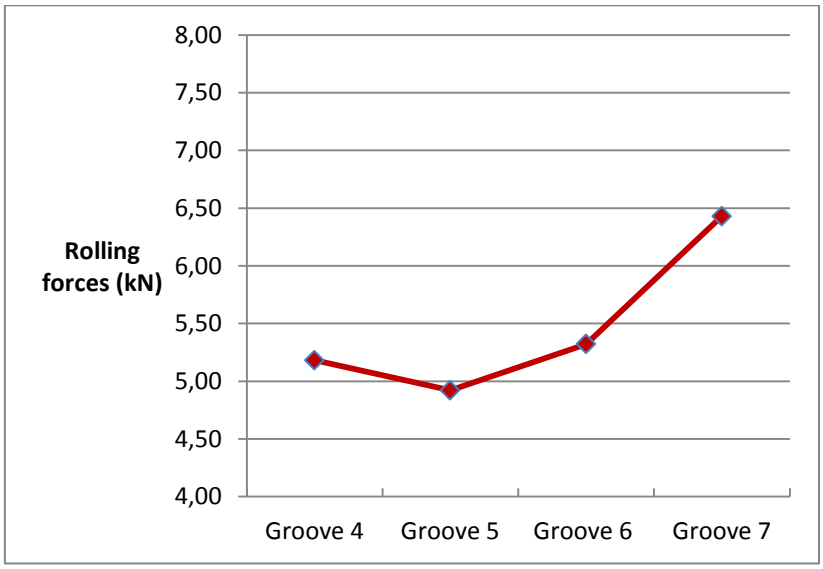

Figure 5-40 Variation of forces in rolling direction on each groove

5.4.2.4. P=3,96 mm

Figure 5-41 shows that the maximum normal force is about 48 kN and the mean is 27 kN. In the case of rolling forces, the maximum is around 7,5 kN and the mean is 4 kN (Figure 5-42).

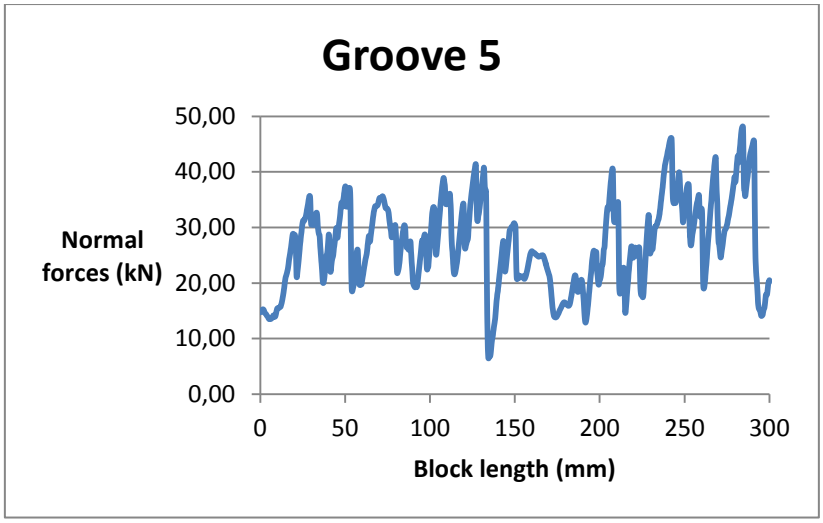

Figure 5-41 Normal force behavior for p=3,96 mm.

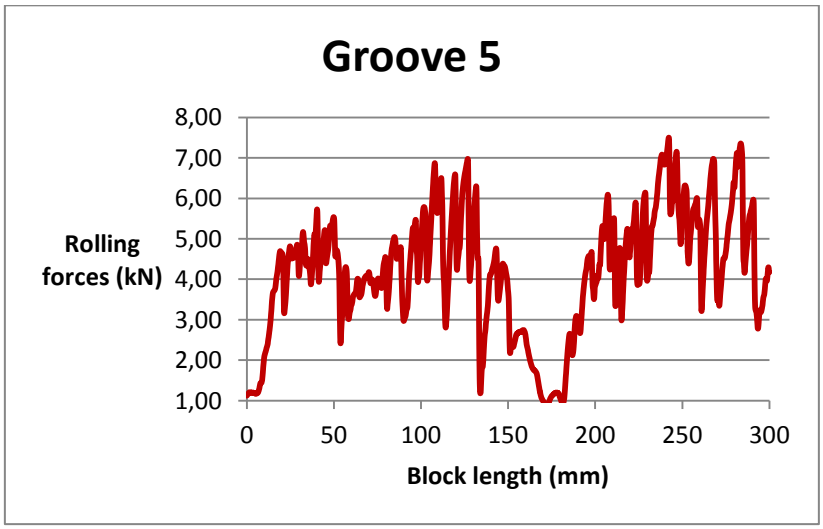

Figure 5-42 Rolling force behavior for p=3,96 mm.

The data showed on Table 5-10 shows as the mean value of rolling forces from groove 4 to groove 6 is 4,19 kN with a small variance of 0,002 kN. The normal forces exhibit a mean of 26,54 kN and a variance of 3,39 kN. Also, in this case, the analogous values for the groove 7 are not so far in magnitude, less than 1 kN for rolling forces and almost 8 kN for normal forces

.Table 5-10 Force values for penetration depth of 3,96 mm.

	Fr mean (kN)	**Fm mean (kN)**
Groove 4	4,14	24,51
Groove 5	4,19	26,99
Groove 6	4,23	28,11
Mean 4-6	**4,19‡0,002**	**26,54‡3,39**
Groove 7	5,42	34,21

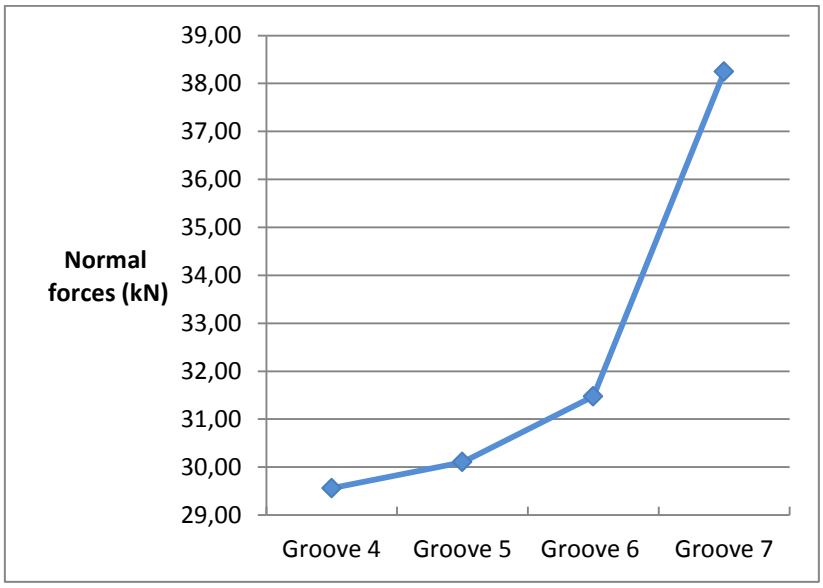

Figure 5-43 Variation of forces in rolling direction on each groove

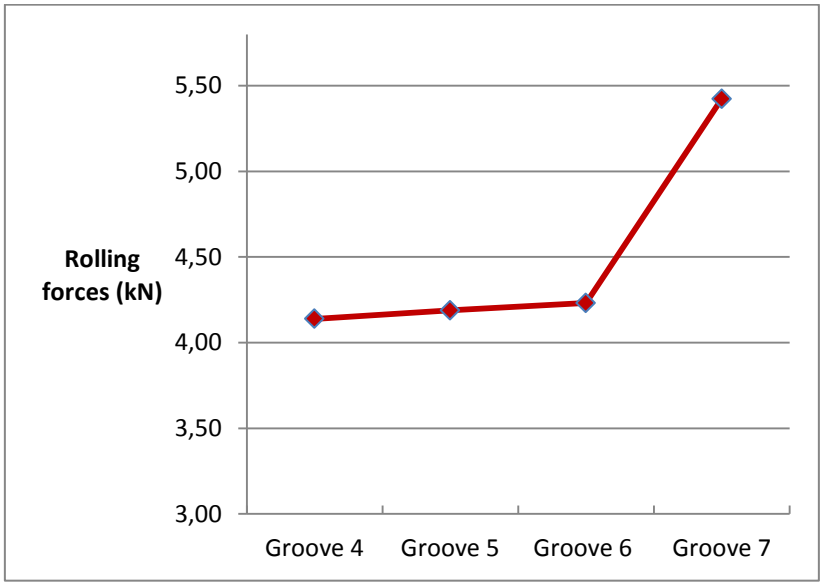

Figure 5-44 Variation of forces in rolling direction on each groove

5.4.2.5. P= 3,51 mm.

The force behavior at this shallower "p" value can be evidenced on Figure 5-45 and Figure 5-46. The maximum normal force is about 42 kN and the mean is 27 kN. In the case of rolling forces, the maximum is around 7 kN and the mean is 4 kN (Figure 5-42). It can be seen as these values have not varied in relation with those obtained with depth penetration of 3,96 mm.

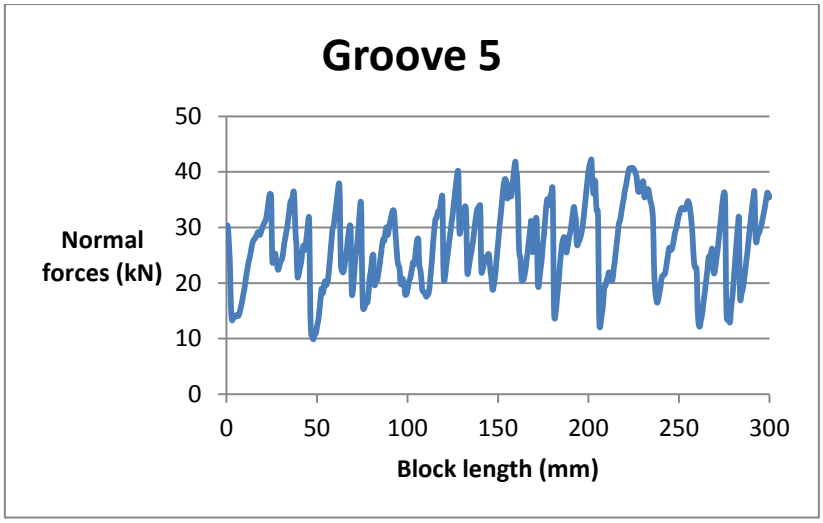

Figure 5-45 Normal force behavior for p=3,51 mm.

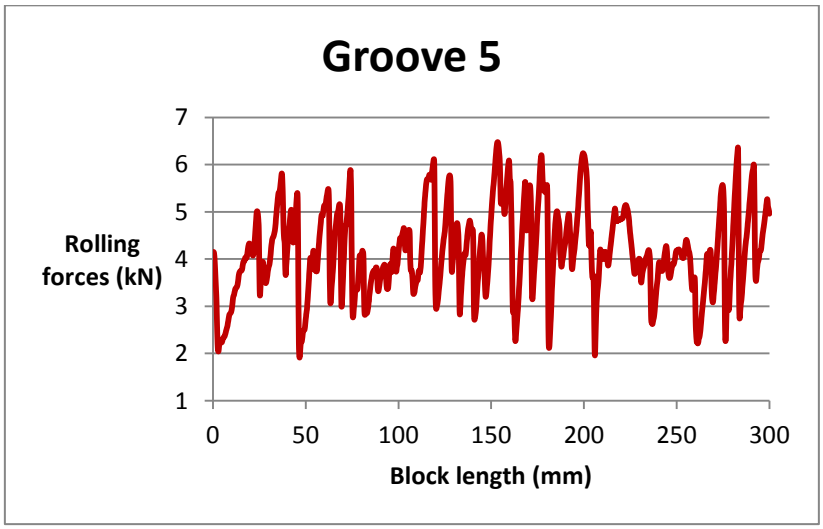

Figure 5-46 Rolling force behavior for p=3,51 mm.

The data showed on .Table 5-11 shows as the mean value of rolling forces from groove 4 to groove 6 is 4,17 kN with a small variance of 0,027 kN. The normal forces exhibit a mean of 27,24 kN and a variance of 1,19 kN. The analogous values for the groove 7 are not so far in magnitude for rolling forces, less than 1 kN, instead for normal forces is about 10 kN.

.Table 5-11 Force values for penetration depth of 3,96 mm.

	Fr mean (kN)	**Fm mean (kN)**
Groove 4	4,01	26,45
Groove 5	4,16	26,75
Groove 6	4,34	28,47
Mean 4-6	**4,17‡0,027**	**27,22‡1,19**
Groove 7	4,92	37,79

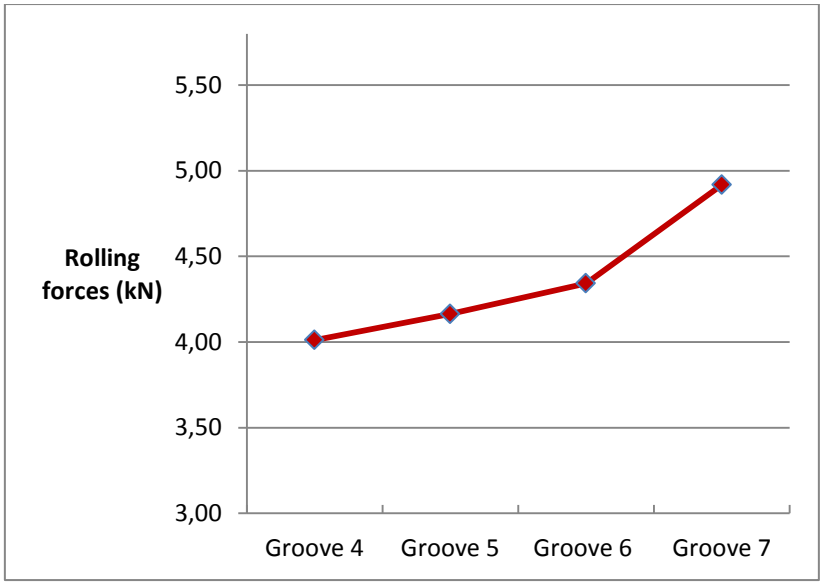

Figure 5-47 Variation of forces in rolling direction on each groove

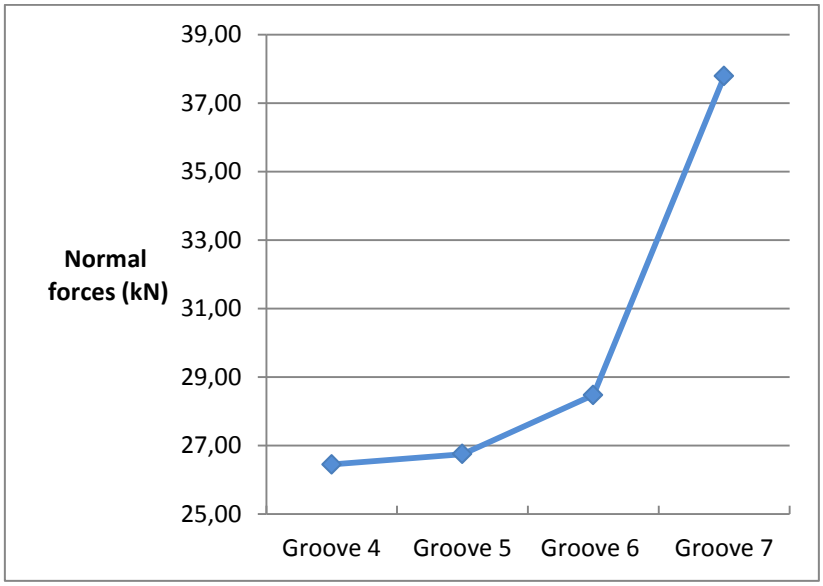

Figure 5-48 Variation of forces in normal direction on each groove

5.4.2.6. Coefficient Cut (CC)

Disc cutting forces increase with increased penetration over the range of penetrations depths tested, from 3,5 to 5,5 mm. The normal forces increase nonlinearly (Figure 5-49), as the rolling forces increase in a more linear way (Figure 5-50). The biggest disc cutting force values reported on the graphs showed below correspond to a penetration depth equal to 5,5 mm. At the same time these values represent the mean of the forces developed during the cutting of grooves considered for calculation of specific energy at this data level. The same consideration is takes for the rest of "p". On the Figure 5-51 is represented the early proved correlation between the forces just discussed, having an R^2= 0,9867.

Although in this study is considered the cut spacing as a constant equal to 40 mm, there exist many others researches where this cutting geometry parameter is variable. For example,

results obtained by (Rostami, 2007) indicate that also with increased spacing both forces tend to increase in a more or less linear way.

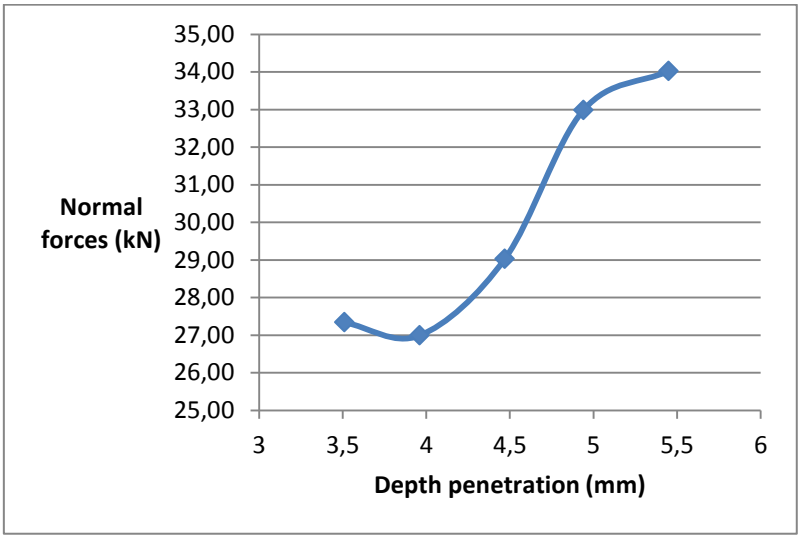

Figure 5-49 Variation of normal forces with penetration

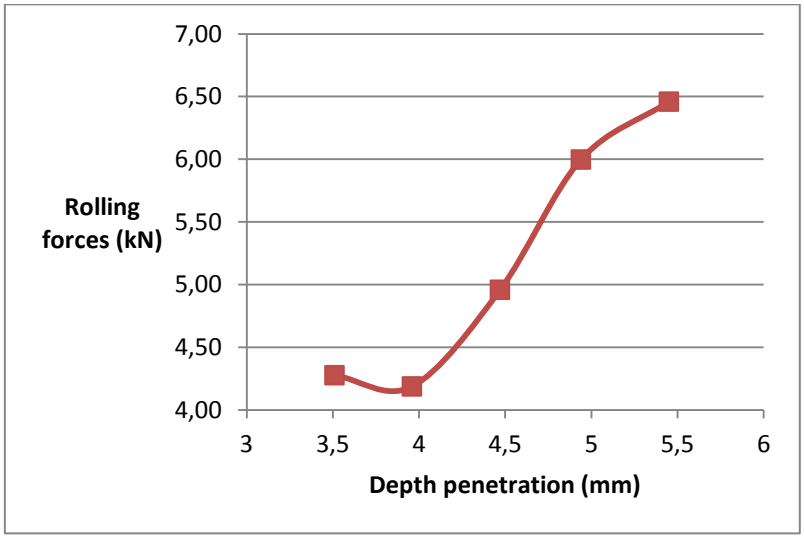

Figure 5-50 Variation of rolling forces with penetration

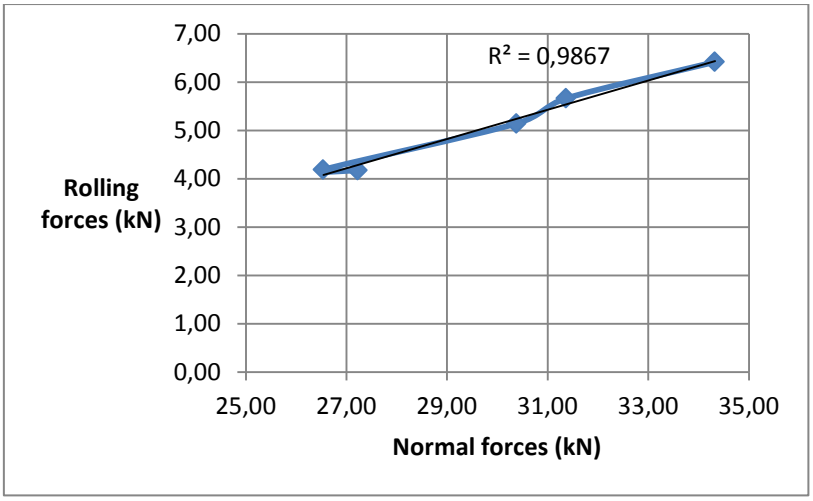

Figure 5-51 Correlation of disc cutting forces

The cutting coefficient, which is the ratio of rolling and normal forces ($CC=F_R/F_N$), also increases with increased penetration. The variation range is delimited between 15% for the shallowest one and almost 19% for the deepest one. Figure 5-52 show the relationship between this coefficient and the penetration depth.

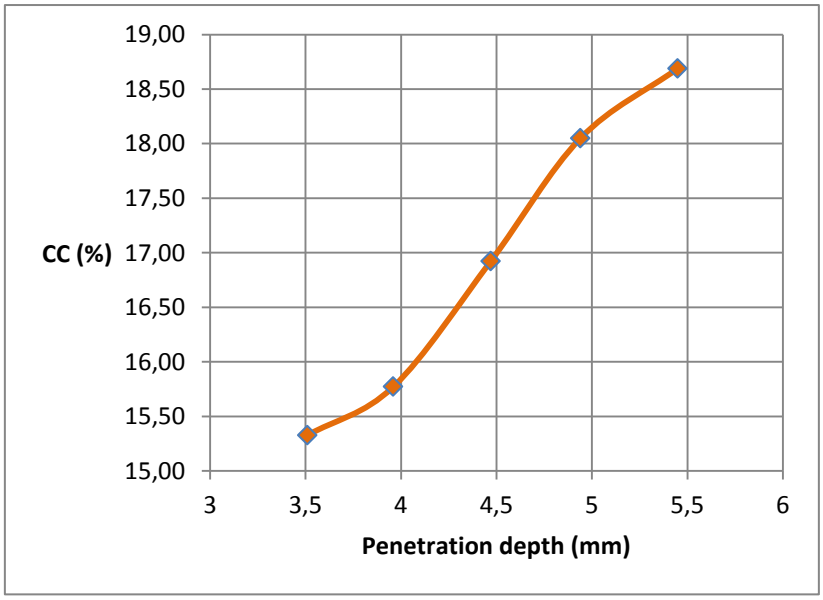

Figure 5-52 Variation of cutting coefficient with penetration

5.4.3. Specific energy

As explained on section 3.1.1, this in one of the main parameters of interest in a study related with a TBM performance. The data showed on Table 5-12 were obtained from the test done with the ILCM. For each penetration depth there is a normal and rolling mean force generated by the rock-tool interaction which has produced a certain volume of chips, as the one showed on Figure 5-53.

Figure 5-53 Chip produced bi rock-tool interaction

For excavating rock with a tool it is spent an amount of energy that is function of the mean rolling force, cutting length and the volume of detritus generated. As the rock fragments are bigger the specific energy tends to be reduced for similar values of forces. The goal is to find the cutting geometry that allows the greatest rock fragmentation in order to use the minimum quantity of energy, in other words to get an optimal s/p ratio Considering the data contained on Table 5-12 and the Figure 5-54, it can be said that for this type of Carraras's marble the optimal s/p ratio is between 8 and 8,6. The penetration at which is obtained this smallest value is approximately 5 mm. and the rolling force necessary for cutting the rock is equal to 6 kN with an associate normal force of 32,98 kN.

Table 5-12 Specific energy and forces for each s/p ratio on study

S (mm)	P(mm)	s/p	F_R (kN)	F_N (kN)	CC (%)	V (cm^3)	SE (MJ/m^3)	SE ($kW\text{-}h/m^3$)
40	3,51	11,40	4,28	27,34	18,69	38,82	33,56	9,29
40	3,96	10,10	4,19	26,99	18,05	31,90	39,38	10,91
40	4,47	8,95	4,96	29,03	16,92	59,71	25,13	6,96
40	4,94	8,10	6,00	32,98	15,77	75,45	23,91	6,62
40	5,45	7,34	6,46	34,02	15,33	73,91	26,38	7,31

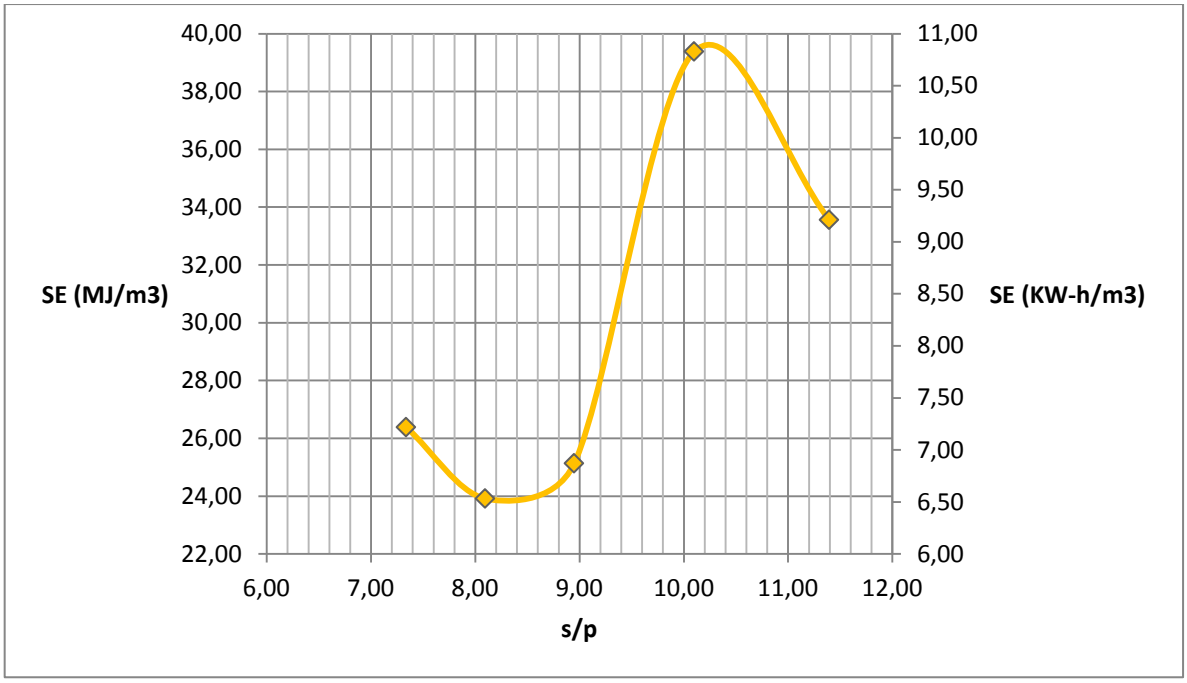

Figure 5-54 Specific energy for "Veined Statuary White" Marble

5.4.4. Variation of forces in function of minerals presence

During cut excavation at the first four levels, specifically by the groove 8, it was evidenced as forces used to reach pikes values at specific points of block length, these points are showed on the graphs represented on Figure 5-56 and Figure 5-57. They are more or less at 54, 260 and 360 mm from the left edge of the block pictured on Figure 5-55. The occurrence of these points coincides with the presence of the before mentioned (Section 5.2) greenish color veins. It cannot be said with sureness because there was not done a proper mineralogical study of these veins but it is presume that it is an occurrence of magnesium oxide.

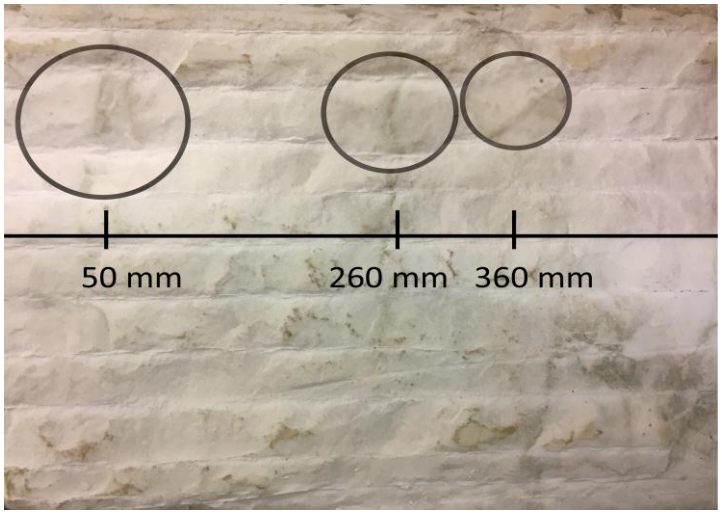

Figure 5-55 Occurrence of greenish color veins

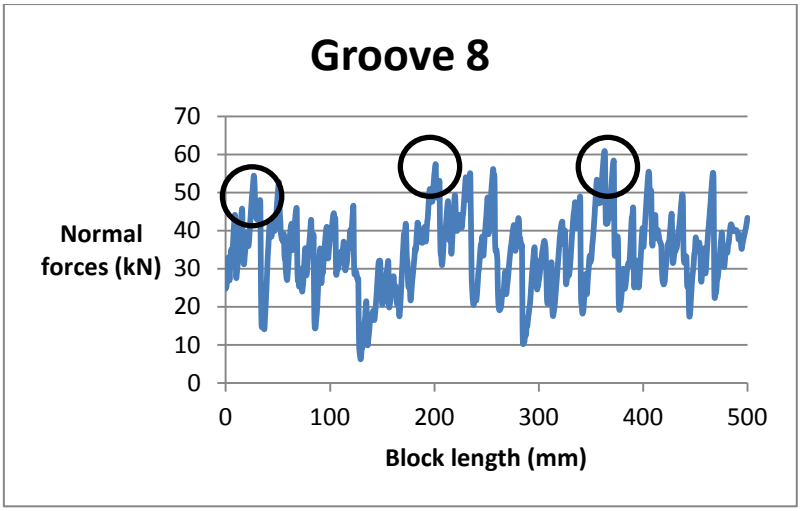

Figure 5-56 Variation of normal force in function of the different minerals on the rock surface

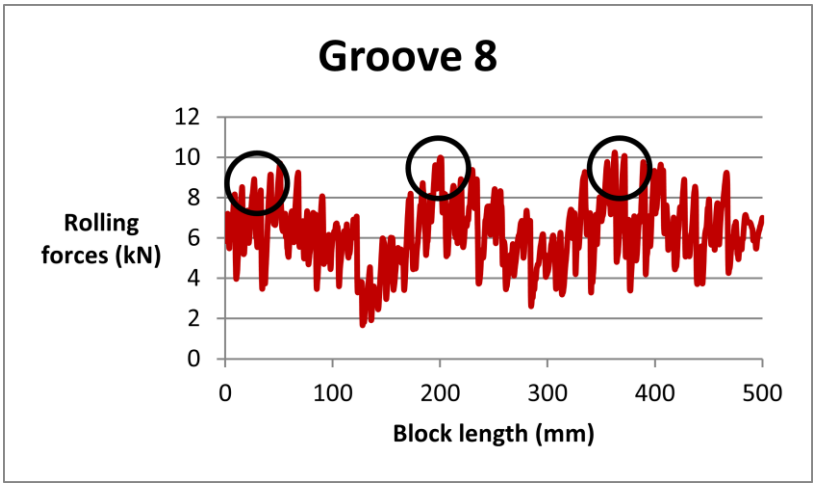

Figure 5-57 Variation of rolling force in function of the different minerals on the rock surface

5.5. Analytical analysis

In order to evaluate the results obtained in a theoretical way and to determinate how reliable they could be for doing a disc cutting forces pre-experimental estimation, have been applied two of the theoretical/empirical models cited on chapter 2. These are the model developed by (Roxborough & Phillips, 1975) and the CSM model. For the last one the data obtained is comparable with experimental results, as for the other one are not so similar. On the next sections are showed and described.

5.5.1. Roxborough and Philips Model

The results showed on Table 5-13 were calculated with the expressions discussed on section 2.5.3.1 and considering a cutter disc with a diameter of 170 mm and edge angle of 60° (Figure 5-58). The rock compressive strength considered is 131 MPa (Blasi, 1998)

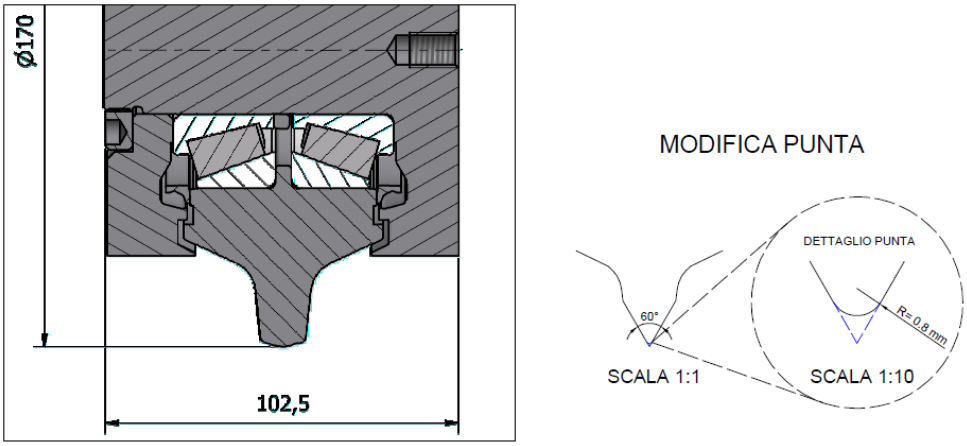

Figure 5-58 Geometry of cutter disc

The discrepancy between forces magnitudes are considerable, taking into account that in the normal direction the differences for all penetrations (Table 5-13) are more or less of 15 kN The theoretical values in this cases underestimates the actual data measured with the ILCM.

On the other hand, the forces on the rolling direction prove to be not so different respect to the experimental data, with a gap of almost 3 kN as the maximum., The forces resulted overestimated for all penetration values except for the 3,5 mm where it is smaller. Figure 5-61 and Figure 5-62 show the R^2, being of 0,884 and 0,938 respectively.

Table 5-13 Theoretical and experimental results

Cutting geometry			**Roraxbough and Philips**				**IlCM**	
S (mm)	**P (mm)**	**s/p**	**l (mm)**	**A (mm2)**	**Fn (kN)**	**Fr (kN)**	**Fn (kN)**	**Fr (kN)**
40	3,51	11,40	48,35	195,95	**13,33**	**3,73**	**27,34**	**4,28**
40	3,96	10,10	51,28	234,50	**14,88**	**4,74**	**26,99**	**4,19**
40	4,47	8,95	54,40	280,80	**16,56**	**6,04**	**29,03**	**4,96**
40	4,94	8,10	57,11	325,77	**18,03**	**7,38**	**32,98**	**6**
40	5,45	7,34	59,89	376,91	**19,53**	**8,99**	**34,02**	**6,46**

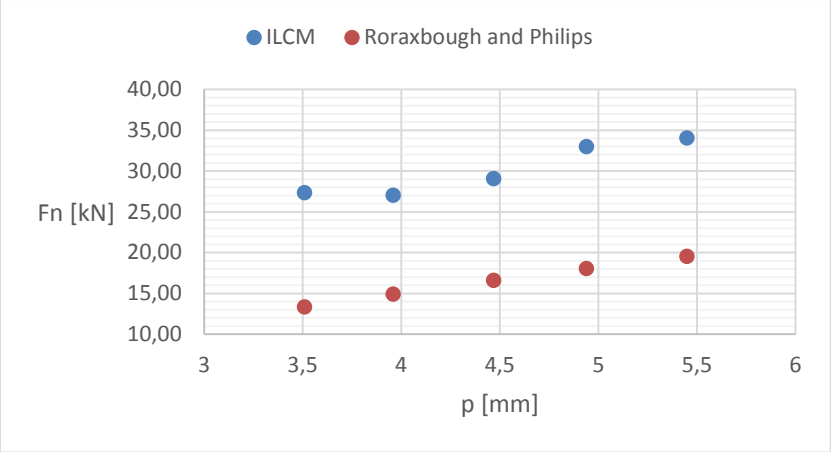

Figure 5-59 Theoretical and experimental normal forces in function of penetration

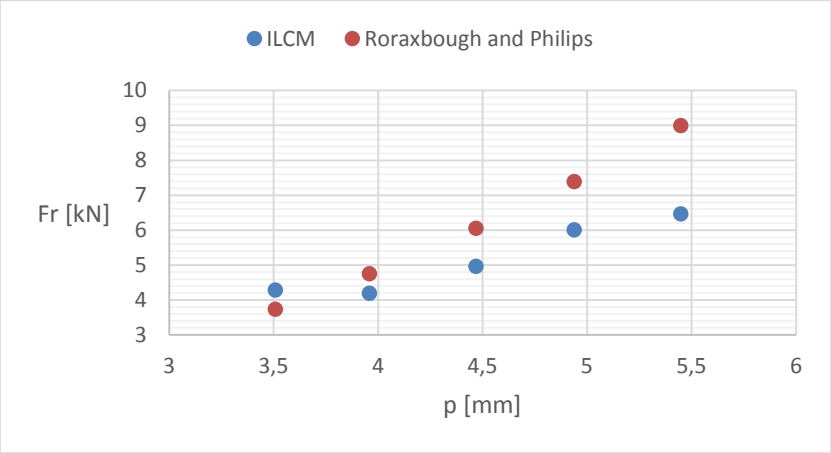

Figure 5-60 Theoretical and experimental rolling forces in function of penetration

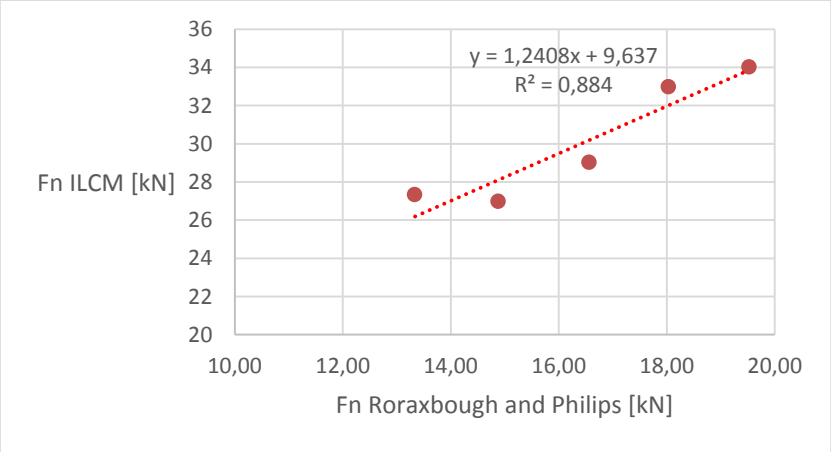

Figure 5-61 Differences between theoretical and experimental normal forces

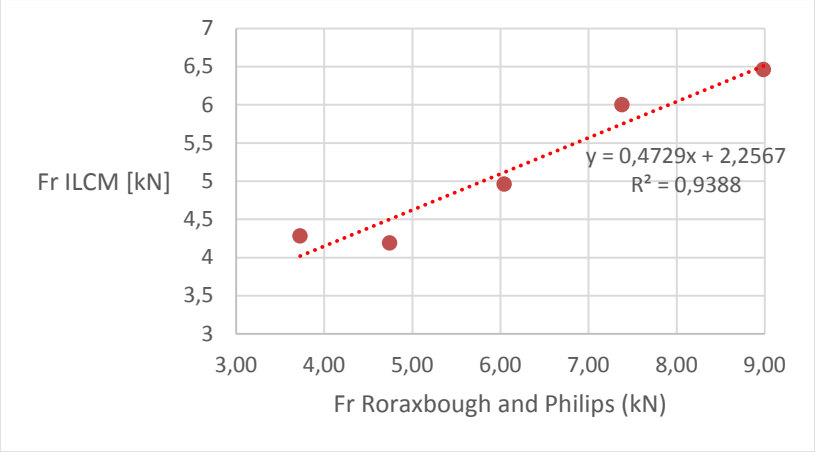

Figure 5-62 Differences between theoretical and experimental rolling forces

5.5.2. CSM model

In the case of this model were used the expressions mentioned on section 2.5.4. for the calculation of the data presented on Table 5-14 and

Table 5-15. It was considered a disc radius of 85 mm and a constant C=2,12. The rock compressive strength, as on the previous model was taken into account as 131 MPa and the tensile strength equal to 8 MPa.

The CSM as a model intended for CCS type discs considers the blade width T as a parameter needed for calculating the average pressure in the contact area P*. Therefore, for a V shaped disc it is not possible to measure it directly. This is why it was used the profile designed on Figure 5-63 for estimating this T value in function of penetration. It was done with a simple trigonometric relation also considering φ=60°

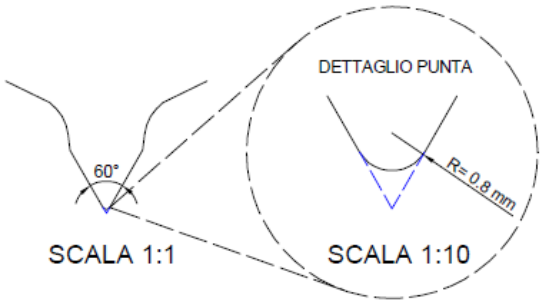

Figure 5-63 V-shaped disc blade

This value was calculated considering two possible sceneries: one that considerers no wearing on the blade and the other which does. The diverse T values are referred as T_{min} and T_{max}.respectively. The nomenclature was taken because of the trend of a bigger value of T when the disc is assumed as worn. As the disc is worn the blade widens and the contact area increases, therefore the pressure P* would be reduced. Table 5-15.

Table 5-14 Experimental and theoretical results considering T_{Min}

Cutting geometry		CSM						ILCM		
P (mm)	s/p	φ	T_{min} (mm)	P* (MPa)	F_N [kN]	F_R [kN]	CC	F_N (kN)	F_R (kN)	CC
3,51	11,40	0,29	4,05	213,82	**21,02**	**3,05**	**0,15**	**27,34**	**4,28**	**0,16**
3,96	10,10	0,31	4,57	205,36	**24,17**	**3,73**	**0,15**	**26,99**	**4,19**	**0,16**
4,47	8,95	0,33	5,16	197,20	**27,81**	**4,57**	**0,16**	**29,03**	**4,96**	**0,17**
4,94	8,10	0,34	5,70	190,71	**31,22**	**5,40**	**0,17**	**32,98**	**6,00**	**0,18**
5,45	7,34	0,36	6,29	184,53	**34,96**	**6,36**	**0,18**	**34,02**	**6,46**	**0,19**

Table 5-15 Experimental and theoretical results considering T max

Cutting geometry		CSM						ILCM		
P (mm])	s/p	φ	T_{max} (mm)	P* (MPa)	F_N (kN)	F_R (kN)	CC	F_N (kN)	F_R (kN)	CC
3,51	11,40	0,29	4,97	206,67	**24,92**	**3,61**	**0,14**	**27,34**	**4,28**	**0,16**
3,96	10,10	0,31	5,49	199,20	**28,15**	**4,35**	**0,15**	**26,99**	**4,19**	**0,16**
4,47	8,95	0,33	6,08	191,90	**31,87**	**5,24**	**0,16**	**29,03**	**4,96**	**0,17**
4,94	8,10	0,34	6,62	186,03	**35,34**	**6,11**	**0,17**	**32,98**	**6,00**	**0,18**
5,45	7,34	0,36	7,21	180,39	**39,16**	**7,13**	**0,18**	**34,02**	**6,46**	**0,19**

The results obtained with this model are really closed with the experimental obtained. In the hypothetical case of a disc without wear there is a maximum difference of 6 kN just for a penetration of 3,51 mm, the rest of the values are really similar between them. When it comes to the case of a worn disc the values continue to be comparable. For all penetration values there is more or less the same difference of 2 kN. The total differences for both scenarios are 13,07 and 13,92 kN respectively

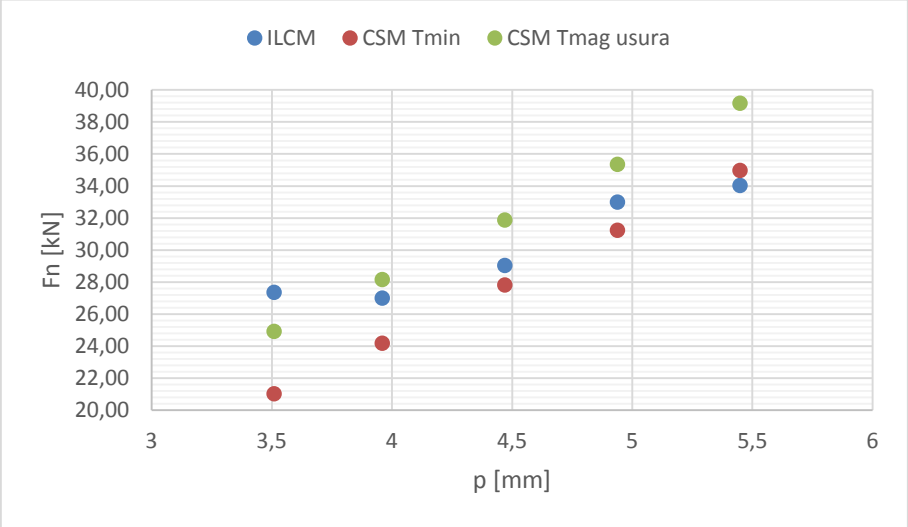

Figure 5-64 Theoretical and experimental normal forces in function of penetration

For rolling forces the differences are yet smaller. When is considered $T_{Min,}$ there is a gap of barely 1 kN for all penetrations the rest are really similar between them. The forces are

slightly underestimated. In the case of T_{Max}. the differences between forces are also into this range but oppositely those derived theoretically are overestimated. The total differences for both scenarios are 2,76 and 1,88 kN respectively. Thus, these close values just discussed are also repeated on cutting coefficients which, in practice, are equal.

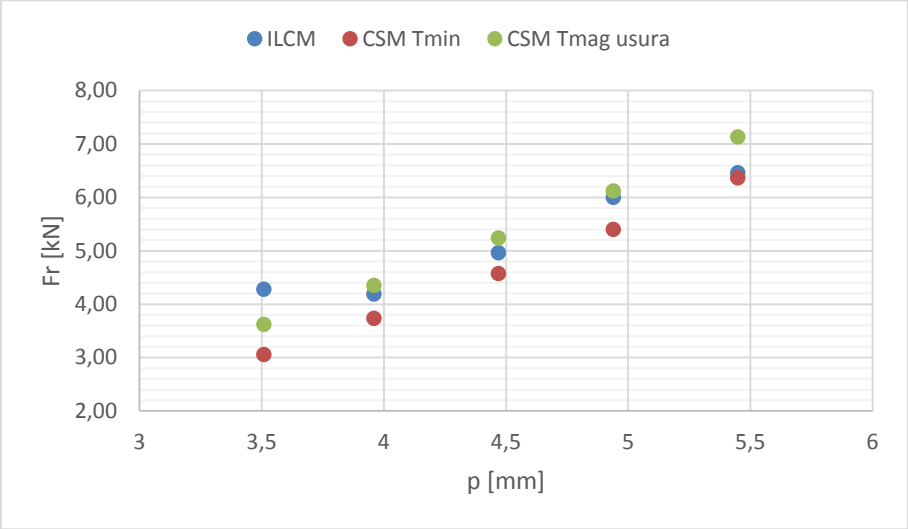

Figure 5-65 Theoretical and experimental rolling forces in function of penetration

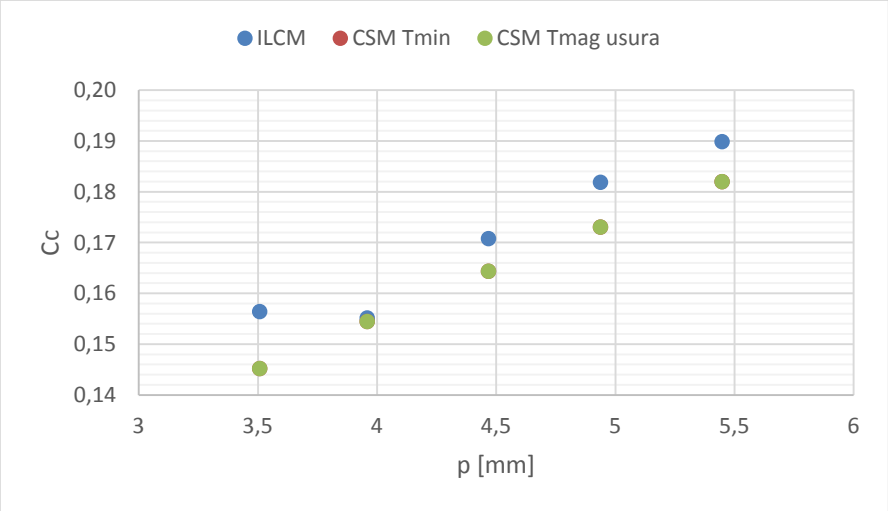

Figure 5-66 Cutting coefficient in function of penetration

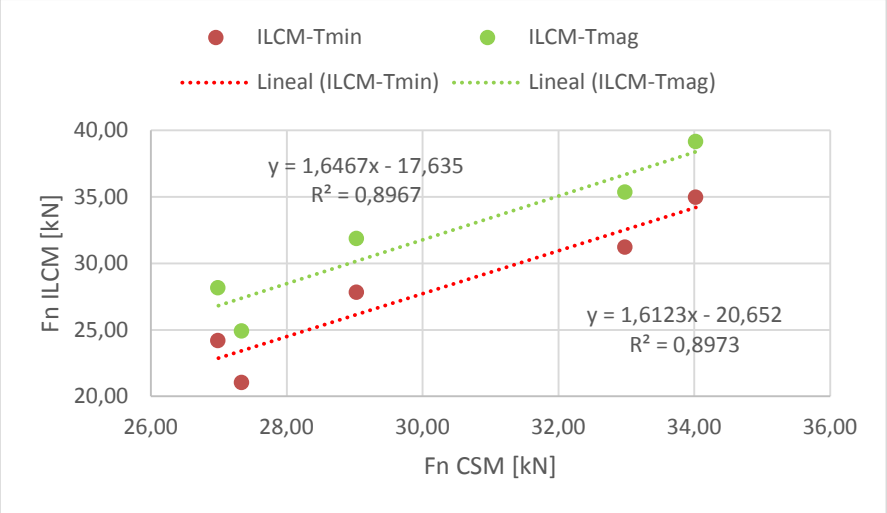

Figure 5-67 Differences between theoretical and experimental normal forces

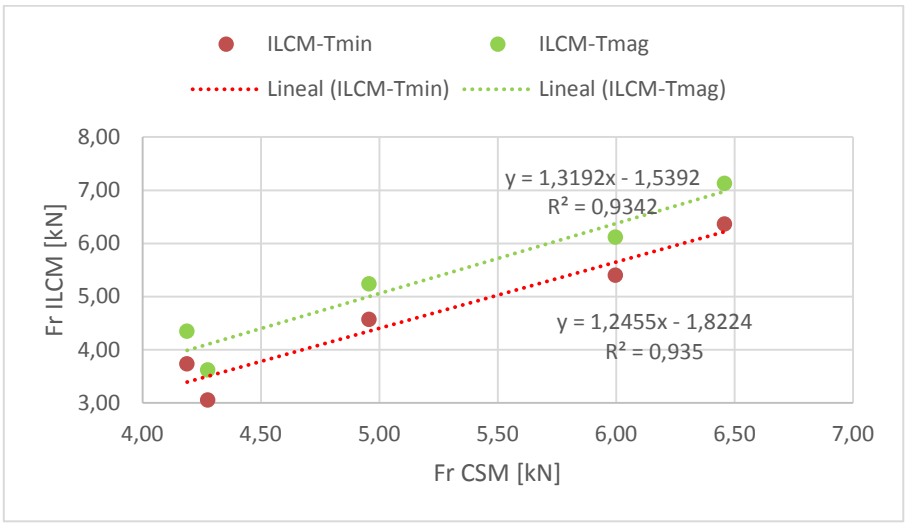

Figure 5-68 Differences between theoretical and experimental rolling forces

Conclusions

The results obtained during the experimental phase has proven that ILCM of Polytechnic of Turin is able to give reliable values of the forces generated during the use of a cutter disc for excavating hard rock at least for this intermediate scale. This affirmation is backed up by the good correlation between normal and rolling forces and the little variations on cutting coefficients.

It was observed as regularizing the rock surface by the conditioning before each data level has caused a more or less constant value of cutting disc force for grooves of the same level. This practice also represents more similar cutting geometry conditions to those generated during the rock excavation with TBM

The sample confinement was improved in comparison with the last experiences with the ILCM, nevertheless could be done some changes in order to reduce the breakage of the cement block edges. Since as a consequence of this, the marble block remained unbounded and therefore could exist the risk of its subsequent breakage near to the borders. This was tried to be avoided by not excavating the more external grooves as the excavation went down, the goal was completed but wasting a considerable amount of time breaking manually with hammer and chisel the marble over the level being excavated.

The step could not be skipped, on the contrary the forces generated on the disc would exceed for long the maximum forces for its optimal operation. Optimizing even more this confinement problem could allow reaching deeper depth penetrations than those reached on this study and therefore generate specific energy values for a bigger range of s/p ratios

The problem mentioned below can be partially solved initiating the test with the greatest values of penetration and to do the shallower ones for the final. Proceeding in this way the forces will not be so high as the levels on study continues to be lower respect to the initial one, also there are reduced the external variants that can modify the results.

The fact that test are done now with a V shaped and not with CCS type disc permitted to reach deeper on penetration values without exceeded forces. Taking into consideration its little diameter and bearings with the old disc could not be possible to excavate this marble, at penetration under 5 mm. without applying greatest forces yet

The models put on study resulted to have different degree of certainty on theoretical determination of forces for the actual setting of the ILCM. The Roraxbough and Philips and model must be used with attention because of the notable underestimation of values. The CSM model, despite it is not properly intended for V-shaped type disc has proved to be very reliable. Having this model into account could be a convenient way to preset convenient cutting geometry for the machine and the cutter disc for future tests.

Deciding which of the two scenarios hypothesized for this model is more convenient to use will depend on disc conditions. However, unless the test is being carried out with a new little worn tool as it was during the execution of the proves, it is advisable to take the model which recreates the forces generated by a blade worn disc.

References

Alber, M., 1996. *Prediction of penetration utilization for Hard Rock TBMs.* Rotterdam, s.n., pp. 721-5.

Balci, C., 2008. Correlation of rock cutting tests with field performance of a TBM in highly gfractured rock formation. A case study in Kozyatagi-kadikoy metro tunnel, Turkey. *Tunneling and underground space tecnhology,* Issue 24, pp. 423-435.

Balci, C. & Bilgin, N., 2007. Corrrelative study of linear small and full-scale rock cutting tests to select mechanized excavations machines. *International Journal of Rock Mechanics & Minig Sciences,* Issue 44, pp. 468-476.

Bilgin, N., Feridunoglu, C. & Tumac, D., 2005. *The performance of a full face tunnel boring machine (TBM) in Tarabya (Istanbul).* Istanbul, Balkema ,Rotterdam, Erdem, Y,Solak T, pp. 821-826.

Blasi, P., 1998. *Le varieta merceologiche dei marmi carraresi*, International marmi e macchine carrara S.P.A: s.n.

Bruland, A., 2014. Prediction model for performance and costs. *Norwegian tunneling society,* pp. 29-34.

Chang, S.-H., Choi, S.-W., Bae, G.-J. & Jeon, S., 2006. Performance prediction of TBM disc cutting on granitic rock by linear cutting disc. *Tunneling and Underground Space Technology* , Issue 21.

Chapman, D., Metje, N. & Stark, A., 2010. *Introduction to tunnel construction.* Oxon: Spon Press.

Cho, J. W., Jeon, S., Yu, S. H. & Chang, S. H., 2009. Optimun spacing of TBM disc cutters: A numerical simulation using the three-dimensional dynamic fracturing methos. *Tunneling and Underground Space Technology.*

Copur, H., 2010. Linear stone cutting tests with chisel tools for identification of cutting principles and predicting performance of chain saw machines. *International Journal of Rock Mechanics & Mining Sciences 47,* pp. 104-120.

Criscuolo, A. & Lisi, S., 2016. Geologia e strutture della formazione dei marmi. *Eurominerals and the society of mining professors 1998.*

Friant, J. E. & Ozdemir, L., 1993. *Tunnel boring technology- Present and future,* s.l.: s.n.

Gertsch, R., Gertsch, L. & Rostami, J., 2007. Disc cutting tests in Colorado Red Granite: Implications for TBM performance prediction. *International Journal of Rock Mechanics & Mining Sciences,* pp. 238-246.

Innaurato, N., Oggeri, C., Oreste, P. & Vinai, R., 2006. *Experimental and Numerical Sudies on Rock Breaking with TBM tools under High Stress Confinement,* Austria: Springer.

Nilsen, B. & Ozdemir, L., 1993. *Hard rock tunnel boring prediction and field performance.* Boston, USA, s.n., pp. 833-852.

Rispoli, A., 2013. *Analisi teorico-sperimentale per l'ottimizzazione dello scavo meccanizzato con utensili a disco,* Torino: s.n.

Roby, J., Sandell, T., Kocab, J. & Lindbergh, L., 2008. *The current state of disc cutter design and development directions.* s.l., s.n., pp. 36-39.

Rostami, J., 2007. *Rock fragmentation by disc cutter, a critical review and update.* s.l., s.n.

Rostami, J. & Ozdemir, L., 1993. A new model for performance prediction of hard rock TBMs. *RECT Proceedings,* pp. 793-809.

Rostami, J., Ozdemir, L. & Neil, D. M., 1994. Performance prediction a key issue in mechanical hard rock mining. *Min. Eng,* Issue 11, pp. 1263-1267.

Rostami, J., Ozdemir, L. & Nilson, B., 1996. *Comparison between CSM and NTH Hard Rock TBM Performance Prediction Model,* s.l.: s.n.

Roxborough, F. F. & Phillips, H. R., 1975. Rock Excavation by Disc Cutter. *Int. J. Rock Mech. Min. Sci & Geomech Vol.12,* pp. 361-366.

Vagnon, F., 2013. *Scavo meccanico in roccia: analisi sperimental, analitica e numerica dei parametri che influenzano l'azione dei dischi delle TBM,* Torino: s.n.

Wanner, H. & Aeberli, U., 1979. *Tunnellling machine performance in jointed rock.* Montreaux, s.n., pp. 573-9.